INFORMATION TO USERS

This manuscript has been reproduced from the microfilm master. UMI films the text directly from the original or copy submitted. Thus, some thesis and dissertation copies are in typewriter face, while others may be from any type of computer printer.

The quality of this reproduction is dependent upon the quality of the copy submitted. Broken or indistinct print, colored or poor quality illustrations and photographs, print bleedthrough, substandard margins, and improper alignment can adversely affect reproduction.

In the unlikely event that the author did not send UMI a complete manuscript and there are missing pages, these will be noted. Also, if unauthorized copyright material had to be removed, a note will indicate the deletion.

Oversize materials (e.g., maps, drawings, charts) are reproduced by sectioning the original, beginning at the upper left-hand corner and continuing from left to right in equal sections with small overlaps.

Photographs included in the original manuscript have been reproduced xerographically in this copy. Higher quality 6" x 9" black and white photographic prints are available for any photographs or illustrations appearing in this copy for an additional charge. Contact UMI directly to order.

Bell & Howell Information and Learning
300 North Zeeb Road, Ann Arbor, MI 48106-1346 USA
800-521-0600

Numerical Simulations of Interactions of Electromagnetic Waves with Lossy Dielectric Surfaces Using Fast Computational Methods

by

Qin Li

A dissertation submitted in partial fulfillment of the requirements for the degree of

Doctor of Philosophy

University of Washington

2000

Program Authorized to Offer Degree: Electrical Engineering

UMI Number: 9964268

Bell & Howell Information and Learning Company
300 North Zeeb Road
P.O. Box 1346
Ann Arbor, MI 48106-1346

In presenting this thesis in partial fulfillment of the requirements for the Doctoral degree at the University of Washington, I agree that the Library shall make its copies freely available for inspection. I further agree that extensive copying of the dissertation is allowable only for scholarly purposes, consistent with "fair use" as prescribed in the U.S. Copyright Law. Requests for copying or reproduction of this dissertation may be referred to UMI Dissertation Services, 300 North Zeeb Road, P.O. Box 1346, Ann Arbor, MI 48106-1346, to whom the author has granted "the right to reproduce and sell (a) copies of the manuscript in microform and/or (b) printed copies of the manuscript made from microform."

Signature 

Date 3-13-2000

University of Washington
Graduate School

This is to certify that I have examined this copy of a doctoral dissertation by

Qin Li

and have found that it is complete and satisfactory in all respects,
and that any and all revisions required by the final
examining committee have been made.

Chair of Supervisory Committee:

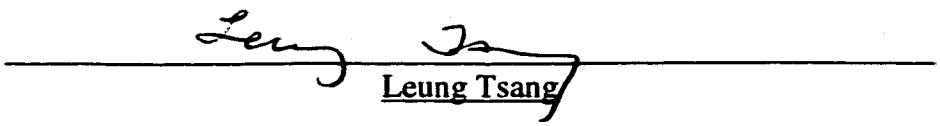

Leung Tsang

Reading Committee:

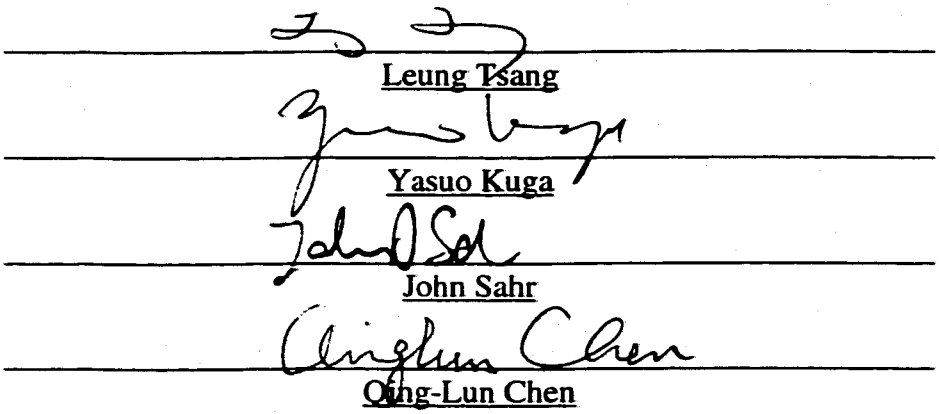

Leung Tsang

Yasuo Kuga

John Sahr

Qing-Lun Chen

Date: March 10, 2000

University of Washington

Abstract

NUMERICAL SIMULATIONS OF INTERACTIONS OF ELECTROMAGNETIC WAVES WITH LOSSY DIELECTRIC SURFACES USING FAST COMPUTATIONAL METHODS

by Qin Li

Chairperson of the Supervisory Committee:
Professor Leung Tsang
Department of Electrical Engineering

The scattering of electromagnetic waves by lossy dielectric random rough surfaces with large permittivity has broad applications in natural media. Because many of natural medium are lossy and with surface roughness. In the application of the Method of Moment to the lossy dielectric rough surfaces with high permittivity, there can be rapid spatial variations of the dielectric medium Green's function and surface fields. A dense discretization of the surface may be required. Therefore there is a large increase in CPU and required memory.

To circumvent the problem, the physics-based two-grid (PBTG) method was developed in this dissertation. In PBTG, two grids are used: a dense grid and a sparse grid. The sparse grid is that of the usual 8 to 10 points per wavelength. The dense grid ranges from 16 or higher number of points per wavelength depending on the relative permittivity of the lossy dielectric medium. The PBTG is based on two observations: (1) the Green's function of the lossy dielectric is attenuative and therefore is space-limited, and (2) the Green's function of free-space is slowly varying on the dense grid compared with the medium Green's function and therefore is spatial frequency-limited. The first observation results in a banded matrix for 1-dimensional rough surface and a sparse

matrix for 2-dimensional rough surface for the Green's function of the lossy dielectric. The second observation allows us, when using the free-space Green's function to act on the surface fields of dense grid, to first average the values of surface unknowns on the dense grid and then place them on the coarse grid. Thus the PBTG speeds up the computation and yet preserves the accuracy of the solution. The surface fields are calculated on the dense grid.

The PBTG can be applied to both 1-dimensional and 2-dimensional rough surfaces and can be easily used in conjunction with the other fast methods. The PBTG is combined with the banded matrix-iterative approach/canonical grid (BMIA/CAG) and the multilevel steepest descent fast multipole method (MLSDFMM) for 1-dimensional random rough surfaces and with sparse matrix canonical grid method (SMCG) for 2-dimensional random rough surfaces in this dissertation.

TABLE OF CONTENTS

LIST OF FIGURES

LIST OF TABLES

ACKNOWLEDGMENTS

I would like to express my sincere appreciation and gratitude to Professor Leung Tsang for his guidance and financial support for four years of graduate study. Without him, this dissertation would not have been possible. I appreciate the contributions of my Ph.D. supervisory committee members, Professors Yasuo Kuga, John Sahr, Eric Thorsos, Qing-Lun Chen, and Barry Hyman. I am grateful to Professor Chi Hou Chan and Dr. Kyung Pak. Whenever I have difficulty, they always give me a quick response. I am grateful to Dr. Jianchen Shi for making his computer resources available for me and to Dr. Kuan Shan Chen for discussing with him during his visit UW. I would like to extend my thanks to Noel Henry for her expertise in editing many of my papers and abstracts

I would like to thank fellow graduate students: Dr. Guifu Zhang, Dr. Chien-Min Lin, Dr. Steve Chan, Ms. Chite Chen, Todd Elson, Leibing Huang, Jun Liu, Seung-Woo Lee, Junho Cha, Carrie Cornish, Houfei Chen, Lin Zhou, Chung-Chi Huang, Jian Jun Guo for their friendship and help. Special thanks give to Mr. John Rockway. He proofread the Chapter one of my dissertation and gave many useful suggestions to me.

I also would like to express my deeply thanks to my parents and my family for their never ending support and encouragement.

DEDICATION

To My wife Dan Lu, my son, Yiran Li, and my parents for their support, encouragement, and patience.

Chapter 1

Introduction

1.1 Introduction

Electromagnetic wave (EM) has been extensively used in communication and radar detection of targets. The usefulness of EM waves is in its ability to propagate long distances and to penetrate into non-metallic mediums. When electromagnetic waves propagate from one place to another, it will interact with the medium it passes through. Therefore it carries some information about that medium. This information is used to determine properties of a medium. Advantage of using EM waves to detect those properties is that it can provide a large data set with low-cost and can be used to measure in a remote area. With development of satellites, EM sensors become especially useful to provide global information about our living environment. These sensors are able to provide important information of weather forecast and environment changes.

In wave propagation, a common problem occurs in describing the scattering at the interface between two medium, such as the interfaces between air and ocean, air and soil, air and vegetation cover, etc... To some extent, all the interfaces will have some degree of roughness, which will complicate the scattering. Thus it is very desirable to understand how EM waves interact with rough surfaces. Furthermore, knowledge of

these wave interactions can then be used to retrieve information on characterizations describing the rough surfaces. Of interests are parameters such as ocean wave height, which is related to the wind speed and direction above ocean, and electric property of the medium such as soil moisture.

There are many studies being conducted on wave scattering from random rough surfaces, using both analytically and numerically techniques. The advantage of analytic theory is that there is a closed form mathematical expression, which can be used to obtain physical insight into the problem. The disadvantage of analytic theory is that its solution is approximate and only valid within some range. The advantage of using numerical methods is that a numerical solution can be obtained for many kinds of rough surfaces. However, the disadvantage of the numerical method it is usually a large-scale computational problem and therefore modern computer and fast computational methods are required. In the following sections, we will review the commonly used analytic theories and numerical methods, which have been developed over the years for wave scattering from random rough surfaces. Finally, we will give an overview of the fast computational methods developed in this dissertation.

1.2 Analytic Theory

Traditional analytic methods for wave scattering from random rough surfaces are the small perturbation method (SPM) and the Kirchhoff approach (KA) [Beckmann, 1963; Bass, 1979, Ishimaru, 1978; Ulaby, 1982; Tsang, 1985]. The small perturbation method assumes the rough surface has a small rms height and a small rms slope compared to the wavelength. It is first assumed that the scattered waves can be expressed as the sum of

plane waves propagating in various directions. Then, the incident field and scattered field are expanded in a series of a small quantity perturbation. This small quantity is usually proportional to the rms height as well as rms slope. The first order solution is found and used as the approximate solution. The range of validity of the SPM has been given by the Monte Carlo simulation results [Thorsos, 1989]. The Kirchhoff approach provides an approximation for the surface fields using the tangent plane approximation. The unknown surface fields at every point on the surface are approximated by the sum of incident fields and reflection fields at the point from the infinite plane parallel to the tangent plane at a point on the surface. Then an integral formulation can be devised to calculate the scattered fields. The KA approximation is valid when the radius of surface curvature at every point on the surface is much larger than the incident wavelength.

To extend the range of these analytic solutions, modern approximate approaches are also developed. These methods are phase perturbation method [Winebrenner, 1985a&b], modified second order Kirchhoff approximation [Ishimaru, 1990; Chen, 1990], small slope method [Voronovich, 1994; Irisov, 1994], and integral equation method [Fung, 1994]. These techniques can be reduced to the solution of SPM for small roughness surfaces and that of KA for the large-scale rough surface where the surface curvature is larger than the wavelength of the incident wave. The second order Kirchhoff approximation [Ishimaru, 1990; Chen, 1990] is developed for the wave scattering from 1-dimensional very rough surfaces. The theory is based on the first order and modified second order Kirchhoff approximations, which also includes shadowing effects of both angular and propagating field tapering. The theory can be applied to very rough surfaces and provide a physical explanation for the backscattering enhancement. The small slope approach [Voronovich, 1994; Irisov, 1994] is derived from the surface integral equation. It has been shown, due to the vertical translation symmetry, that all the surface fields are proportional to the factor of $\exp(-ik_z f(x, y))$, where k_z is the free space wavenumber in

z direction and $f(x, y)$ is the surface height. Thus this factor can be extracted from the unknown surface fields which leads to removing the height of the rough surface dependence. Moreover, the surface fields are then solved by expanding the fields in a small slope series. Another important achievement of small slope method is that Irisov [Irisov, 1997] showed that the small slope method and the small perturbation method give an identical formula for the thermal emission from random rough surfaces. That allows us to calculate thermal emission from random rough surfaces using the small perturbation method even for surface with large rms height but small rms slope.

1.3 Numerical Methods

Numerical simulations have been extensively used to study the wave scattering from random rough surfaces because of the analytic approaches limited range of validity. Monte-Carlo simulations of wave scattering from random surfaces were first used to prove the range of validity for the approximate analytic solutions. Also to provide a benchmark result for wave scattering from an arbitrary surface [Axline, 1978; Thorsos, 1988; Thorsos, 1989]. With the development of fast computational methods and the advance of modern computer, it is possible to demonstrate wave scattering from random rough surfaces with arbitrary profiles [Lou, 1990; Thorsos, 1991; Devayya, 1992; Kim, 1992; Tsang, 1993 a&b; Li, 1994; Chen, 1995; Tsang, 1995; Holliday, 1996; Michielssen, 1996; Kapp, 1996; Chan, 1998; Chou, 1998; Donhue, 1998; Holliday, 1998; Johnson, 1998; Lin, 1998; Tran, 1998; Li, 1999]. The most common method used in numerical simulation is the surface integral equation and its solution by the method of moments (MoM) [Harrington, 1968]. Conventional implementation of MoM produces a N by N full matrix equation and therefore requires $O(N^3)$ operations and $O(N^2)$ computer memory storage for Gaussian elimination method or other traditional solvers of matrix

equation, where N is the number of surface unknowns. This limits the simulations to small and moderate surface lengths with no more than a few thousand surface unknowns. To solve the practical problem, researchers turn to the finite element method (FEM) [Lou, 1990], the finite-difference time-domain method (FDTD) [Chan, 1991] and the iterative MoM [Thorsos, 1991; Devayya, 1992; Tsang, 1993 a&b; Tsang, 1995; Holliday, 1996; Michielssen, 1996; Kapp, 1996; Chan, 1998; Chou, 1998; Donhue, 1998; Holliday, 1998; Johnson, 1998; Lin, 1998; Tran, 1998; Li, 1999]. The finite element method has an advantage of resulting in a banded matrix equation but a discretization away from the rough surface boundary is required. This will increase the total number of unknown fields. The advantages of the FDTD approach are that matrix inversion of any kind has been completely eliminated, time-domain response is readily available and scattering intensities at different frequencies can be obtained simultaneously.

The iterative MoM uses iterative techniques to solve the matrix equations instead of traditional solvers. The CPU and memory requirements of iterative techniques are determined by the matrix-vector multiplication time and the number of iterations required. Mathematically, there are two classes of iterative procedures for solving matrix equation resulting from the standard moment method, stationary and non-stationary [West, 1999]. The stationary algorithms give the quickest convergence when applied to the well-conditioned systems that result in many circumstances, but the non-stationary techniques prove more robust in other more ill-conditioned situations [West, 1999]. Thus, most of the fast computational methods facilitate computation by either reducing the number of iteration with stationary approaches [Thorsos, 1991; Holliday, 1996; Kapp, 1996; Chou, 1998; Holliday, 1998; Tran, 1998] or reducing computational steps of the matrix-vector multiply with non-stationary techniques [Tsang, 1993 a&b; Tsang, 1995; Michielssen, 1996; Chan, 1998; Chou, 1998; Johnson, 1998; Lin, 1998; Tran, 1998; Li, 1999]. The Kirchhoff iterative approach [Thorsos, 1991], the forward-backward method (FBM) [Holliday, 1996; Holliday 1998], and the method of ordered multiple interactions

(MOMI) [Kapp, 1996] belong to the stationary techniques. In the Kirchhoff iterative approach [Thorsos, 1991; West, 1999], the integral equation is cast into the Fredholm equation of the second kind with the first term being the Kirchhoff approximation. The integral equation is then directly iterated leading to the Neumann expansion. The current is updated by applying the surface boundary conditions to the scattered field associated with the previous iteration's current. The FBM and MOMI [Holliday, 1996; Kapp, 1996; West, 1999] update current values as they become available, choosing the ordering of the updates to follow multiple scattering paths on the surface. These approaches have been proven quickly convergent in solving the systems that result from the magnetic field integral equations (MFIE). But the computational complexity is $O(N^2)$. The non-stationary iterative approaches are of conjugate-direction based procedures. Investigators focused on finding different ways to facilitate the matrix-vector multiplication. The method proposed by Michielssen [Michielssen, 1996], the fast multipole method (FMM) [Rokhlin, 1983; Rokhlin, 1990; Engheta, 1992; Coifman, 1993; Lu, 1993; Michielssen, 1994], and the banded-matrix iterative approach/canonical grid method (BMIA/CAG) [Tsang, 1993 a&b; Tsang, 1995; Chan, 1998; Johnson, 1998] are examples of those techniques. The algorithm proposed by Michielssen uses a recursive formula with a computational complexity of $O(N \log^2 N)$ for a quasi-planar surface. The banded-matrix iterative approach/canonical grid method (BMIA/CAG) permits the solution of large-scale random rough surface problems. The essence of the method consists of decomposing the interaction into near and non-near field interactions. The non-near field interactions are then expanded on a canonical grid of a horizontal surface by Taylor series so that the Fast Fourier Transform (FFT) can be applied. The computational complexity and the memory requirements for BMIA/CAG are $O(N\ log(N))$ and $O(N)$, respectively. The BMIA/CAG is also applied to dielectric rough surface [Chan, 1998]. The idea of the FMM is to reduce the number of scattering centers. If a scattering object is discretized into N segments and the interactions among them are computed directly, N^2 operations are required. Instead of calculating them directly, the FMM divides the segments into

groups according to the distances among them. The scattered field of each segment within a group is translated to group center by aggregation. The interactions among the elements of neighboring groups are calculated as before. For the interactions of the elements of non-near groups, only the interactions of group centers are calculated. Thus, the number of scattering centers is reduced. After each group center receives all the scattered fields from other non-near group centers, it redistributes these fields to the subscatterers belonging to the group. In this way, the single level FMM can reduce the computational complexity to $O(N^{1.5})$. For the multilevel FMM, the multi-sized groups are formed. The small sized group is used to calculate the interactions among the near elements and large sized group is used to calculate the interactions among far away elements. With the aid of interpolation and anterpolation, the computational complexity of the multilevel FMM is O(NlogN) for the arbitrary shape of surfaces.

There is also a tendency to use the stationary techniques with the speeding up of matrix vector multiply. Tran [Tran, 1998] has combined the MOMI with the BMIA/CAG and Admas [Admas, 1999] combined the MOMI with the two-level FMM. Zhou and Johnson [Chou, 1998] use the FBM with the spectrum acceleration of matrix vector multiply. Those methods take the advantage of quickest convergence of stationary techniques and also with the reduced computational complexity of matrix vector multiply. But as we mentioned before in the introduction, the stationary techniques have convergent problem for some cases. Thus the non-stationary techniques have more general applications.

However for 2-dimensional random rough surfaces of 3-dimensional scattering problem, there are only three iterative methods of the MoM have been applied. They are the Kirchhoff iteration approach [Tran, 1994 a&b], the sparse matrix canonical grid

method (SMCG) [Tsang, 1993; Tsang, 1994; Pak, 1995; Johnson, 1996; Pak, 1997], and the Fast Multipole Method (FMM) [Wagner, 1997; Jandhyala, 1998 a&b].

The Kirchhoff iteration approach has the convergence problem for the large incidence angle and surface with moderate rms slope [Wingham 1992] and is with the computational complexity of $O(N^2)$. The SMCG is the extension of the BMIA/CAG to the 2-dimensional rough surfaces therefore with the computational complexity of O(NlogN). Monte Carlo simulations of wave scattering from 2-D PEC rough surfaces based on the SMCG has been compared with the controlled millemeter wave experiments, the excellent agreement between them is obtained both for co-polarization and cross polarization. The results show the backscattering enhancement. There are several versions of the FMM. For the method used by Wagner [Wagner, 1997], the computational complexity is with O(NlogN). For the method used by Jandhyala [Jandhyala, 1998 a&b], the steepest descent path is chosen to calculate Green's function. Using the quasi-planar property of rough surface, the number of computational steps can be reduced to $O(N)$ with the multilevel FMM.

1.4 This Dissertation

The scattering of electromagnetic waves by lossy dielectric and random rough surfaces with large permittivity has broad applications because of the similarities to natural media. For example, the relative permittivity of wet soil can be as high as 17 + 2i and that of ocean can be as high as 40 + 40i at microwave frequency. In the application of MoM to rough surface scattering problem, a common implementation is to use a grid of 8 to 10 points per wavelength to discretize the surface. We shall call such a gridding a single coarse grid (SCG). However for lossy dielectric rough surfaces with high permittivity, two Green functions are required. One is the free-space Green function. The other is the

Green's function of the dielectric medium characterized by the wavenumber corresponding to the dielectric medium. Because that wavenumber can be much larger than the free-space wavenumber, there can be rapid spatial variations of the dielectric medium Green's function and surface fields. Thus a much denser discretization of the surface in the implementation of the method of moments (MOM) may be required. Depending on the dielectric constant, one may require a dense grid of 20 to 50 points per wavelength. We shall call such a gridding a single dense grid (SDG). The disadvantage of the SDG is that there is a large increase in CPU and required memory. To avoid this problem, the use of the impedance boundary condition has been common [Johnson, 1998] for problems with a large dielectric constant. The impedance boundary condition ignores the propagation through the dielectric medium. It is a good approximation for the wave scattering from metallic surfaces with very large permittivity because the wave in the medium can not propagate very far. However, it is difficult to validate the accuracy of the impedance boundary condition for the case of a moderate dielectric constant. For example, between 5 to 50, the accuracy of the impedance boundary condition is dubious. Also one of the applications of scattering by lossy dielectric surfaces is the calculation of emissivity for applications in passive microwave remote sensing. The calculation of emissivity has to be calculated to within 0.01, which corresponds to a brightness temperature difference of about 3 degrees. This means that the surface fields have to be calculated accurately.

To circumvent the problem, the physics-based two-grid (PBTG) method will be developed in this dissertation. It is an improvement over the past two alternatives in that it has the same accuracy as the single dense grid and yet has CPU comparable with that of the single coarse grid. In PBTG, two grids are used: a dense grid and a sparse grid. The sparse grid is that of the usual 8 to 10 points per wavelength. The dense grid ranges from 16 or higher number of points per wavelength depending on the relative permittivity of the lossy dielectric medium. The surface fields are calculated on the dense grid. In the formulation of the surface integral equations, two Green's functions are used. The free

space Green's function and the Green's function of the lossy dielectric medium. The PBTG is based on two observations: (1) the Green's function of the lossy dielectric is attenuative and therefore is space-limited, and (2) the Green's function of free-space is slowly varying on the dense grid compared with the medium Green's function and therefore is spatial frequency-limited. Because of Kramer-Kronig relation, a large real part of dielectric constant is usually associated with a large imaginary part at microwave frequency. The first observation results in a banded matrix for 1-D rough surface and a sparse matrix for 2-D rough surface for the Green's function of the lossy dielectric. When this Green's function acts on the surface fields on the dense grid, it will be just the product of a banded or sparse matrix and a column vector. The second observation allows us, when using the free-space Green's function to act on the surface fields of dense grid, to first average the values of surface unknowns on the dense grid and then place them on the coarse grid. Thus the PBTG speeds up the CPU and yet preserves the accuracy of the solution. The PBTG can be applied to both 1-D and 2-D rough surfaces and can be easily used in conjunction with the other fast methods such as the BMIA/CAG, the SMCG, and FMM.

In Chapter 2, we show that both surface fields and bistatic scattering coefficients computed by the single coarse grid show large differences with those computed by the single dense grid for 1-dimensional rough surfaces. It illustrates that the single dense gird is required. Then we describe the physics-based two-grid method (PBTG) for solving the problem of scattering of waves by lossy dielectric surfaces for TE wave incidence. The numerical results show that the PBTG can give the same accurate results as the single dense grid and only require the same CPU as the coarse grid.

In Chapter 3, we (i) combine the PBTG method with the BMIA/CAG method for improving of CPU and memory requirements, (ii) study bistatic scattering coefficients and emissivity for TM case and compare TM and TE results, and (iii) apply to low grazing scattering. We use it to treat a rough surface with a large surface length since the

edge effects have to be avoided for low-grazing angle incidence. The computational complexity and the memory requirements of non-near field interactions for present algorithm are O(N *log(N)*) and O(N), respectively, where N is the number of surface unknowns on the coarse grid. Using this approach, we illustrate numerical results of TE and TM wave scattering up to surface length of 500 wavelengths and 30,000 surface unknowns.

In Chapter 4, we (i) extend the PBTG to 2-D rough surface (3-D scattering problem). (ii) combine the PBTG method with the sparse matrix canonical grid method (SMCG) for improving CPU and memory requirements, (iii) study bistatic scattering coefficients and emissivity for wave scattering from 2-D dielectric rough surface with high permittivity. The approach is denoted as PBTG/SMCG. The computational complexity and the memory requirements for the algorithm are O(N_{scg} *log*(N_{scg})) and O(N_{scg}) for non-near field interactions and O(N_{sdg}) for near field interactions, respectively, where N_{scg} and N_{sdg} are the number of grid points on the coarse grid and dense grid, respectively. Using this approach, we illustrate numerical results of wave scattering from 2-Dimensional rough surface with permittivity as high as 17 + 2i. Also the numerical results of emissivity are compared with that of approximately analytic solutions of the small perturbation method (SPM). The SPM agrees with the small slope approximation of emissivity calculation [Irisov, 1997] for half space case. It is to be emphasized that to apply SPM, the slope has to be small. But for many natural surfaces, including band limited fractal surfaces [Mandelbrot, 1983], the slopes are not small. Thus comparisons of emissivities are made with that of the second order small perturbation method (SPM).

In Chapter 5, we simulate the thermal emission of wet soil with surface roughness using the PBTG/SMCG. The thermal emission of soils with rough surfaces is determined by the surface roughness, soil moisture, soil type, and physical temperature. The measurements of brightness temperature can provide information about soil moisture

content. Soil moisture is an important parameter that affects global climate change. The brightness temperatures of soils will be measured by the new generations of satellites such as ADEOS II and EOS-PM. In this chapter, we report and show extensive illustrations and tabulations of the results of emissivities for rough soils with Gaussian spectrum at L and C bands. The same physical roughness parameters are used at L and C bands. The results are important to better understand the effects of surface roughness on the microwave thermal emission of soils.

In Chapter 6, we combine the PBTG with the FMM. We use the steepest-descent path fast multipole method to compute the non-near field interactions on the coarse grid. Thus the computational complexity and memory requirement are proportional to the number of sampling points on the coarse grid for non-near field interactions and on the dense grid for the near field interactions. Using the proposed algorithm of the PBTG-FMM, we study the wave scattering from Gaussian and non-Gaussian random rough surfaces. A modified power-law spectrum is proposed to generate random rough surfaces. The feature of the proposed spectrum is that it can become Gaussian spectrum and the spectrum of exponential correlation function by properly choosing the power index and with fixed rms height and correlation length.

Chapter 2

Numerical Solution of Scattering of Waves by Lossy Dielectric Surfaces Using a Physics-Based Two-Grid Method

2.1 Introduction

The scattering of waves by lossy dielectric surfaces has broad applications. The method of moments (MOM) has been successfully applied to solve such problems [Axline, 1978; Nieto-Vesperinas, 1987; Rino, 1992]. In the two-media problem, two Green functions are required. One is the free-space medium Green function. The other is the Green's function of the dielectric medium with the wavenumber of the dielectric medium. Because that wavenumber can be much larger than the free-space wavenumber, a much denser discretization of the surface in the implementation of the method of moments (MOM) may be required. For example, the usual MOM requires a sampling of 10 points per wavelength. In a lossy dielectric problem, depending on the dielectric constant, one may require a dense grid of 20 to 50 points per wavelength. An increase of the number of unknowns by as many as five times requires much more CPU and memory. To avoid this problem, the use of the impedance boundary condition has been common [Mitzner, 1967] for problems with a large dielectric constant. However, it is difficult to validate the accuracy of the impedance boundary condition. Moreover, for the case of a moderate dielectric constant, for example, between 5 to 50, the accuracy of the impedance boundary condition is dubious.

In this paper, we use a physics-based two-grid method (PBTG) for solving the problem of scattering of waves by lossy dielectric surfaces. There are two grids used: a dense grid and a sparse grid. The sparse grid is that of the usual 10 points per wavelength. The dense grid is based on the wavenumber of the dielectric medium and can range from 20 to 50 points per wavelength. The method is based on the following two observations. (1) Green's function of the lossy dielectric is attenuative, and (2) Green's function of free-space is slowly varying on the dense grid. The first property gives a sparse matrix for the Green's function of the lossy dielectric. The second property allows us, when using the free-space Green's function on the dense grid, to first average the values of surface unknowns on the dense grid and then place them on the sparse grid . This method speeds up the CPU and yet preserves the accuracy of the solution. In this paper, the method is illustrated for scattering of waves by random surfaces. Such problems have attracted attention in microwave, optical and acoustic scattering [Axline, 1978; Nieto-Vesperinas, 1987; Rino, 1992]. Recently, we have developed a fast numerical method for such rough surface simulations. The method is known as the banded-matrix iterative approach and the banded-matrix iterative approach with canonical grid [Tsang, 1994a; Tsang, 1994b; Tsang, 1995]. The method decomposes into near and non-near field interaction. The non-near field interaction is translated into a canonical grid so that the Fast Fourier Transform (FFT) can be applied. Using this method, we have solved a rough surface problem with more than 25,000 surface unknowns which is a two-dimensional problem with a one-dimensional surface. However, such random rough surface simulations have not addressed the dense grid requirement for dielectric surfaces with a large dielectric constant which is dealt with in this paper.

In Section II, the formulation of the problem of the Transverse Electrical (TE) wave impinging upon a dielectric surface is given in terms of integral equations. The bistatic scattering coefficients and the emissivity are defined. The integral equations are converted into a matrix equation using a single grid discretization. In Section III, we show the numerical results using single grids. We compare the results of a single sparse

grid of 10 points per wavelength and a single dense grid of up to 40 points per wavelength. It is shown that the use of a dense grid is required, and that the use of a coarse grid can lead to erroneous results for the surface fields, the bistatic scattering coefficients and the emissivities of the surface. In Section IV, we develop the physics-based two-grid algorithm. In Section V, we illustrate the numerical results of the physics-based two-grid method using examples of scattering from soil surfaces. It is shown that the physics-based two-grid method can give accurate results over the single coarse grid and at a substantial savings of CPU time over the single dense grid.

2.2 Formulation and Single Grid Implementation

Consider a tapered plane wave, $\psi_{inc}(x, z)$, with time dependence, $\exp(-i\omega t)$, impinging upon a 1-D rough surface with a random height profile $z = f(x)$. It is tapered so that the illuminated rough surface can be confined to surface length L

$$\psi_{inc}(\bar{r}) = e^{i\bar{k}\cdot\bar{r}[1+W(\bar{r})]} e^{-(x+z\tan\theta_{inc})^2/g^2} \tag{2.1}$$

where $W(\bar{r}) = [2(x+z\tan\theta_{inc})^2/g^2 - 1]/(kg\cos\theta_{inc})^2$, $\bar{k} = k(\hat{x}\sin\theta_{inc} - \hat{z}\cos\theta_{nc})$, and g is the parameter that controls the tapering of the incident wave. We set the tapering parameter to be $g = L/4$. The scattered field from a dielectric rough surface can be solved using the coupled integral equation. Let ψ and ψ_1, denote respectively, the wave functions for the upper medium and lower medium. They satisfy the following surface integral equations:

$$\frac{1}{2}\psi(\bar{r}') - \int_s [\psi(\bar{r})\frac{\partial G(\bar{r},\bar{r}')}{\partial \hat{n}} - G(\bar{r},\bar{r}')\frac{\partial \psi(\bar{r})}{\partial \hat{n}}]ds = \psi_{inc}(\bar{r}') \tag{2.2}$$

$$\frac{1}{2}\psi_1(\bar{r}') + \int_s [\psi_1(\bar{r})\frac{\partial G_1(\bar{r},\bar{r}')}{\partial \hat{n}} - G_1(\bar{r},\bar{r}')\frac{\partial \psi_1(\bar{r})}{\partial \hat{n}}]ds = 0 \tag{2.3}$$

where $\int_S$ denotes a Cauchy integral and G and G_1 are the Green's function of the upper and lower medium. The wave functions Ψ and Ψ_1 are related through the boundary conditions on the surface S, namely,

$$\psi_1(\bar{r}) = \psi(\bar{r}) \qquad \text{and} \qquad \frac{\partial \psi_1(\bar{r})}{\partial \hat{n}} = \rho \frac{\partial \psi(\bar{r})}{\partial \hat{n}} \tag{2.4}$$

where ρ equals μ_1/μ and $\varepsilon_1/\varepsilon$ for TE and TM polarization, respectively. The integral equations can be converted into a matrix equation. We apply the boundary conditions in conjunction with the collocation method. Let the surface be discretized into a single grid of N points for x between -L/2 and L/2, so that $N\Delta x = L$. Thus the x_m points are at

$x_m = (m-0.5)\Delta x - \frac{L}{2}$, m=1, 2, ..., N.

$$\sum_{n=1}^{N} a_{mn} u(x_n) + \sum_{n=1}^{N} b_{mn} \psi(x_n) = \psi_{inc}(x_m) \tag{2.5}$$

$$\sum_{n=1}^{N} a_{mn}^{(1)} \rho u(x_n) + \sum_{n=1}^{N} b_{mn}^{(1)} \psi(x_n) = 0 \tag{2.6}$$

where $u(x) = \sqrt{1+[f'(x)]^2}\, \partial\psi / \partial n$. The matrix elements a_{mn}, b_{mn}, $a_{mn}^{(1)}$, and $b_{mn}^{(1)}$ are given below:

for $m \neq n$

$$a_{mn} = \Delta x \frac{i}{4} H_0^{(1)}(k r_{mn}) \tag{2.7}$$

$$b_{mn} = -\Delta x \frac{ik}{4} \frac{f'(x_n)(x_n - x_m) - [f(x_n) - f(x_m)]}{r_{mn}} H_1^{(1)}(k r_{mn}) \tag{2.8}$$

$$a_{mn}^{(1)} = -\Delta x \frac{i}{4} H_0^{(1)}(k_1 r_{mn}) \tag{2.9}$$

$$b_{mn}^{(1)} = \Delta x \frac{ik_1}{4} \frac{f'(x_n)(x_n - x_m) - [f(x_n) - f(x_m)]}{r_{mn}} H_1^{(1)}(k_1 r_{mn}) \tag{2.10}$$

where $r_{mn} = \sqrt{(x_n - x_m)^2 + [f(x_n) - f(x_m)]^2}$ and k and k_1 are the wavenumbers in the upper region and lower region, respectively.

for m = n

$$a_{mm} = \Delta x \frac{i}{4} H_0^{(1)}[k\Delta x \gamma_m /(2e)] \tag{2.11}$$

$$b_{mn} = \frac{1}{2} - \frac{f''(x_m)}{4\pi} \frac{\Delta x}{\gamma_m^2} \tag{2.12}$$

$$a_{mm}^{(1)} = -\Delta x \frac{i}{4} H_0^{(1)}[k_1 \Delta x \gamma_m /(2e)] \tag{2.13}$$

$$b_{mm}^{(1)} = \frac{1}{2} + \frac{f''(x_m)}{4\pi} \frac{\Delta x}{\gamma_m^2} \tag{2.14}$$

where $\gamma_m = \sqrt{1 + [f'(x_m)]^2}$, e = 2.71828183, $f'(x_m)$ and $f''(x_m)$ represent the first and second derivative of f(x) evaluated at x_m, respectively. The accuracy of the solution depends on the sampling frequency. The matrix equation in (5) and (6) is in the form of a single grid. Let n_d = N/L be the number of points per wavelength. Usually a sample frequency of n_d = 10 is taken meaning that we have 10 points per wavelength. We shall call such a sampling a coarse grid. If the sampling is two or more times denser than the coarse grid, we shall call it a dense grid. The dense grid that we use ranges from n_d = 20 to n_d = 50. As we shall show in the next section, the dense grid becomes necessary when the lower medium has a large dielectric constant.

2.3 Bistatic Scattering Coefficient and Emissivity

After the matrix equation is solved, the surface field can be calculated. The bistatic scattering coefficient $\sigma(\theta_s, \theta_i)$ is a measure of the scattering from incident angle θ_i into scattered angle θ_s. It is defined by:

$$\sigma(\theta_s,\theta_i)=\frac{\left|\int_{-\infty}^{\infty} dx[ik\psi(x)(\frac{df}{dx}\sin\theta_s-\cos\theta_s)-u(x)]\exp(-ik\alpha(\theta_s,x))\right|^2}{8\pi g\sqrt{\frac{\pi}{2}}k\cos\theta_i(1-\frac{1+2\tan^2\theta_i}{2k^2g^2\cos^2\theta_i})} \tag{2.15}$$

In (15), $\alpha(\theta_s, x) = \sin\theta_s\, x + \cos\theta_s\, f(x)$. The bistatic scattering coefficient has been normalized by the incident power impinging upon the rough surface. For scattering by a perfect conducting surface, the energy conservation test is that $\int\sigma(\theta_s,\theta_i)d\theta_s=1$. For scattering by a dielectric surface, the emissivity of the rough surface at incident angle θ_i is

$$e(\theta_i)=1-\int d\theta_s\sigma(\theta_s,\theta_i) \tag{2.16}$$

Thus emissivity is a measure of energy conservation in a scattering calculation. Because of reciprocity, emissivity is the same as absorptivity which is the amount of power absorbed by the dielectric in a scattering problem. In passive remote sensing, the brightness temperature T_B of the medium is measured at incident angle θ_i. The brightness temperature is

$$T_B(\theta_i)=e(\theta_i)T \tag{2.17}$$

where T is the physical temperature of the medium in Kelvin degrees. The brightness temperature can be measured to an accuracy of 1 degree K. For the case of $T = 300$K, an error of calculation in the emissivity of 0.03 gives an error of 9K in brightness temperature which is not acceptabe. It is important that the scattering calculation obey energy conservation to within 0.01, so that the error in brightness temperature is limited to 3 degrees K.

2.4 Numerical Results Illustrating the Need for a Dense Grid

In this section, we illustrate the numerical results of rough surface scattering with a dielectric constant of 25+i using a single grid. Simulations are based on Gaussian random rough surfaces with Gaussian correlation functions. If $n_d = 10$, we call it a coarse grid, and for $n_d \geq 20$, we call it a dense grid. In Figures 1a and 1b, we compare respectively the results of the real and imaginary parts of a surface field of scattering by a single realization of rough surface for rms height $h = 0.5\lambda$, correlation length $\ell = 0.6\lambda$, incident angle $\theta_I = 30^o$, and surface length $L = 30\ \lambda$, where λ is the wavelength. We compare the cases of using n_d=10, 30, and 40 points per wavelength. We note that the results of n_d=30 and n_d=40 are very close to each other. The results of n_d=10 are quite different. Obviously, the results based on n_d=10 points per wavelength are not accurate enough. In Table I, we compare the emissivities calculated for using one realization for each of the different n_d. We found that for n_d=10, the emissivity is 0.5316, while for n_d=40, the emissivity is 0.6257. The difference of emissivities of 0.0941 leads to the difference of 300K x 0.0941 = 28.23K in brightness temperature. The cases of $n_d = 30$ and $n_d = 40$ are very close to each other. These examples illustrate the need of using a dense grid for a problem of moderate to large permittivity. In Table I, we also compare the CPU time. Although 40 points per wavelength provides enough accuracy, the CPU time is many times higher than 10 points per wavelength. The solutions of the matrix equation of all these cases are computed using the banded-matrix iterative approach (BMIA) [Tsang, 1994a; Tsang, 1994b; Tsang, 1995]. In Figure 2, we compare the bistatic scattering coefficients averaged over 20 realizations. We see large differences between $n_d = 10$ and $n_d = 30$. Therefore if a single grid discretiztion is used, the grid has to be dense to provide the accuracy.

2.5 Physics-Based Two-Grid Method

Although a dense grid can give accurate numerical results, there can be a large increase in CPU and memory requirements as the number of unknowns is 2 to 5 times that of the coarse grid. In this section, we describe the physics-based two-grid method which was developed to reduce CPU and memory requirements.

Note that the lower medium is lossy, so the relative permittivity for the lower medium can be written as:

$$\varepsilon_1 = \varepsilon_1'(1+iLT) \tag{2.18}$$

where LT stands for loss tangent. Let

$$n_1 = \mathrm{int}eger(\sqrt{\frac{\varepsilon_1'}{\varepsilon}}) \tag{2.19}$$

In the physics-based two-grid method, we use two grid samplings n_{dc} (coarse grid) and n_{dg} (dense grid).

We assume a dense grid with N_{dg} points and a coarse grid with N points.

$$N_{dg} = n_{dg}\frac{L}{\lambda} \tag{2.20}$$

$$N = n_{dc}\frac{L}{\lambda} \tag{2.21}$$

Usually $n_{dc} = 10$ and $n_{dg} = 10n_1$

We first re-write equations (5) and (6) using the dense grid.

$$\sum_{n=1}^{N_{dg}} a_{mn}u(x_n) + \sum_{n=1}^{N_{dg}} b_{mn}\psi(x_n) = \psi_{inc}(x_m) \tag{2.22}$$

$$\sum_{n=1}^{N_{dg}} a_{mn}^{(1)}\rho u(x_n) + \sum_{n=1}^{N_{dg}} b_{mn}^{(1)}\psi(x_n) = 0 \tag{2.23}$$

The Roman numeral subscripts m,n denote indexing with the dense grid. The matrix elements a_{mn}, b_{mn} represent Green's function of the upper medium while $a_{mn}^{(1)}, b_{mn}^{(1)}$ represents Green's function of the lower medium of the lossy dielectric. We make the following three observations.

1) For non-near field interaction, Green's function for the upper medium is slowly varying compared with Green's function of the lossy dielectric lower medium. Thus when performing matrix and column vector multiplication on the dense grid as indicated in (22), Green's function of the upper medium is essentially constant over an interval of n_1 points. Thus we can write

$$\sum_{l=-\frac{n_1-1}{2}}^{\frac{n_1-1}{2}} a_{m(n+l)} u_{n+l} \approx a_{mn} \sum_{l=-\frac{n_1-1}{2}}^{\frac{n_1-1}{2}} u_{n+l} = n_1 a_{mn} \left(\frac{1}{n_1} \sum_{l=-\frac{n_1-1}{2}}^{\frac{n_1-1}{2}} u_{n+l}\right) \tag{2.24}$$

2) The slowly varying nature of Green's function of the upper medium only applies to non-near field interaction. For near field interaction, Green's functions G and G_1 have roughly the same rate of variation. Thus we need to separate out a distance, say 1λ, outside of which G_1 is much more rapidly varying than G.

3) The Green's function in the lower region is heavily attenuative. Let k_1" be the imaginary part of k_1. If $k_1 "r > C$, where C is a constant, then the field interaction between the mth and the nth point is vanishingly small. We can define a distance limit as dictated by dissipative loss:

$$r_\ell = \frac{C}{k_1"} \tag{2.25}$$

outside of which the lower medium Green's function can be set equal to zero. The constant C varies from case to case.

Based on the observations above, we calculate the left-hand sides of (22) and (23) as follows.

a) We first approximate

$$a_{mn}^{(1)} \approx \tilde{a}_{mn}^{(1)} \tag{2.26}$$

$$b_{mn}^{(1)} \approx \tilde{b}_{mn}^{(1)} \tag{2.27}$$

where $\tilde{a}_{mn}^{(1)} = a_{mn}^{(1)}$, $\tilde{b}_{mn}^{(1)} = b_{mn}^{(1)}$ for $r_{mn} \le r_\ell$ and $\tilde{a}_{mn}^{(1)} = \tilde{b}_{mn}^{(1)} = 0.0$ for $r_{mn} > r_\ell$, where r_{mn} is the distance between the mth point and the nth point on the dense grid. Thus $\tilde{a}_{mn}^{(1)}$ and $\tilde{b}_{mn}^{(1)}$ are banded matrices and Equation (23) becomes

$$\sum_{n=1}^{N_{de}} \tilde{a}_{mn}^{(1)} \rho u(x_n) + \sum_{n=1}^{N_{de}} \tilde{b}_{mn}^{(1)} \psi(x_n) = 0 \tag{2.28}$$

b) Next we decompose the upper medium Green's function into near field and non-near field interactions

$$\sum_{n=1}^{N_{de}} a_{mn} u(x_n) = \sum_{n=1}^{N_{de}} a_{mn}^{s} u_n + \sum_{n=1}^{N_{de}} a_{mn}^{ns} u_n \tag{2.29}$$

$$\sum_{n=1}^{N_{de}} b_{mn} \psi(x_n) = \sum_{n=1}^{N_{de}} b_{mn}^{s} \psi_n + \sum_{n=1}^{N_{de}} b_{mn}^{ns} \psi_n \tag{2.30}$$

where $a_{mn}^{s} = a_{mn}$, $b_{mn}^{s} = b_{mn}$ for $r_{mn} \le r_f$ and $a_{mn}^{s} = b_{mn}^{s} = 0$ for $r_{mn} > r_f$. Also $a_{mn}^{ns} = a_{mn}$, $b_{mn}^{ns} = b_{mn}$ for $r_{mn} > r_f$ and $a_{mn}^{ns} = b_{mn}^{ns} = 0$ for $r_{mn} \le r_f$. Here we call r_f to be the distance outside which the Green's function of the lower medium is fast varying compared with that of free space Green's function. Outside r_f, the upper medium Green's function is slowly varying on the dense grid.

c) We apply a coarse grid of 10 points per wavelength to the non-near field interaction of the upper medium Green's function corresponding to matrix elements of a_{mn}^{ns} and b_{mn}^{ns}. Let α and β be used to denote the coarse grid index. The coarse grid has surface unknowns $\tilde{u}$ and $\tilde{\psi}$, which are averages of the dense grid surface unknowns. Thus if $\bar{r}_\beta$ is centered in the middle of the n_1 dense grid points of n+1, n+2, ..., n+n_1, we have

$$\tilde{u}_\beta = \frac{u_{n+1} + u_{n+2} + \cdots + u_{n+n1}}{n_1} \tag{2.31}$$

$$\tilde{\psi}_\beta = \frac{\psi_{n+1} + \psi_{n+2} + \cdots + \psi_{n+n1}}{n_1} \tag{2.32}$$

For the coarse grid, we calculate Green's function of the upper medium at the coarse grid value which we represent by $\tilde{a}_{\alpha\beta}$ and $\tilde{b}_{\alpha\beta}$.

$$\tilde{a}_{\alpha\beta} = \Delta\tilde{x} \frac{i}{4} H_0^{(1)}(k r_{\alpha\beta}) \tag{2.33}$$

$$\tilde{b}_{\alpha\beta} = -\Delta\tilde{x}\frac{ik}{4}\frac{f'(x_\beta)(x_\beta - x_\alpha) - [f(x_\beta) - f(x_\alpha)]}{r_{\alpha\beta}} H_1^{(1)}(kr_{\alpha\beta}) \tag{2.34}$$

for $r_{\alpha\beta} > r_f$ and $\tilde{a}_{\alpha\beta} = \tilde{b}_{\alpha\beta} = 0.0$ for $r_{\alpha\beta} \le r_f$. If $\Delta\tilde{x}$ is the coarse grid sampling, then $\Delta\tilde{x} = n_1 \Delta x$, where Δx is the dense grid sampling.

Thus Equation (22) becomes

$$[\sum_{n=1}^{N_{dg}} a_{mn}^s u(x_n) + \sum_{n=1}^{N_{dg}} b_{mn}^s \psi(x_n)] + [\sum_{\beta=1}^{N} \tilde{a}_{\alpha\beta}\tilde{u}(x_\beta) + \sum_{\beta=1}^{N} \tilde{b}_{\alpha\beta}\tilde{\psi}(x_\beta)]_{\text{int } p} = \psi_{inc}(x_m) \tag{2.35}$$

Note in Equation (35) that $\sum_{n=1}^{N_{dg}} a_{mn}^s u(x_n)$ includes N_{dg} values of m=1, 2, •••, N_{dg}, while $\sum_{\beta=1}^{N} \tilde{a}_{\alpha\beta}\tilde{u}(x_\beta)$ only has N values of α=1, 2, •••, N. Thus we first compute $\sum_{\beta=1}^{N} \tilde{a}_{\alpha\beta}\tilde{u}(x_\beta)$. Then we use linear interpolation to find N_{dg} on the dense grid. In Equation (35), we use subscript intp to represent that interpolation. Finally, we use BMIA to solve matrix Equation (28) and (35) instead of (22) and (23).

The usual memory requirement of method of moments is the square of the number of unknowns. However, most of the matrix elements belong to non-near field interactions. PBTG has substantial savings in CPU time. For the upper medium free space Green's function, PBTG, as indicated in Equation (35) only stores the non-near field interaction on the coarse grid. For the lower medium Green's function of the lossy dielectric, the PBTG takes into account the lossy nature of the dielectric and needs only to store the banded matrix.

2.6. Numerical Results and CPU Comparisons

In this section, we show the numerical results based on the physics-based two-grid method and compare the results and CPU time with that of the single grid of a dense grid. We show that the PBTG is as accurate as using the dense grid and yet is many times

faster than the dense grid. In Figures 3a and 3b, we compare respectively the results of the real and imaginary parts of surface field of scattering by a single realization of rough surface using a single grid and PBTG. For the single grid results, we use $n_d = 40$ which is a dense grid and gives results of sufficient accuracy. For PBTG, the two grids used have $n_{dc} = 10$ and $n_{dg} = 40$. For PBTG, we also use two different r_f of 1λ and 4λ. The case of $r_f = 4\lambda$ is almost identical to the single dense grid result. In Table II, we compare the emissivities calculated and the CPU required. The emissivity calculated by PBTG is also very close to that of single dense grid. The CPU comparison shows that it is a factor of 2 less than the single dense grid for the case of surface length $L = 30\lambda$. The CPU advantages get better for long surfaces. This is because the dense grid is still used for distance separations less than r_f, and $r_f = 4\lambda$ is substantial compared with the surface length of $L = 30\lambda$. To show the computational advantage for longer surfaces, we show in Figure 5 the results of a bistatic scattering coefficient of a surface length of $L = 120\lambda$. For the single grid, we use the coarse grid of the usual n_d=10 points per wavelength, and for the PBTG, we use the two grids of $n_{dc} = 10$ and $n_{dg} = 30$. The single coarse grid is not accurate as shown in the results in Figure 5. In Table II, we show the comparisons of CPU. We note that the ratio of CPU is 9545.4/6586.6=1.45 This means that PBTG provides the accuracy with only a 45% percent increase in CPU over the inaccurate single coarse grid. On the other hand, the estimated CPU for a single dense grid of $n_d = 30$ corresponding to 7200 surface unknowns is about 9 times more. This single dense grid of $n_d = 30$ is not computed because of the large memory requirements. On the other hand, the PBTG of $n_{dc} = 10$ and $n_{dg} = 30$ can be performed as indicated because PBTG also has substantial savings in memory.

2.7 Conclusions

In this paper, we have developed and applied the PBTG method to address the dense grid requirement for dielectric surfaces with a large lossy dielectric constant. The method saves both CPU and memory and provides the required accuracy. We are presently combining it with the canonical grid method and extending the approach to 3-dimensional problems.

Table 2.1: Comparison of CPU and emissivities for one realization based on single grid method with various number of n_d

Method	Surface length (λ)	n_d	# of surface unknowns	CPU time (s)	Emissivity
SG*	30	10	600	396.9	0.5316
SG	30	20	1200	1287.1	0.5813
SG	30	30	1800	2428.1	0.6172
SG	30	40	2400	4616.1	0.6257

SG = Single Grid

Table 2.2: Comparison of CPU and emissivities based on PBTG and single grid method with various values of n_d and r_f

Method	# of realization	Surface length(λ)	n_d	# of surface unknowns	r_f	CPU time(s)	Emissivity
SG	1	30	40	2400		4,616.1	0.6257
PBTG	1	30	10 and 40	2400	1.0	1,371.2	0.6418
PBTG	1	30	10 and 40	2400	2.0	1,748.2	0.6314
PBTG	1	30	10 and 40	2400	3.0	2,253.1	0.6203
PBTG	1	30	10 and 40	2400	4.0	2,430.1	0.6280
SG	1	120	10	2400		6,586.6	
SG	1	120	30	7200		60,000*	
PBTG	1	120	10 and 30	7200	1.0	9,545.4	
SG	20	30	10	600			0.4827
SG	20	30	30	1800			0.6041
PBTG	20	30	10 and 30	1800	2.0		0.5914

*estimated values only

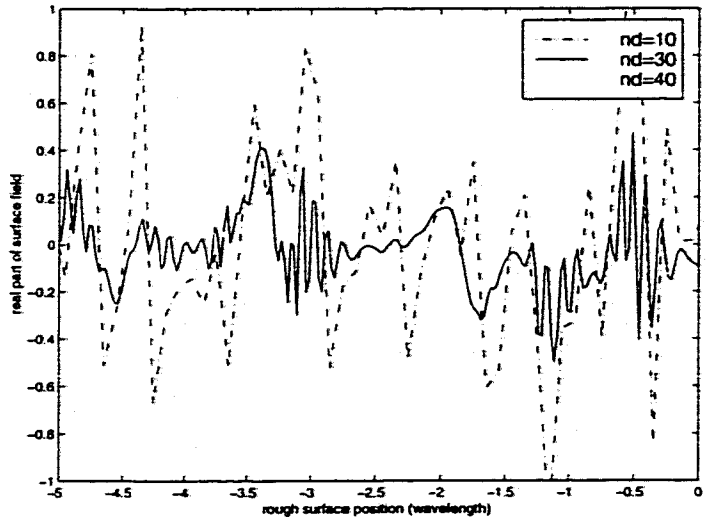

(a)

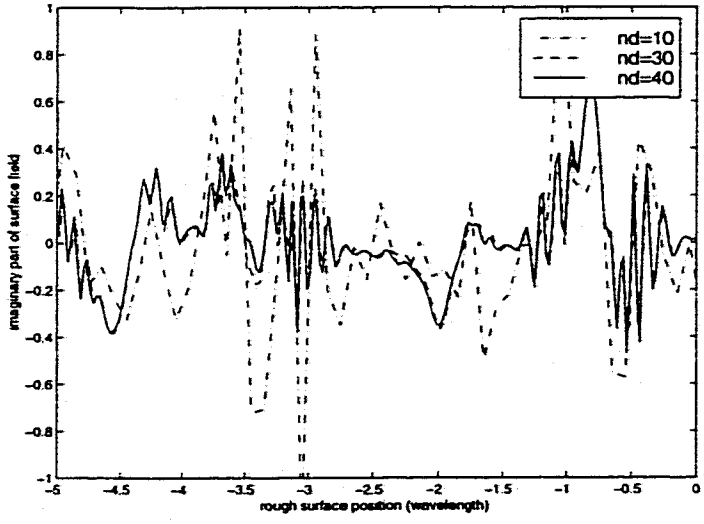

(b)

Figure 2.1. Comparison of surface fields for different n_d, (number of sampling points per wavelength) for one realization with h=0.5λ, $\ell = 0.6\lambda$, θ_i=30°, L=30λ, ε_r=25+i, g=L/4, (a) real part of surface field (b) imaginary part of surface field.

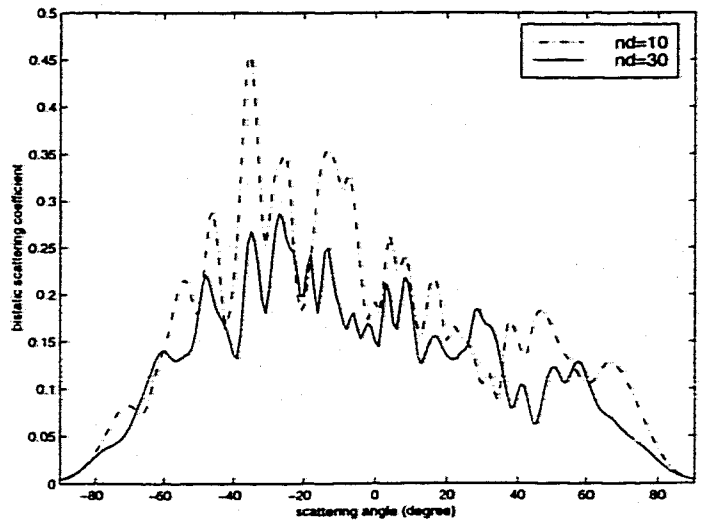

Figure 2.2. Comparison of bistatic scattering coefficient for different n_d, (number of sampling points per wavelength) for 20 realizations with h=0.5λ, $\ell = 0.6\lambda$, θ_i=30°, L=30λ, ε_r=25+i, g=L/4.

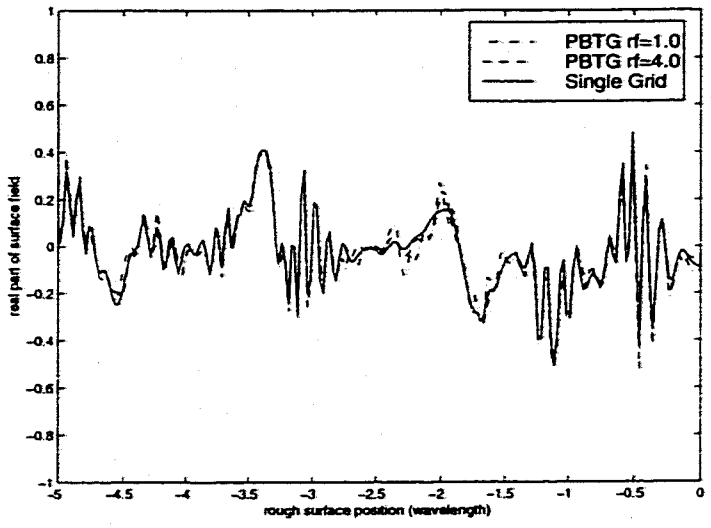

(a)

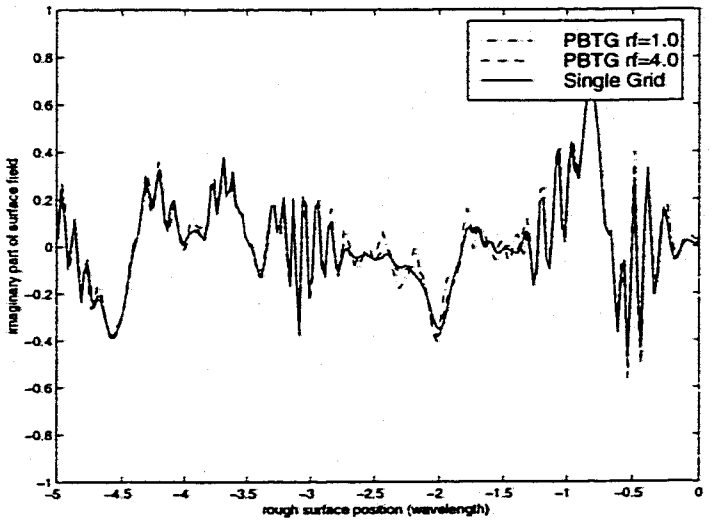

(b)

Figure 2.3. Comparison of surface field between SINGLE GRID method and physics based two grid method PBTG for one realization with h=0.5λ, $\ell = 0.6\lambda$, θ_i=30°, L=30λ, ε_r=25+i, g=Ltw/4. For the single grid $n_d = 40$, For PBTG, $n_{dc} = 10$, $n_{dg} = 40$ (a) real part of surface field (b) imaginary part of surface field.

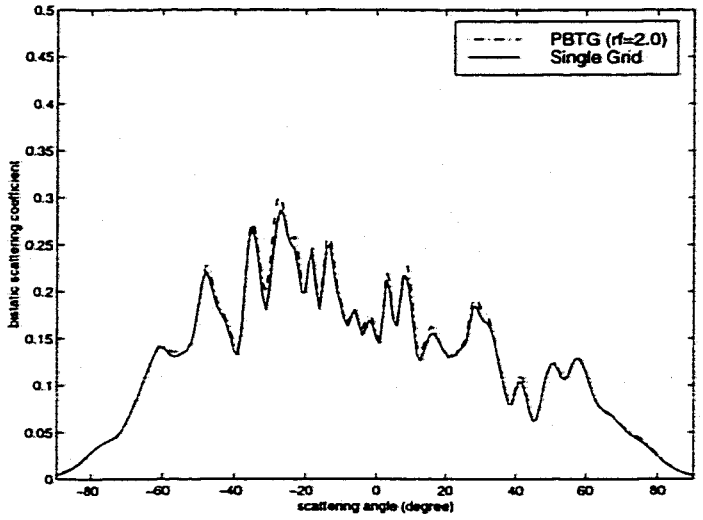

Figure 2.4. Comparison of bistatic scattering coefficient between SINGLE GRID and PBTG for 20 realizations with h=0.5λ, ℓ=0.6λ, θ_i=30°, L =30.0λ, ε_r=25.0+i, g=L/4. For the single grid $n_d = 30$, For PBTG, $n_{dc} = 10$, $n_{dg} = 30$.

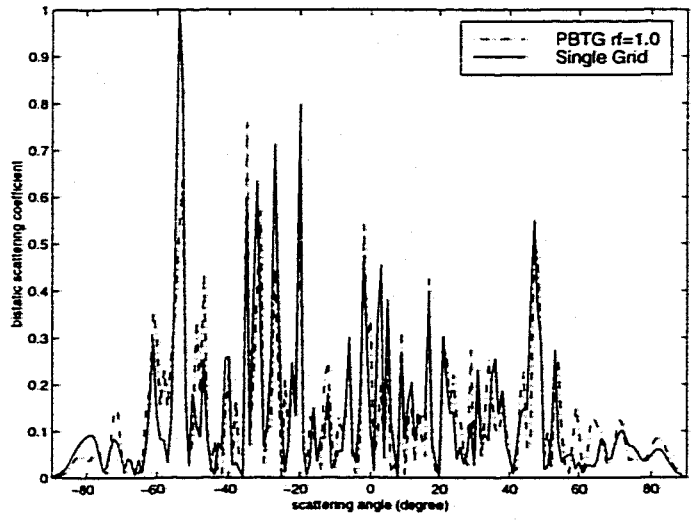

Figure 2.5. Comparison of bistatic scattering coefficient between SINGLE GRID and PBTG for one realization with h=0.5λ, ℓ=0.6λ, θ_i=30°, L =120λ, ε_r=25.0+i, g=L/4. For the single grid of $n_d = 10$, For PBTG, $n_{dc} = 10$, $n_{dg} = 30$.

Chapter 3

Monte-Carlo Simulations of Wave Scattering from Lossy Dielectric Random Rough Surfaces Using the Physics-Based Two-grid Method and the Canonical Grid Method

3.1 Introduction

The scattering of waves from random rough surfaces has been a topic of continued study for many years because of its broad applications. Recently, Monte-Carlo simulations of the wave scattering problem have been a common approach because of the advent of modern computers and the development of fast numerical methods. Monte Carlo simulations performed by all authors require at least 20 wavelengths because the surface must have enough valleys and peaks to be a legitimate statistical sample (realization) in random rough surface simulations. The most common method that has been used in numerical simulations is the integral equation method [Axline, 1978; Maradudin, 1990; Thorsos, 1988; Chen, 1990; Nieto-Vesperinas, 1987; Rino, 1992; Kim, 1992; Maystre, 1991; Chen, 1995]. Conventional implementation of the integral equation method requires an $O(N^3)$ operation and an $O(N^2)$ computer memory storage. Therefore, the simulation has been limited to small to moderate surface length with no more than a few thousand surface unknowns. Over the past few years, there are several fast numerical methods that have been developed [Donohue, 1998; Jandhyala, 1998; Michielssen, 1996; Tsang, 1993a; Tsang, 1993d; Tsang, 1994a; Li, 1994; Tsang, 1995; Chan, 1993; Chan, 1998]. One of them is the banded-matrix iterative approach/canonical grid method (BMIA/CAG) that permits the solution of large-scale random rough surface problems

[Tsang, 1993a; Tsang, 1993d; Tsang, 1994a; Li, 1994; Tsang, 1995; Chan, 1993; Chan, 1998]. The essence of the method consists of decomposing the interaction into near and non-near field interactions. The non-near field interactions are then expanded on a canonical grid of a horizontal surface so that the Fast Fourier Transform (FFT) can be applied. The computational complexity and the memory requirements for BMIA/CAG are $O(N\ log(N))$ and $O(N)$, respectively. Another method for the 1-D case is by Michielssen's etal [1996], which has computational complexity of $O(N \log^2 N)$. For the case of PEC, the paper by Michielssen etal reports a CPU of 8 to 12 minutes for 4000 unknowns while the BMIA/CAG method as reported in Table II of reference 17 reports a CPU of 20 minutes for 8000 unknowns. Thus the two methods are comparable in CPU time for the PEC case. The BMIA/CAG is also applied to dielectric rough surface [Chan, 1998]. The experience with dielectric surface is that the CPU increases much more than the PEC case.

In the application of method of moments to rough surface scattering problem, a common implementation is to use a grid of 10 points per wavelength to discretize the surface. We shall call such a gridding a single coarse grid (SCG). But, to study scattering by lossy dielectric rough surfaces with high permittivity, there can be rapid spatial variation of surface fields. Two alternatives were used. The first alternative is to use impedance boundary condition [Johnson, 1998]. The disadvantage of this alternative is that an approximation is used in the problem without any error estimate. The second alternative is to use a dense grid with a large number of points (say more than 20 points) per wavelength. We shall call such a gridding a single dense grid (SDG). The disadvantage of this second alternative is that there is a large increase in CPU and required memory. The physics-based two-grid (PBTG) method [Tsang, 1997] is an improvement over these two alternatives in that it has the same accuracy as the single dense grid and yet has CPU comparable with that of the single coarse grid. Another improvement is that the PBTG method can calculate the emissivity accurately because the method obeys energy conservation accurately. In PBTG, two grids were used: a

dense grid and a sparse grid. The sparse grid is that of the usual 10 points per wavelength. The dense grid ranges from 20 to higher number points per wavelength depending on the relative permittivity of the lossy dielectric medium. The key point of PBTG is based on the following two observations. (1) Green's function of the lossy dielectric is attenuative, and (2) Green's function of free-space is slowly varying on the dense grid. Because of Kramer-Kronig relation, a large real part of dielectric constant is usually associated with a large imaginary part. The first property of lossy dielectric gives a banded submatrix for the Green's function of the lossy dielectric. The second property allows us, when using the free-space Green's function on the dense grid, to first average the values of surface unknowns on the dense grid and then place them on the sparse grid. PBTG speeds up the CPU and yet preserves the accuracy of the solution. It needs to be mentioned the PBTG is different from multigrid method. The multigrid method [Donohue, 1998; Brigs, 1987] tries to facilitate the convergence of iteration in iterative techniques. It entails discretization of the structure into various grid sizes. The coarse grid corresponds to the low frequency portion of the solution while the fine grid corresponds to that of the high frequency solution. An iterative solution is obtained for each level of discretization and the solutions are interpolated from the coarse grid to the fine grid. The solution is first obtained in the coarse grid and then one moves to the next level of fine grid. Once the iterative solution is obtained in the fine grid, then one has to go back to the coarse grid to refine the solution. The present method that we have is based on scattering physics. The purpose of PBTG is to speed up the matrix-vector product of two Green's functions convolving with the surface fields on the dense grid.

In the previous paper [Tsang, 1997], we developed PBTG for TE case. In this paper, we (i) combine the PBTG method with the BMIA/CAG method for improving of CPU and memory requirements, (ii) study bistatic scattering coefficients and emissivity for TM case and compare TM and TE results, and (iii) apply to low grazing scattering. We use it to treat a rough surface with a large surface length since the edge effects have to be avoided for low-grazing angle incidence [Tsang, 1995; Johnson, 1998]. We use two grids, a dense

grid and a coarse grid. The interaction is divided into (1) very near field of less than 1 wavelength, (2) near field of between 1 wavelength and r_d wavelengths, and (3) non-near field beyond r_d wavelengths. In numerical simulations, r_d is an adjustable parameter so that BMIA/CAG can be used to solve the equations. In this paper, r_d is fixed at 10 wavelengths. For very near-field interactions, we use a dense grid which is represented by four banded submatrics. For near-field and non-near field interactions, the free space Green's function is slowly varying on the dense grid. We can first average the fields on the dense grid to get fields on the sparse grid. The non-near field interactions are also expanded on a canonical grid of a horizontal surface so that the fast Fourier Transform (FFT) can be applied. In the lower medium, non-near field interactions were neglected because of lossy properties of the lower medium. The approach is denoted as PBTG-BMIA/CAG. The computational complexity and the memory requirements for present algorithm are $O(N\ log(N))$ and $O(N)$, respectively, where N is the number of surface unknowns on the coarse grid. Using this approach, we illustrate numerical results of TE and TM wave scattering up to surface length of 500 wavelengths and 30,000 surface unknowns. Note that all the surface unknowns on the dense grid are calculated by this method. The salient features of the numerical results are

(1) A single coarse grid (SCG) has poorer accuracy for TM case than for TE case.

(2) PBTG-BMIA/CAG speeds up CPU and preserves the accuracy. It has accuracy comparable to single dense grid and yet has CPU comparable to single coarse grid. It also gives surface fields on the dense grid and can give accurate results of the surface fields when the surface fields have rapid spatial variation.

(3) PBTG-BMIA/CAG gives accurate results for emissivity calculations and also for low grazing backscattering problems (LBGA).

Thus PBTG-BMIA/CAG produces accurate results on the dense grid at CPU comparable with that of single coarse grid.

In Section II, the formulation of the problem of TE and TM wave impinging upon a dielectric surface is given in terms of integral equations. Then the integral equations are converted into a matrix equation using a single grid discretization. In Section III, we implement the physics-based two-grid algorithm and combine it with the BMIA/CAG method. In section IV, the bistatic scattering coefficients and the emissivity are defined. In Section V, the numerical results are illustrated.

3.2Formulation and Single Grid Implementation

Consider a tapered plane wave, $\psi_{inc}(x, z)$, with a time dependence of $e^{-i\omega t}$, impinging upon a 1-D rough surface with a random height profile z = f (x). It is tapered so that the illuminated rough surface can be confined to surface length L [Chan, 1998]. The incident wave is

$$\psi_{inc}(x, f(x)) = \frac{g}{2\sqrt{\pi}} \int_{-\infty}^{\infty} dk_x e^{i(k_x x - k_z z)} e^{\frac{(k_x - k_{ix})^2 g^2}{4}} \tag{3.1}$$

where $k_{ix} = k \sin \theta_i$, $k_z^2 = k^2 - k_x^2$ with a proper choice of the branch cut, k is the wavenumber of the free space, and g is the parameter that controls the tapering of the incident wave. Let ψ and ψ_1, denote respectively, the wave functions for the upper medium and lower medium. They satisfy the following surface integral equations [Tsang, 1985]

$$\frac{1}{2}\psi(\bar{r}') - \int_s [\psi(\bar{r}) \frac{\partial G(\bar{r}, \bar{r}')}{\partial \hat{n}} - G(\bar{r}, \bar{r}') \frac{\partial \psi(\bar{r})}{\partial \hat{n}}] ds = \psi_{inc}(\bar{r}') \tag{3.2}$$

$$\frac{1}{2}\psi_1(\bar{r}') + \int_s [\psi_1(\bar{r}) \frac{\partial G_1(\bar{r}, \bar{r}')}{\partial \hat{n}} - G_1(\bar{r}, \bar{r}') \frac{\partial \psi_1(\bar{r})}{\partial \hat{n}}] ds = 0 \tag{3.3}$$

where $\int_S$ denotes a Cauchy integral and G and G_1 are the 2-dimensional Green's function of the upper and lower medium which are given by

$$G(\bar{r},\bar{r}') = \frac{i}{4} H_0^{(1)}(k|\bar{r}-\bar{r}'|) \tag{3.4}$$

$$G_1(\bar{r},\bar{r}') = \frac{i}{4} H_0^{(1)}(k_1|\bar{r}-\bar{r}'|) \tag{3.5}$$

$H_0^{(1)}$ is the zeroth order Hankel function of the first kind and k_1 is the wavenumber of the lower medium. The wave functions Ψ and Ψ_1 are related through the boundary conditions on the surface S, namely,

$$\psi_1(\bar{r}) = \psi(\bar{r}) \qquad \text{and} \qquad \frac{\partial \psi_1(\bar{r})}{\partial \hat{n}} = \rho \frac{\partial \psi(\bar{r})}{\partial \hat{n}} \tag{3.6}$$

where ρ equals μ_1/μ and $\varepsilon_1/\varepsilon$ for TE and TM polarization, respectively. The integral equation is next discretized using an evenly spaced single grid. The surface is discretized into a single grid of N points for x between -L/2 and L/2 and the x_m points are at

$x_m = (m-0.5)\Delta x - \frac{L}{2}$, m=1, 2, ..., N.

$$\sum_{n=1}^{N} a_{mn} u(x_n) + \sum_{n=1}^{N} b_{mn} \psi(x_n) = \psi_{inc}(x_m) \tag{3.7}$$

$$\sum_{n=1}^{N} a_{mn}^{(1)} \rho u(x_n) + \sum_{n=1}^{N} b_{mn}^{(1)} \psi(x_n) = 0 \tag{3.8}$$

where $u(x) = \sqrt{1+[f'(x)]^2}\, \partial\psi / \partial n$. The matrix elements a_{mn}, b_{mn}, $a_{mn}^{(1)}$, and $b_{mn}^{(1)}$ are given by [Li, 1994]:

$$a_{mn} = \begin{cases} \Delta x \frac{i}{4} H_0^{(1)}(k r_{mn}) & m \neq n \\ \Delta x \frac{i}{4} H_0^{(1)}[k \Delta x \gamma_m / (2e)] & m = n \end{cases} \tag{3.9}$$

$$b_{mn}=\begin{cases}-\Delta x\dfrac{ik}{4}\dfrac{f'(x_n)(x_n-x_m)-[f(x_n)-f(x_m)]}{r_{mn}}H_1^{(1)}(kr_{mn}) & m\neq n\\ \dfrac{1}{2}-\dfrac{f''(x_m)}{4\pi}\dfrac{\Delta x}{\gamma_m^2} & m=n\end{cases} \tag{3.10}$$

$$a_{mn}^{(1)}=\begin{cases}-\Delta x\dfrac{i}{4}H_0^{(1)}(k_1 r_{mn}) & m\neq n\\ -\Delta x\dfrac{i}{4}H_0^{(1)}[k_1\Delta x\gamma_m/(2e)] & m=n\end{cases} \tag{3.11}$$

$$b_{mn}^{(1)}=\begin{cases}\Delta x\dfrac{ik_1}{4}\dfrac{f'(x_n)(x_n-x_m)-[f(x_n)-f(x_m)]}{r_{mn}}H_1^{(1)}(k_1 r_{mn}) & m\neq n\\ \dfrac{1}{2}+\dfrac{f''(x_m)}{4\pi}\dfrac{\Delta x}{\gamma_m^2} & m=n\end{cases} \tag{3.12}$$

where $r_{mn}=\sqrt{(x_n-x_m)^2+[f(x_n)-f(x_m)]^2}$ and $\gamma_m=\sqrt{1+[f'(x_m)]^2}$, e = 2.71828183, $H_1^{(1)}$ is the first order Hankel function of the first kind, $f'(x_m)$ and $f''(x_m)$ represent the first and second derivative of f(x) evaluated at x_m, respectively. The matrix equation in (7) and (8) is in the form of a single grid. Let n = N/L be the number of points per wavelength. Usually a sample frequency of n = 10 is taken meaning that we have 10 points per wavelength. We shall call such a sampling a single coarse grid (SCG). If the sampling frequency is two or more times denser than the coarse grid, we shall call it a single dense grid (SDG). The dense grid that we use ranges from n = 20 to n = 30 in the paper.

3.3 Physics-Based Two-Grid Method Combined with Banded Matrix Iterative Approach/Canonical Grid Method

In this section, we describe the physics-based two-grid method correlated the BMIA/CAG.

Assume that the upper medium is the free space and the lower medium is lossy with the following relative permittivity:

$$\varepsilon_1 = \varepsilon_1'(1 + i\tan\delta) \tag{3.13}$$

where $\tan\delta$ stands for loss tangent. Let λ and λ_1 represent the wavelength of the wave with the identical frequency in the free space and the lower medium, respectively, and

$$n_1 = \mathrm{int}eger(\sqrt{\varepsilon_1'}) \tag{3.14}$$

Then, the relationship between λ and λ_1 can be expressed approximately by

$$\lambda_1 \approx \frac{\lambda}{n_1} \tag{3.15}$$

The number of sampling points needed in the lower medium should be n_1 times more than that in the free space.

In the physics-based two-grid method, we use two grids with samplings per wavelength of n_{cg} (coarse grid) and n_{dg} (dense grid), respectively. Let N_{dg} and N be respectively the total number of points on the dense grid and the coarse grid.

$$N_{dg} = n_{dg}\frac{L}{\lambda} \tag{3.16}$$

$$N = n_{cg}\frac{L}{\lambda} \tag{3.17}$$

Usually $n_{cg} = 10$ and $n_{dg} = 10n_1$. We first re-write equations (7) and (8) using the dense grid.

$$\sum_{n=1}^{N_{dg}} a_{mn}u(x_n) + \sum_{n=1}^{N_{dg}} b_{mn}\psi(x_n) = \psi_{inc}(x_m) \tag{3.18}$$

$$\sum_{n=1}^{N_{dx}} a_{mn}^{(1)} \rho u(x_n) + \sum_{n=1}^{N_{dx}} b_{mn}^{(1)} \psi(x_n) = 0 \tag{3.19}$$

The Roman numeral subscripts m,n denote indexing with the dense grid. Note that in the method of PBTG, the surface field at the dense grid are calculated. It is when the Green's function is multiplied with the surface fields on the dense grid, we can make substantial CPU saving by using PBTG. The matrix elements a_{mn}, b_{mn} represent Green's function of the upper medium while $a_{mn}^{(1)}, b_{mn}^{(1)}$ represents Green's function of the lower medium of the lossy dielectric. To reduce the calculation, we make the following three observations.

1) The Green's function in the lower region is heavily attenuative. A medium with a large real part of dielectric constant is normally associated with a large imaginary part. Let k_1" be the imaginary part of k_1. If $k_1 "r > C$, where C is a constant, then the field interaction between the mth and the nth point is vanishingly small. We can define a distance limit as dictated by dissipative loss:

$$r_t = \frac{C}{k_1 "} \tag{3.20}$$

outside of which the lower medium Green's function can be set equal to zero. The constant C depending on the loss tangent $\tan\delta$ varies from case to case. In this paper, C was fixed at 1.5.

Based on this observation, we calculate the left-hand sides of (19) as follows. We approximate

$$a_{mn}^{(1)} \approx \tilde{a}_{mn}^{(1)} = \begin{cases} a_{mn}^{(1)} & r_{mn} \le r_t \\ 0 & r_{mn} \ge r_t \end{cases} \tag{3.21}$$

$$b_{mn}^{(1)} \approx \tilde{b}_{mn}^{(1)} = \begin{cases} b_{mn}^{(1)} & r_{mn} \le r_t \\ 0 & r_{mn} \ge r_t \end{cases} \tag{3.22}$$

where r_{mn} is the distance between the mth point and the nth point on the dense grid. Thus $\tilde{a}_{mn}^{(1)}$ and $\tilde{b}_{mn}^{(1)}$ are banded matrices and Equation (19) becomes

$$\sum_{n=1}^{N_{dg}} \tilde{a}_{mn}^{(1)} \rho u(x_n) + \sum_{n=1}^{N_{dg}} \tilde{b}_{mn}^{(1)} \psi(x_n) = 0 \tag{3.23}$$

2) For non-near field interaction, Green's function for the upper medium is slowly varying compared with Green's function of the lossy dielectric lower medium. Thus when performing matrix and column vector multiplication on the dense grid as indicated in (18), the Green's function of the upper medium is essentially constant over an interval of n_1 points on the dense grid. Thus we can write

$$\sum_{l=1}^{n_1} a_{(m+l)(n+l)} u_{n+l} \approx a_{m_{mp} n_{mp}} \sum_{l=1}^{n_1} u_{n+l} = n_1 a_{m_{mp} n_{mp}} \left(\frac{1}{n_1} \sum_{l=1}^{n_1} u_{n+l}\right) \tag{3.24}$$

where $l = 1, 2, \ldots, n_1$ and the points with indexes m_{mp} and n_{mp} are the middle points of the $(m+1)th$ point and the $(m+n_1)th$ point and the $(n+1)th$ point and the $(n+n_1)th$ point, respectively. What is done in (24) is that the surface fields on the dense grid are first averaged before multiplied by the upper medium Green's function.

3) The slowly varying nature of Green's function of the upper medium only applies to non-near field interaction. For near field interaction, Green's functions G and G_1 have roughly the same rate of variation. Thus we need to separate out a distance, say 1λ, outside of which G_1 is much more rapidly varying than G.

Based on the observations above, we decompose the upper medium Green's function into near field and non-near field interactions

$$\sum_{n=1}^{N_{dg}} a_{mn} u(x_n) = \sum_{n=1}^{N_{dg}} a_{mn}^{s} u_n + \sum_{n=1}^{N_{dg}} a_{mn}^{ns} u_n \tag{3.25}$$

$$\sum_{n=1}^{N_{dg}} b_{mn} \psi(x_n) = \sum_{n=1}^{N_{dg}} b_{mn}^{s} \psi_n + \sum_{n=1}^{N_{dg}} b_{mn}^{ns} \psi_n \tag{3.26}$$

where a_{mn}^{s}, b_{mn}^{s}, a_{mn}^{ns}, and b_{mn}^{ns} are determined by

$$a_{mn}^{s} = \begin{cases} a_{mn} & r_{mn} \le r_f \\ 0 & r_{mn} \ge r_f \end{cases} \tag{3.27}$$

$$b_{mn}^{s}=\begin{cases} b_{mn} & r_{mn}\le r_f \\ 0 & r_{mn}\ge r_f \end{cases} \tag{3.28}$$

$$a_{mn}^{ns}=\begin{cases} 0 & r_{mn}\le r_f \\ a_{mn} & r_{mn}\ge r_f \end{cases} \tag{3.29}$$

$$b_{mn}^{ns}=\begin{cases} 0 & r_{mn}\le r_f \\ b_{mn} & r_{mn}\ge r_f \end{cases} \tag{3.30}$$

Thus r_f is the distance outside which the Green's function of the lower medium is fast varying compared with that of free space Green's function.

Let α and β denote the coarse grid indices. The coarse grid has surface unknowns $\tilde{u}$ and $\tilde{\psi}$, which are averages of the dense grid surface unknowns. Thus if $\bar{r}_\beta$ is centered in the middle of the n_1 dense grid points of n+1, n+2, ..., n+n_1, we have

$$\tilde{u}_\beta=\frac{u_{n+1}+u_{n+2}+\cdots+u_{n+n1}}{n_1} \tag{3.31}$$

$$\tilde{\psi}_\beta=\frac{\psi_{n+1}+\psi_{n+2}+\cdots+\psi_{n+n1}}{n_1} \tag{3.32}$$

We calculate Green's function of the upper medium on the coarse grid. These are represented by $\tilde{a}_{\alpha\beta}$ and $\tilde{b}_{\alpha\beta}$.

$$\tilde{a}_{\alpha\beta}=\begin{cases} \Delta\tilde{x}\dfrac{i}{4}H_0^{(1)}(kr_{\alpha\beta}) & r_{\alpha\beta}>r_f \\ 0 & r_{\alpha\beta}\le r_f \end{cases} \tag{3.33}$$

$$\tilde{b}_{\alpha\beta}=\begin{cases} -\Delta\tilde{x}\dfrac{ik}{4}\dfrac{f'(x_\beta)(x_\beta-x_\alpha)-[f(x_\beta)-f(x_\alpha)]}{r_{\alpha\beta}}H_1^{(1)}(kr_{\alpha\beta}) & r_{\alpha\beta}>r_f \\ 0 & r_{\alpha\beta}\le r_f \end{cases} \tag{3.34}$$

where $\Delta\tilde{x}$ is the coarse grid sampling, $\Delta\tilde{x}=n_1\Delta x$, and Δx is the dense grid sampling. Thus Equation (18) becomes

$$[\sum_{n=1}^{N_{dg}} a^s_{mn} u(x_n) + \sum_{n=1}^{N_{dg}} b^s_{mn} \psi(x_n)] + [\sum_{\beta=1}^{N} \tilde{a}_{\alpha\beta} \tilde{u}(x_\beta) + \sum_{\beta=1}^{N} \tilde{b}_{\alpha\beta} \tilde{\psi}(x_\beta)]_{\text{int } p} = \psi_{inc}(x_m) \tag{3.35}$$

Note in Equation (35) that $\sum_{n=1}^{N_{dg}} a^s_{mn} u(x_n)$ includes N_{dg} values of m=1, 2, •••, N_{dg} , while $\sum_{\beta=1}^{N} \tilde{a}_{\alpha\beta} \tilde{u}(x_\beta)$ only has N values of α=1, 2, •••, N. Thus we first compute $\sum_{\beta=1}^{N} \tilde{a}_{\alpha\beta} \tilde{u}(x_\beta)$. Then we use linear interpolation to find N_{dg} on the dense grid. In Equation (35), we use subscript intp to represent that interpolation.

In the original PBTG, the BMIA is used to solve matrix Equation (23) and (35). In this paper, we use BMIA/CAG to solve matrix equation. We further divide non-near field interactions into two regions which are separated by r_d. For the interactions between r_f and r_d, we implement matrix and vector multiplication directly. For the interactions larger than r_d, we expand $\tilde{a}_{\alpha\beta}$ and $\tilde{b}_{\alpha\beta}$ in Taylor series as in the BMIA/CAG so that the FFTs can be used to compute this part of the matrix-vector multiplication. The Taylor series expansion is given below

$$H(k\sqrt{x_d^2 + z_d^2}) = \sum_{m=0} a_m(x_d) \left(\frac{z_d}{x_d} \right)^{2m} \tag{3.36}$$

Here $H(k\sqrt{x_d^2 + z_d^2})$ represents both $H_0^{(1)}(k\sqrt{x_d^2 + z_d^2})$ and $\frac{H_1^{(1)}(k\sqrt{x_d^2 + z_d^2})}{\sqrt{x_d^2 + z_d^2}}$, $x_d = (x - x')$ and $z_d = (z - z') = f(x) - f(x')$. The first three terms of the expansion coefficients are given in [Chan, 1998].

The accuracy of Taylor series expansion depends on the ratio of z_d / x_d which in turn dictates the bandwidth of the stored near-field interactions.

3.4 Bistatic Scattering Coefficient and Emissivity

After the matrix equation is solved, the surface field can be calculated. The bistatic scattering coefficient $\sigma(\theta_s, \theta_i)$ is a measure of the scattering from incident angle θ_i into scattered angle θ_s. It is defined by:

$$\sigma(\theta_s,\theta_i)=\frac{\left|\int_{-\infty}^{\infty} dx[ik\psi(x)(\frac{df}{dx}\sin\theta_s-\cos\theta_s)-u(x)]\exp(-ik\alpha(\theta_s,x))\right|^2}{4\pi g^2\int_{-k}^{k} dk_x k_z \exp[-(k_x-k\sin\theta_i)^2 g^2/2]} \tag{3.37}$$

In (37), $\alpha(\theta_s, x) = \sin\theta_s\, x + \cos\theta_s\, f(x)$, and $k_z=\sqrt{k^2-k_x^2}$. The bistatic scattering coefficient has been normalized by the incident power impinging upon the rough surface. For scattering by a perfect conducting surface, the energy conservation test is that $\int\sigma(\theta_s,\theta_i)d\theta_s=1$. For scattering by a dielectric surface, the emissivity of the rough surface at incident angle θ_i is

$$e(\theta_i)=1-\int d\theta_s\sigma(\theta_s,\theta_i) \tag{3.38}$$

Thus emissivity is a measure of energy conservation in a scattering calculation. Because of reciprocity, emissivity is the same as absorptivity which is the amount of power absorbed by the dielectric in a scattering problem. In passive remote sensing, the brightness temperature T_B of the medium is measured at incident angle θ_i. The brightness temperature is

$$T_B(\theta_i)=e(\theta_i)T \tag{3.39}$$

where T is the physical temperature of the medium in Kelvin degrees. Brightness temperatures are commonly measured by instruments mounted on satellites and aircrafts. The brightness temperature can be measured to an accuracy of 1 degree K. For the case of T = 300K, an error of calculation in the emissivity of 0.03 gives an error of 9K in brightness temperature and will not be acceptable. It is important that the scattering

calculation obey energy conservation to less than 0.01, so that the error in brightness temperature is limited to less than 3 degrees K.

3.5 Numerical Results and Discussion

In this section, we illustrate the numerical simulation results of wave scattering from rough lossy dielectric surface for both TE and TM waves. Simulations are based on Gaussian random rough surfaces with Gaussian correlation functions. First, we show the comparisons of bistatic scattering coefficients and surface fields based on a single dense grid (SDG) and a single coarse grid (SCG) with a dielectric constant of 25+i, surface length of 100 wavelengths and at an incidence angle of 30 degrees. The results show that the dense grid is required for the case with large dielectric constant. We shall regard the SDG results to be correct. Next, we compare the results based on PBTG-BMIA/CAG with that of SDG. Then we use the new method to calculate the cases with large surface length at different incident angles and compare with SDG. Results indicate that the method still works well for large surface length and at near-grazing incidence angle. It is important to note that the PBTG-BMIA/CAG calculates the surface fields on the dense grid.

Our numerical results for rms heights less than a wavelength indicate that it requires a long surface to have accurate solutions of close to grazing incidence since the edge effects have to be avoided [Tsang, 1995]. It has been reported that the surface length of 8192 wavelengths is needed for the incidence angle of 89° [Johnson, 1998]. For the case of small incidence angle, the required surface length can be much shorter. However, the advantage of the present method is for long surfaces and that is why the examples deal with cases with rms height less than a wavelength.

To avoid the edge effects, the tapering parameter was taken to be $L/4$ for the case of surface length of 100 wavelengths and $L/8$ for the case of surface length of 500

wavelengths at near-grazing incidence. The critical distance of r_f that defines the very near field is fixed at 1 wavelength in this paper. The cases with surface length of 100 wavelengths were run on SPARC 20 workstation and the cases with surface length of 500 wavelengths were run on Pentium-Pro Personal Computer with the clock rate of 200MHz. The random rough surfaces used in the simulation are Gaussian random rough surfaces. The dielectric constant is set at 25 + i.

a) Comparison between single dense grid and single coarse grid.

In Figures 1a and 1b, we compare respectively the results of the bistatic scattering coefficients of a single realization of rough surface and averaged over 20 realizations for TE wave, at incident angle $\theta_i = 30^o$, and surface length L = 100 λ, where λ is the wavelength. The rms height and correlation length are 0.5 and 0.6 wavelength, respectively. We compare the cases of SCG of n_d=10 and SDG of 30 points per wavelength. We note that the results of SCG and SDG are quite different both for one realization and for averages over 20 realizations. Obviously, the results based on SCG are not accurate enough. The comparisons were also made in Figures 2a and 2b for TM wave with the same parameters. It is noted that the performance of SCG is poorer for TM case. This is because the more energy is transmitted into the lower medium for TM case than for the TE case and the lower medium dielectric requires a dense discretization. In Figures 3a and 3b, we compare the surface electric fields between SDG and SCG for TE and TM waves, respectively. It is obvious that the coarse grid can not give rapid spatial variation of the surface fields. In Table I, we compare the emissivities calculated for using one realization and 20 realizations for SCG and SDG for both TE and TM waves. We found that for SCG, the emissivity is 0.614097, while for SDG, the emissivity is 0.592344 for one realization of TE wave. The difference of emissivities of 0.021753 can give a difference of 300K x 0.021753 = 6.53K in brightness temperature. Even after averaging over 20 realizations, the emissivity for SCG still has -0.013456 difference from

that of SDG. For TM wave, the difference of emissivity is much larger. It is -0.061699 for one realization and -0.092587 for 20 realizations. This gives differences of 18.5K and 27.78K in brightness temperatures, respectively. Thus SCG is not accurate for problems of large dielectric constant and cannot be used to calculate the emissivities. In Table II, we compare the CPU. We note that although SDG is accurate, it requires much more CPU than SCG. We regard the SDG results as accurate.

b) Comparison between PBTG combined with BMIA/CAG and single dense grid.

In Figures 4a and 4b, we compare the results of the bistatic scattering coefficients respectively obtained from a single realization of rough surface and averaged over 20 realizations of rough surfaces using SDG and PBTG-BMIA/CAG for TE wave. For PBTG-BMIA/CAG, the two grids are used with $n_{cg} = 10$ and $n_{dg} = 30$. The result obtained by PBTG-BMIA/CAG is almost identical to the SDG result. In Figures 5a and 5b, the comparisons are made for TM wave that also shows PBTG-BMIA/CAG can give almost the same results as SDG. The comparisons of the surface electric fields between SDG and PBTG-BMIA/CAG for TE and TM cases are shown in Figures 6a and 6b, respectively. The agreements are good since the PBTG-BMIA/CAG computes the surface fields on the dense grid. The emissivities calculated by SDG and PBTG-BMIA/CAG are compared in Table I. The emissivity calculated by PBTG-BMIA/CAG is very close to that of SDG for TE and TM waves. The difference of emissivities averaged over 20 realizations between SDG and PBTG-BMIA/CAG is -0.007889 for TE wave and -0.002933 for TM wave that will lead to maximum differences of 2.3667K and 0.8799K in brightness temperatures, respectively. We also compare the CPU between PBTG-BMIA/CAG, SDG, and SCG. In Table II, we give the comparisons of the total CPU and CPU per iteration based on PBTG-BMIA/CAG and single grid methods for one realization. It is shown that the CPU per iteration is the smallest for PBTG and the largest for SDG. The total CPU of PBTG is slightly more than that of SCG because PBTG-BMIA/CAG requires more number of iterations. But the CPU of PBTG-BMIA/CAG is

still several times less than that of SDG. The CPU for PBTG-BMIA/CAG is also comparable to SCG.

c) Comparison between PBTG-BMIA/CAG and SDG for large surface length case.

In Figures 7a and 7b, the bistatic scattering coefficients obtained by PBTG-BMIA/CAG and SDG, respectively, are compared for the case of a large surface length of 500 wavelengths, rms height of 0.3λ, correlation length of 0.5λ, and dielectric constant of $17+i$ at incidence angle of 30 degrees for one realization for both TE and TM waves. In this case, SDG has 20 points per wavelength. PBTG-BMIA/CAG is with $n_{cg}=10$ and $n_{dg}=20$. The agreements are good. The comparisons of emissivities and CPU are shown in Table III.

d) Backscattering coefficients from rough surface with large dielectric constant at near-grazing incidence angle.

We also compare the bistatic scattering coefficients between PBTG-BMIA/CAG and SDG at incidence angle of 85 degrees in Figures 8a and 8b. In this case, other parameters used are the same as the Figures 7a and 7b. The agreements are good except in the forward scattering directions. The agreement in the forward direction is reasonable. It is important to note that PBTG-BMIA/CAG gives accurate results in backscattering direction.

In Figure 9a, we show the bistatic scattering coefficients of TE wave at 85° incidence angle averaged over various number of realizations. In Figure 9b, we zoom in and show the bistatic scattering coefficients in the vicinity of backscattering direction. In Figures 10a and 10b, we show the corresponding results for TM wave. We take the surface length of 500 wavelengths, rms height of 0.5λ, correlation length of 0.6λ, dielectric constant of

$25+i$. In PBTG-BMIA/CAG, we use two grids of 10 points per wavelength and 30 points per wavelength. We did not calculate the results of SDG because of large CPU and memory requirements. We found that 50 realizations are required for convergence of backscattering coefficients for TE and 70 realizations are required for TM waves.

3.6 Conclusions

In this paper, we have combined PBTG method with BMIA/CAG to calculate the wave scattering from rough surfaces of large surface length with a large lossy dielectric constant. The method saves both CPU and memory and provides the required accuracy. The computational complexity and the memory requirements of the present algorithm are O(N *log*(N)) and O(N), respectively, where N is the number of surface unknowns on the coarse grid. We also applied the method to calculate the backscattering coefficients from rough surface at near-grazing incidence angle and also the emissivities. The PBTG-BMIA/CAG gives accurate results when compared with SDG and with CPU time comparable with SCG. The method can be extended to the 3-D case. Results for 3-D case have been obtained and are being prepared for a separate publication.

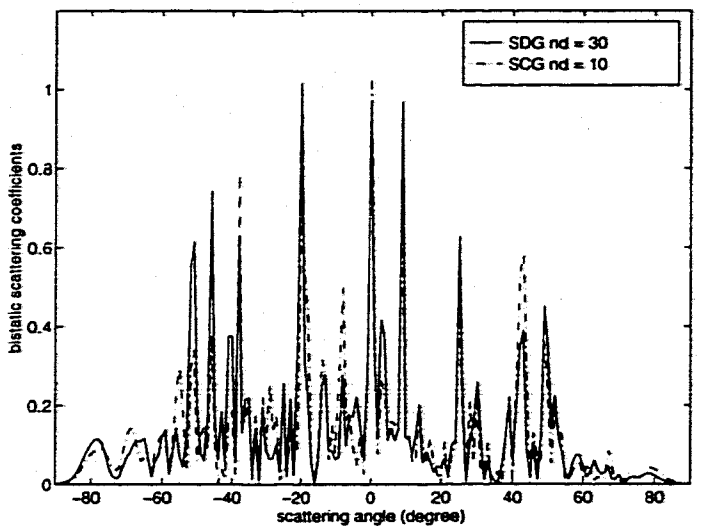

(a)

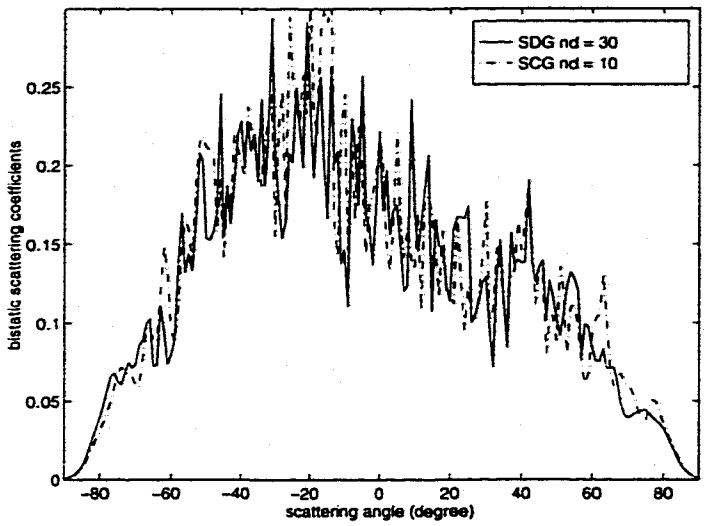

(b)

Figure 3.1 Comparison of the bistatic scattering coefficients between the single dense grid of 30 points per wavelength and the single coarse grid of 10 points per wavelength. TE wave, rms $h = 0.5\lambda$, correlation length of $l = 0.6\lambda$, dielectric constant of $\varepsilon_r = 25 + i$, surface length of $L = 100\lambda$, and tapering parameter of $g = L/4$ at incidence angle of $\theta_i = 30°$. a). one realization b). 20 realizations

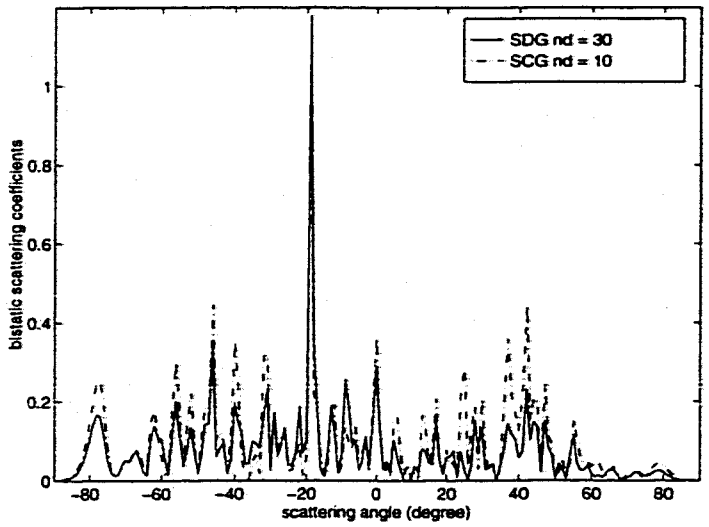

(a)

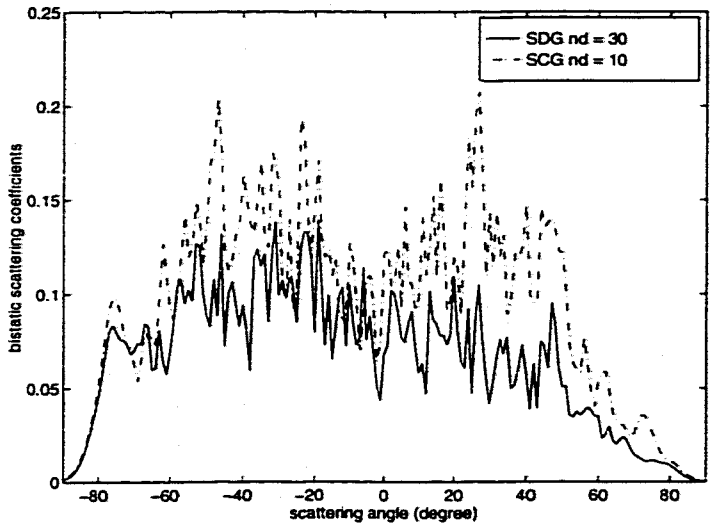

(b)

Figure 3.2 Comparison of the bistatic scattering coefficients between the single dense grid of 30 points per wavelength and the single coarse grid of 10 points per wavelength. TM wave, rms $h = 0.5\lambda$, correlation length of $l = 0.6\lambda$, dielectric constant of $\varepsilon_r = 25 + i$, surface length of $L = 100\lambda$, and tapering parameter of $g = L/4$ at incidence angle of $\theta_i = 30°$. a). one realization b). 20 realizations

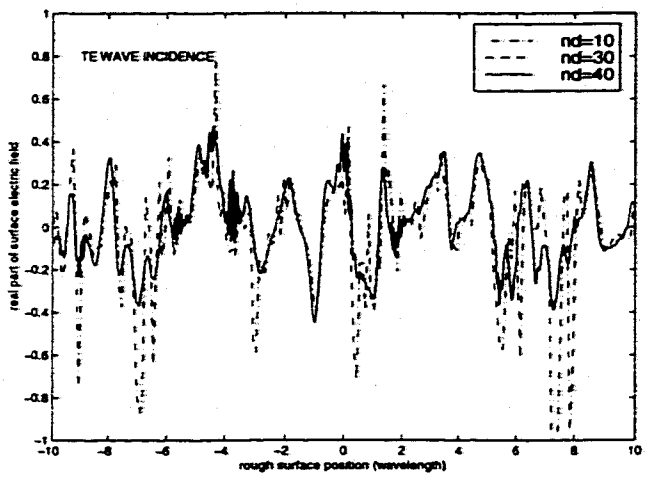

(a)

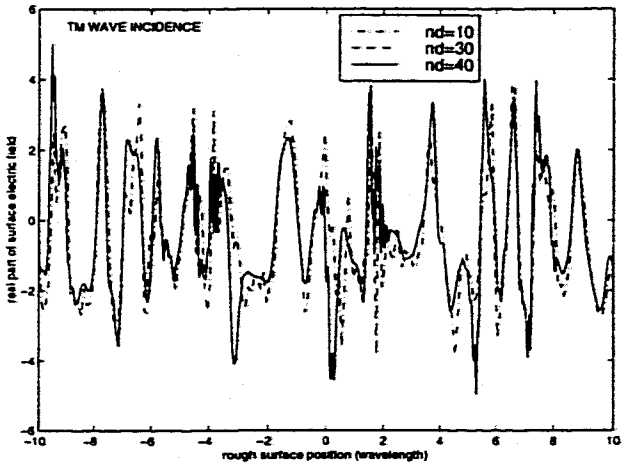

(b)

Figure 3.3 Comparison of the surface fields between the single dense grid of 30 points per wavelength and the single coarse grid of 10 points per wavelength. rms $h = 0.5\lambda$, correlation length of $l = 0.6\lambda$, dielectric constant of $\varepsilon_r = 25 + i$, surface length of $L = 100\lambda$, and tapering parameter of $g = L/4$ at incidence angle of $\theta_i = 30°$. a). TE wave b). TM wave

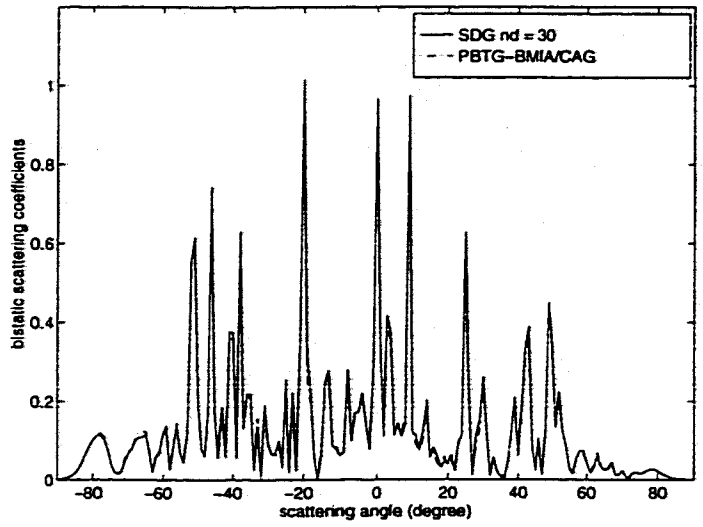

(a)

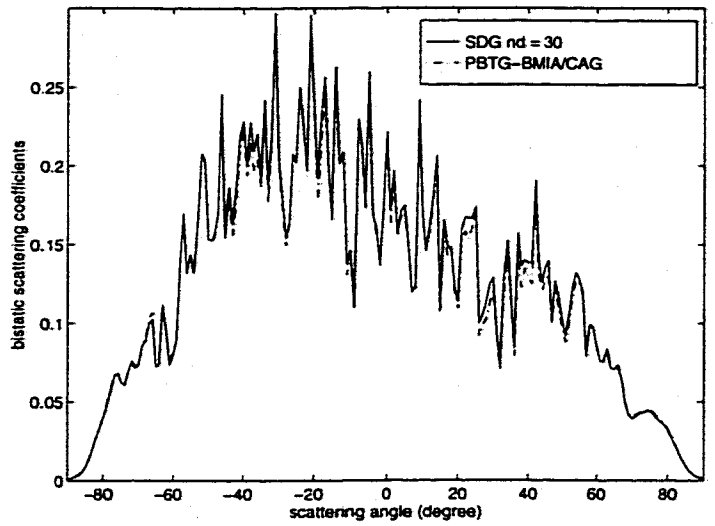

(b)

Figure 3.4 Comparison of the bistatic scattering coefficients between the single dense grid of 30 points per wavelength and the PBTG-BMIA/CAG with $r_f = 1\lambda$. TE wave, rms $h = 0.5\lambda$, correlation length of $l = 0.6\lambda$, dielectric constant of $\varepsilon_r = 25 + i$, surface length of $L = 100\lambda$, and tapering parameter of $g = L/4$ at incidence angle of $\theta_i = 30°$. a). one realization b). 20 realizations

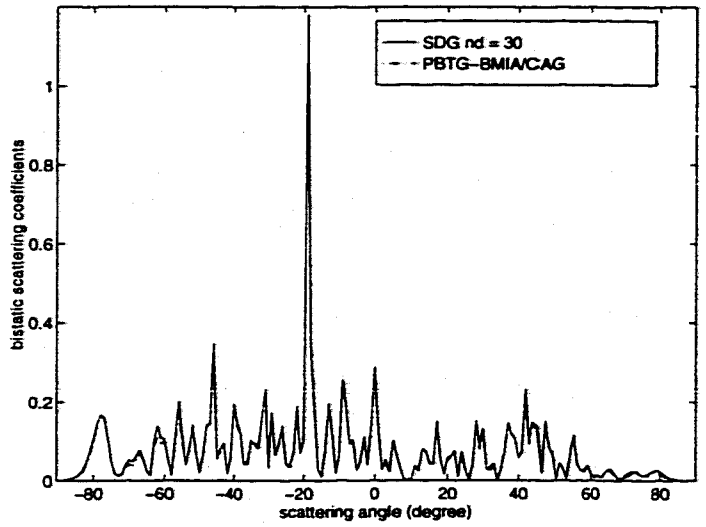

(a)

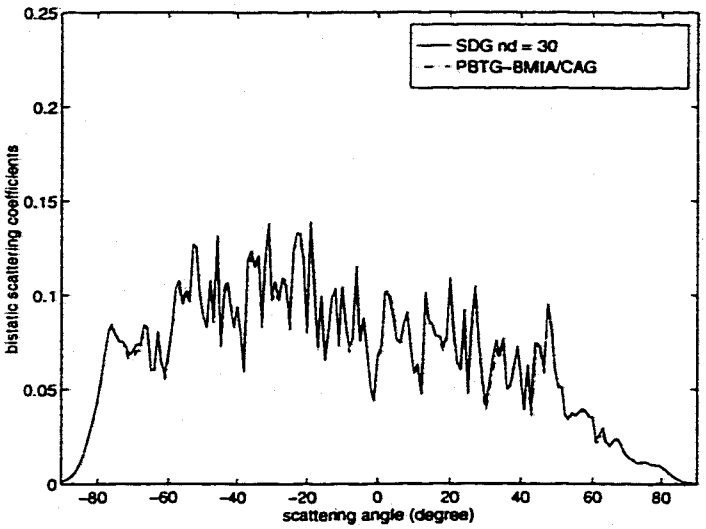

(b)

Figure 3.5 Comparison of the bistatic scattering coefficients between the single dense grid of 30 points per wavelength and the PBTG-BMIA/CAG with $r_f = 1\lambda$. TM wave, rms $h = 0.5\lambda$, correlation length of $l = 0.6\lambda$, dielectric constant of $\varepsilon_r = 25 + i$, surface length of $L = 100\lambda$, and tapering parameter of $g = L/4$ at incidence angle of $\theta_i = 30°$. a). one realization b). 20 realizations

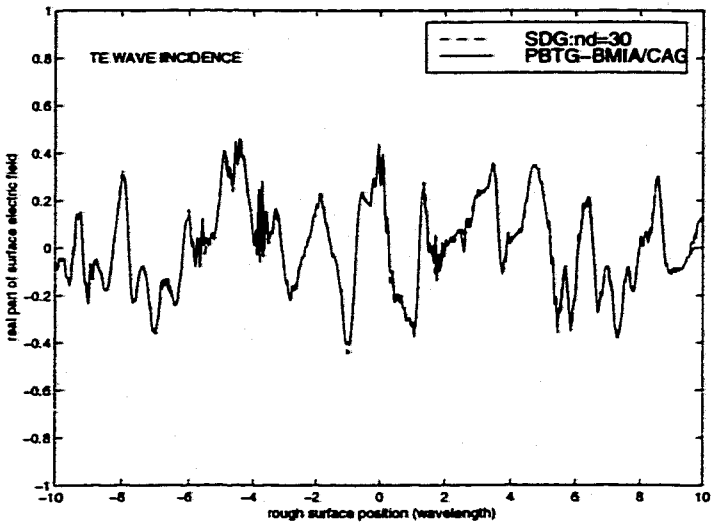

(a)

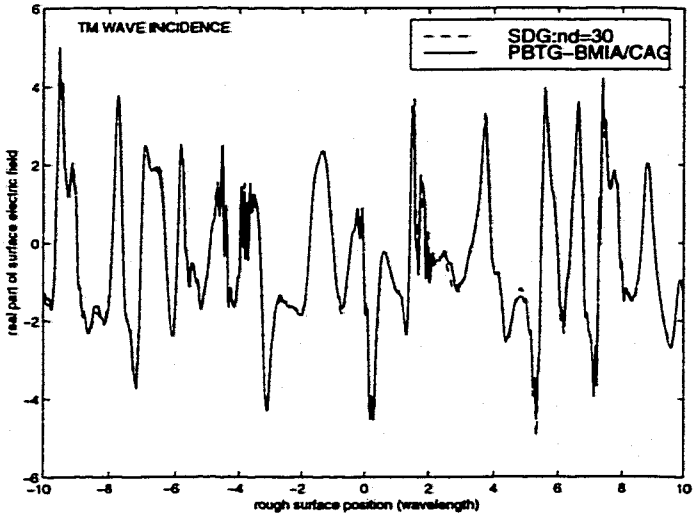

(b)

Figure 3.6 Comparison of the surface fields between the single dense grid of 30 points per wavelength and the PBTG-BMIA/CAG with $r_f = 1\lambda$. rms $h = 0.5\lambda$, correlation length of $l = 0.6\lambda$, dielectric constant of $\varepsilon_r = 25 + i$, surface length of $L = 100\lambda$, and tapering parameter of $g = L/4$ at incidence angle of $\theta_i = 30°$. a). TE wave b). TM wave

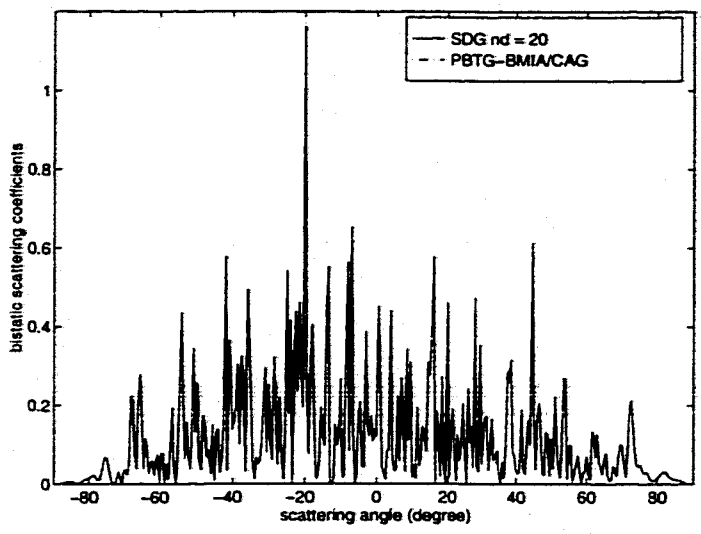

(a)

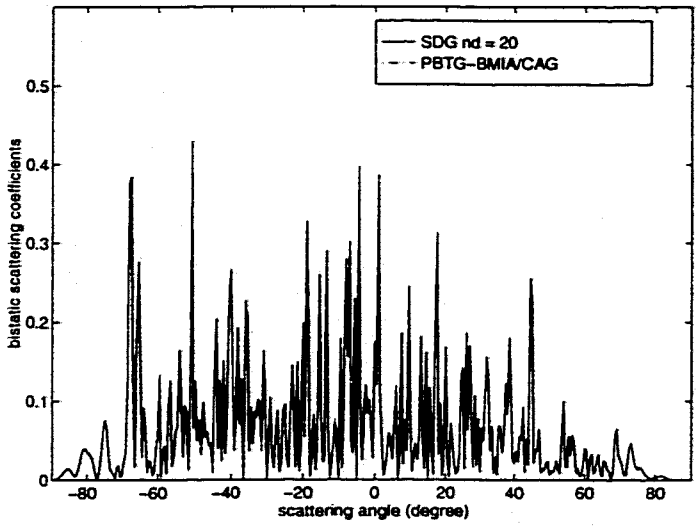

(b)

Figure 3.7 Comparison of the bistatic scattering coefficients between the single dense grid of 20 points per wavelength and the PBTG-BMIA/CAG with $r_f = 1\lambda$ for one realization. rms $h = 0.3\lambda$, correlation length of $l = 0.5\lambda$, dielectric constant of $\varepsilon_r = 17 + i$, surface length of $L = 500\lambda$, and tapering parameter of $g = L/8$ at incidence angle of $\theta_i = 30°$. a). TE wave b). TM wave

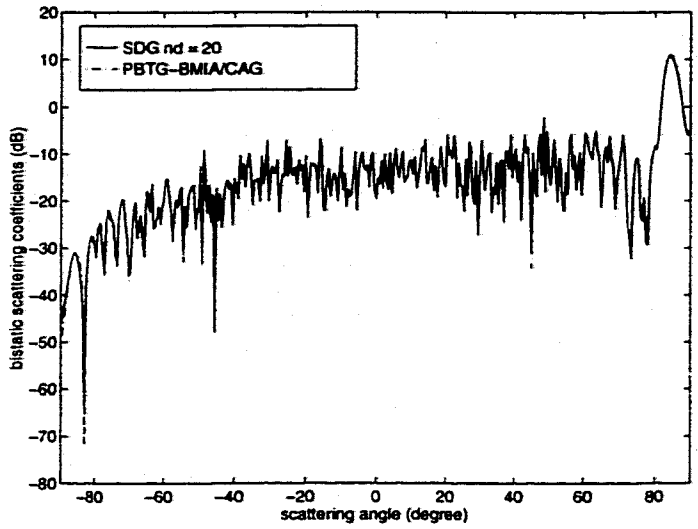

(a)

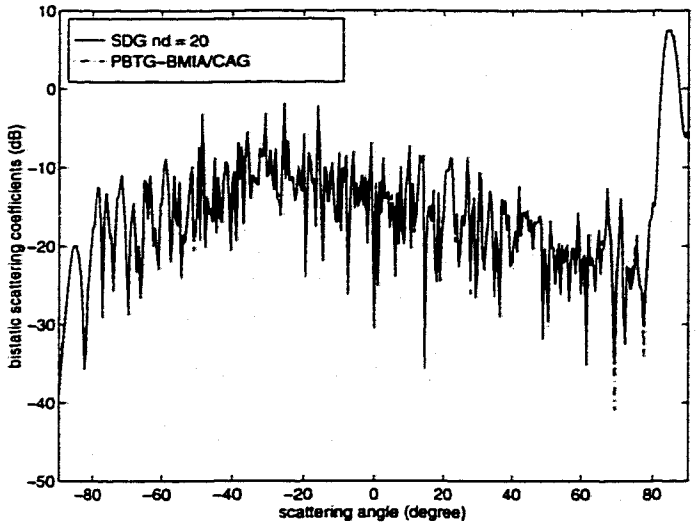

(b)

Figure 3.8 Comparison of the bistatic scattering coefficients between the single dense grid of 20 points per wavelength and the PBTG-BMIA/CAG with $r_f = 1\lambda$ for one realization. rms $h = 0.3\lambda$, correlation length of $l = 0.5\lambda$, dielectric constant of $\varepsilon_r = 17 + i$, surface length of $L = 500\lambda$, and tapering parameter of $g = L/8$ at incidence angle of $\theta_i = 85°$. a). TE wave b). TM wave

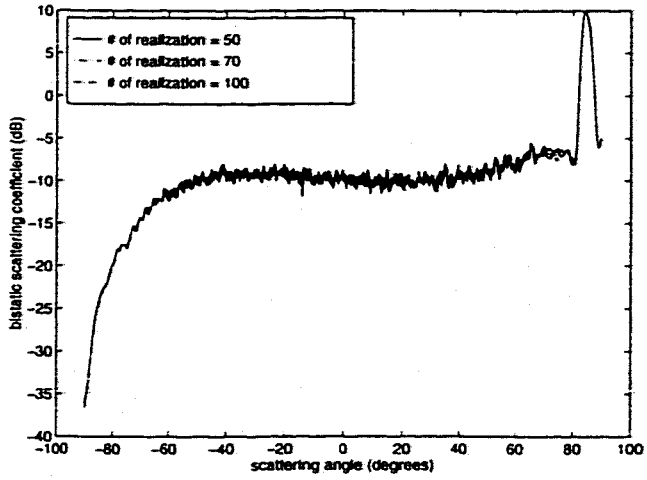

(a)

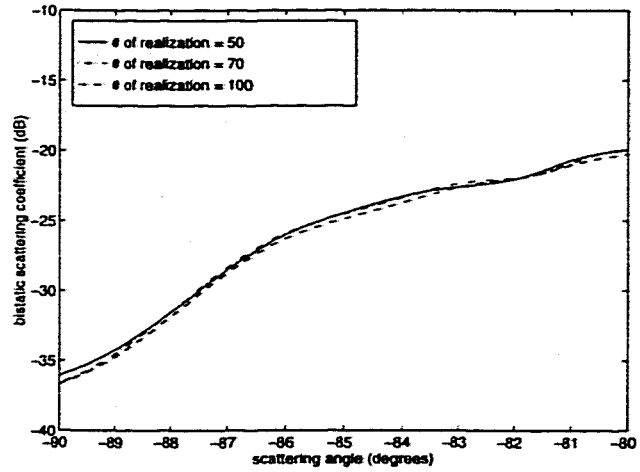

(b)

Figure 3.9 Comparison of the bistatic scattering coefficients averaged over various number of realizations calculated by PBTG-BMIA/CG with $r_f = 1\lambda$ and using the dense grid of 30 points per wavelength and the coarse grid of 10 points per wavelength. TE wave, rms $h = 0.5\lambda$, correlation length of $l = 0.6\lambda$, dielectric constant of $\varepsilon_r = 25 + i$, surface length of $L = 500\lambda$, and tapering parameter of $g = L/8$ at incidence angle of $\theta_i = 85°$. a). entire range of scattering angles b). vicinity of backscattering direction

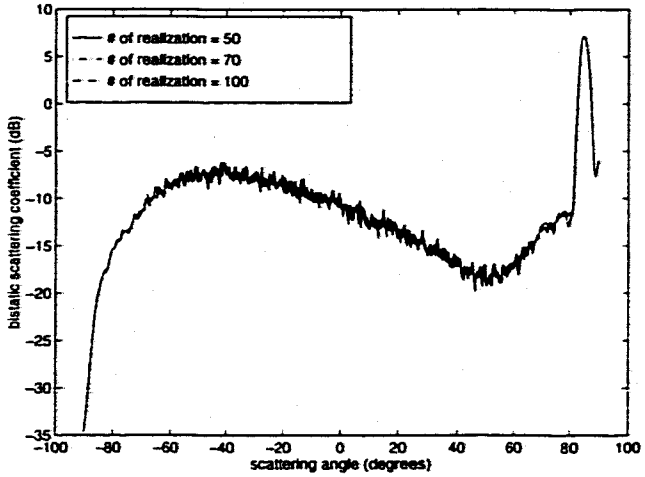

(a)

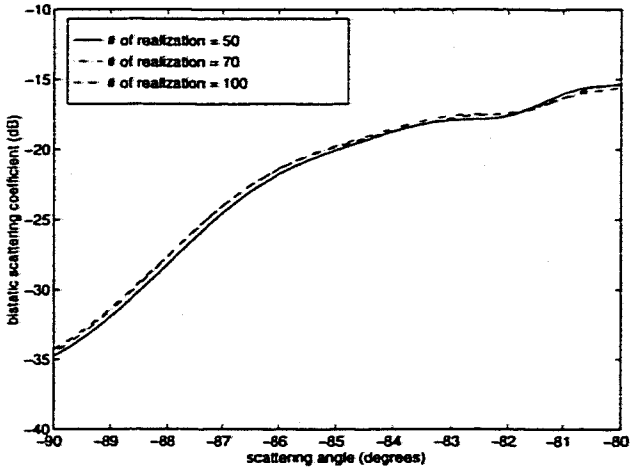

(b)

Figure 3.10 Comparison of the bistatic scattering coefficients averaged over different realization number calculated by the PBTG-BMIA/CAG with $r_f = 1\lambda$ and using the dense grid of 30 points per wavelength and the coarse grid of 10 points per wavelength. TM wave, rms $h = 0.5\lambda$, correlation length of $l = 0.6\lambda$, dielectric constant of $\varepsilon_r = 25 + i$, surface length of $L = 500\lambda$, and tapering parameter of $g = L/8$ at incidence angle of $\theta_i = 85°$. a). entire range of scattering angles b). vicinity of backscattering direction

Table 3.1 Comparison of emissivities based on PBTG-BMIA/CAG and single grid method (L = 100 wavelength)

Method	n_d	Polarization	# of realization	Emissivity	difference of emissivity***
SCG*	10	TE	1	0.614097	+0.021753
SDG**	30	TE	1	0.592344	0
PBTG-BMIA/CAG	10 and 30	TE	1	0.602337	0.0099
SCG	10	TM	1	0.703530	-0.061699
SDG	30	TM	1	0.765229	0
PBTG-BMIA/CAG	10 and 30	TM	1	0.768926	0.003697
SCG	10	TE	20	0.592318	-0.013456
SDG	30	TE	20	0.605774	0
PBTG-BMIA/CAG	10 and 30	TE	20	0.613663	0.007889
SCG	10	TM	20	0.701566	-0.092587
SDG	30	TM	20	0.794153	0
PBTG-BMIA/CAG	10 and 30	TM	20	0.797086	-0.002933

SCG = Single Coarse Grid, SDG = Single Dense Grid, The difference of emissivity means the emissivity minus the emissivity of SDG.

Table 3.2 Comparison of CPU based on PBTG-BMIA/CAG and single grid method (1 realization and L = 100 wavelength)

Method	n_d	# of surface unknowns	Polar.	CPU time (s) per iteration	# of iteration	CPU time(s)
SCG	10	2000	TE	14.5	416	6064.8
SDG	30	6000	TE	75.0	383	28757.0
PBTG-BMIA/CAG	10 and 30	6000	TE	11.6	662	7708.1
SCG	10	2000	TM	14.51	108	1595.0
SDG	30	6000	TM	77.0	108	8333.2
PBTG-BMIA/CAG	10 and 30	6000	TM	12.2	135	1655.0

Table 3.3 Comparison of Emissivity and CPU based on PBTG-BMIA/CAG and SDG method (1 realization and L = 500 wavelength)

Method	# of surface unknowns	incident angle	Polarization	emissivity	CPU time (s) per iteration	# of iteration	CPU time(mins)
SDG	20000	30	TE	0.639483	42.87	792	566
PBTG-BMIA/CAG	20000	30	TE	0.645528	9.84	1579	259
SDG	20000	30	TM	0.803430	34.52	252	145
PBTG-BMIA/CAG	20000	30	TM	0.804980	9.57	326	52
SDG	20000	85	TE	0.140942	40.72	358	243
PBTG-BMIA/CAG	20000	85	TE	0.073925	9.23	604	93
SDG	20000	85	TM	0.508661	35.58	145	86
PBTG-BMIA/CAG	20000	85	TM	0.47590	9.83	183	30
PBTG-BMIA/CAG	30000	85	TE		13.1	1323	290
PBTG-BMIA/CAG	30000	85	TM		13.6	292	68

Chapter 4

Bistatic Scattering and Emissivities of Random Rough Dielectric Lossy Surfaces with the Physics-Based Two-Grid Method in Conjunction with the Sparse-Matrix Canonical Grid Method

4.1 Introduction

The problem of electromagnetic wave scattering from random rough surfaces continues to attract research interest because of its broad applications. Classical analytic approaches are limited in regimes of validity. With the advent of modern computers and the development of fast numerical methods, Monte-Carlo simulations of the wave scattering problem have become an attractive approach. The most common method that has been used in numerical simulations is the surface integral equation method [Axline, 1978; Maradudin, 1990; Thorsos, 1988; Nieto-Vesperinas, 1987; Rino, 1992; Chen, 1995] and its solution by the method of moments (MoM). Conventional implementation of the MoM requires an $O(N^3)$ operation and an $O(N^2)$ computer memory storage. Fast numerical methods have been developed for 1-D random rough surface (2-D scattering problem) [Tsang, 1995; Johnson, 1998; Michelssen, 1996, Kapp, 1996; Chou, 1998] and 2-D random rough surfaces (3-D scattering problem) [Tsang, 1994; Johnson, 1996; Pak, 1995; Pak, 1997; Jandhyala, 1998a & b]. However for 2-D random rough surfaces of 3-dimensional scattering problem, only two fast numerical methods have been used and they are the sparse matrix canonical grid method (SMCG) [Tsang, 1994; Johnson, 1996; Pak, 1995; Pak, 1997] and the Fast Multipole Method (FMM) [Jandhyala, 1998a & b].

Both methods have been applied to perfect electric conducting surfaces and dielectric surfaces.

Recently, we studied the scattering of electromagnetic waves by lossy dielectric surfaces with large permittivity [Tsang, 1997; Li, 1999] which has broad applications in natural media. For wet soil, the relative permittivity can be as high as 17 + i2.0 at 1.4 GHz. For ocean surfaces, the permittivity can be as high as 39.7+i40.2 at 14 GHz. In the application of MoM to perfectly electric conducting rough surface scattering problem, only free space Green's function is needed because the wave cannot penetrate into the lower medium. A common implementation of MoM is to use a grid of 8 to 10 points per wavelength to discretize the surface. We shall call such a gridding a single coarse grid (SCG). For the wave scattering from metallic surfaces with very large permittivity, impedance boundary condition could be used because the wave in the medium can not propagate to the other points. However for lossy dielectric rough surfaces with high permittivity, there can be rapid spatial variations of the dielectric medium Green's function and surface fields. Thus a dense grid is needed. Also one of the applications of scattering by lossy dielectric surfaces is the calculation of emissivity for applications in passive microwave remote sensing. The calculation of emissivity has to be calculated to within 0.01 which corresponds to a brightness temperature difference of about 3 degrees. This means that the surface fields have to be calculated accurately.

Two alternatives were used to treat lossy dielectric surfaces. The first alternative is to use impedance boundary condition [Johnson, 1998]. The impedance boundary condition ignores the propagation from one point to all other points through the dielectric medium. Thus the disadvantage of this method is that an approximation is used in the problem without any error estimate. The error can affect the accuracy of emissivity which has an required accuracy of 0.01. The second alternative is to use a dense grid with a large number of points (say 16 to 20 points) per wavelength. We shall call such a gridding a single dense grid (SDG). The disadvantage of this SDG is that there is a large increase in

CPU and required memory. Recently we have developed the physics-based two-grid (PBTG) method [Tsang, 1997; Li, 1999]. It is an improvement over the past two alternatives in that it has the same accuracy as the single dense grid and yet has CPU comparable with that of the single coarse grid. The PBTG method can calculate the emissivity accurately. In PBTG, two grids are used: a dense grid and a sparse grid. The sparse grid is that of the usual 8 to 10 points per wavelength. The dense grid ranges from 16 or higher number of points per wavelength depending on the relative permittivity of the lossy dielectric medium. The surface fields are calculated on the dense grid. In the formulation of the surface integral equations, two Green's functions are used. The free space Green's function and the Green's function of the lossy dielectric medium. The PBTG is based on two observations. (1) the Green's function of the lossy dielectric is attenuative (spatial limited), and (2) the Green's function of free-space is slowly varying on the dense grid (spatial frequency limited). Because of Kramer-Kronig's relation, a large real part of dielectric constant is usually associated with a large imaginary part at high frequency. The first observation results in a sparse matrix for the Green's function of the lossy dielectric. When this Green's function acts on the surface fields on the dense grid, it will be just the product of a sparse matrix and a column vector. The second observation allows us, when using the free-space Green's function to act on the surface fields of dense grid, to first average the values of surface unknowns on the dense grid and then place them on the coarse grid. Thus the PBTG speeds up the CPU and yet preserves the accuracy of the solution. It needs to be mentioned that the PBTG is different from multi-grid method. The multi-grid method [Briggs, 1987; Donohue, 1998] tries to facilitate the convergence of iteration in iterative techniques. The present method is based on scattering physics. The purpose of PBTG is to speed up the matrix-vector product that corresponds to the convolution of two Green's functions with the surface fields on the dense grid.

In the previous papers [Tsang, 1997; Li, 1999], the PBTG method was implemented for 1-D surface (2-D scattering problem). In this paper, we (i) extend the PBTG to 2-D

rough surface (3-D scattering problem). (ii) combine the PBTG method with the sparse matrix canonical grid method (SMCG) for improving CPU and memory requirements, (iii) study bistatic scattering coefficients and emissivity for wave scattering from 2-D dielectric rough surface with high permittivity. We use two grids, a dense grid and a coarse grid. The wave interaction in the rough surface is divided into (1) very near field of distance of separation less than half wavelength, (2) near field of separation between half wavelength and r_d wavelengths, and (3) non-near field beyond r_d wavelengths. For very near-field interactions, we use the usual product of sparse matrix and column vector. For near-field and non-near field interactions, the free space Green's function is slowly varying on the dense grid. We first average the fields on the dense grid to get fields on the coarse grid. For the non-near field interactions, we further expand free space Green's function on a canonical grid of a horizontal surface so that the fast Fourier Transform (FFT) can be applied (SMCG). In the lower medium, the non-near field interactions are neglected because of lossy properties of the lower medium. The approach is denoted as PBTG/SMCG. The computational complexity and the memory requirements for the algorithm are $O(N_{scg}\ log(N_{scg}))$ and $O(N_{scg})$, respectively, where N_{scg} is the number of grid points on the coarse grid. Using this approach, we illustrate numerical results of wave scattering from 2-Dimensional rough surface with permittivity as high as 17 + 2i. Also the numerical results of emissivity are compared with that of approximately analytic solutions. The common analytic method to emissivity is the small perturbation method (SPM) [Tsang, 1985; Yueh, 1994] because it obeys energy conservation. For example, the second order SPM obeys energy conservation to order of h^2 where h is the rms height. Furthermore, the SPM agrees with the small slope approximation of emissivity calculation [Voronovich, 1994; Irisov, 1997] for half space case. It is to be emphasized that to apply SPM, the slope has to be small. But for many natural surfaces, including band limited fractal surfaces [Mandelbrot, 1983], the slopes are not small. Thus comparisons of emissivities are made with that of the second order small perturbation method (SPM).

In Section II, the formulation of the problem of wave impinging upon a 2-D dielectric surface (3-D scattering problem) is given in terms of surface integral equations. Then the surface integral equations are converted into a matrix equation using a single grid discretization. In Section III, we describe the physics-based two-grid algorithm and combine it with the sparse matrix canonical grid method. In section IV, the mathematical expressions of the bistatic scattering coefficients and the emissivity are given. In Section V, the numerical results are illustrated.

4.2 Formulation and Single Grid Implementation

Consider an electromagnetic wave, $\overline{E}_i(\overline{r})$ and $\overline{H}_i(\overline{r})$, with a time dependence of $e^{-i\omega t}$, impinging upon a 2-D dielectric rough surface with a random height profile $z = f(x, y)$. It is tapered so that the illuminated rough surface can be confined to the surface area $L_x \times L_y$ [Pak, 1997]. The direction of incident wave is $\hat{k}_i = \sin\theta_i \cos\phi_i \hat{x} + \sin\theta_i \sin\phi_i \hat{y} - \cos\theta_i \hat{z}$.

The incident fields are given as

$$\overline{E}_i(\overline{r}) = \int_{-\infty}^{+\infty} dk_x \int_{-\infty}^{+\infty} dk_y \exp(ik_x x + ik_y y - ik_z z) E(k_x, k_y) \hat{e}(-k_z) \tag{4.1}$$

$$\overline{H}_i(\overline{r}) = -\frac{1}{\eta_1} \int_{-\infty}^{+\infty} dk_x \int_{-\infty}^{+\infty} dk_y \exp(ik_x x + ik_y y - ik_z z) E(k_x, k_y) \hat{h}(-k_z) \tag{4.2}$$

For TE wave incidence

$$\hat{e}(-k_z) = \frac{1}{k_\rho}(\hat{x}k_y - \hat{y}k_x) \tag{4.3}$$

$$\hat{h}(-k_z) = \frac{k_z}{kk_\rho}(\hat{x}k_x + \hat{y}k_y) + \frac{k_\rho}{k}\hat{z} \tag{4.4}$$

and for TM wave incidence

$$\hat{h}(-k_z) = -\frac{1}{k_\rho}(\hat{x}k_y - \hat{y}k_x) \tag{4.5}$$

$$\hat{e}(-k_z) = \frac{k_z}{kk_\rho}(\hat{x}k_x + \hat{y}k_y) + \frac{k_\rho}{k}\hat{z} \tag{4.6}$$

with $k_z = \sqrt{k_1^2 - k_\rho^2}$ and $k_\rho = \sqrt{k_x^2 + k_y^2}$. In the above k_1 and η_1 are the wavenumber and wave impedance of free space, respectively. The spectrum of the incident wave, $E(k_x, k_y)$, is given as

$$E(k_x, k_y) =$$

$$\frac{1}{4\pi^2}\int_{-\infty}^{\infty} dx \int_{-\infty}^{\infty} dy \exp(-ik_x x - ik_y y)\exp[i(k_{ix}x + k_{iy}y)(1+w)]\exp(-t) \tag{4.7}$$

where $t = t_x + t_y = (x^2 + y^2)/g^2$ and

$$t_x = \frac{(\cos\theta_i \cos\phi_i x + \cos\theta_i \sin\phi_i y)^2}{g^2 \cos^2\theta_i} \tag{4.8}$$

$$t_y = \frac{(-\sin\phi_i x + \cos\phi_i y)^2}{g^2} \tag{4.9}$$

$$w = \frac{1}{k_1^2}\left(\frac{2t_x - 1}{g^2\cos^2\theta_i} + \frac{2t_y - 1}{g^2}\right) \tag{4.10}$$

The parameter g controls the tapering of the incident wave. Let $\bar{r}' = \hat{x}x' + \hat{y}y' + \hat{z}f(x', y')$ denote a source point and $\bar{r} = \hat{x}x + \hat{y}y + \hat{z}f(x, y)$ denote a field point on the rough surface. Then the fields satisfy the following surface integral equations [Pak, 1997]

$$\frac{\bar{E}_1(\bar{r})}{2} - \left\{\iint \hat{n}' \times \bar{H}_1(\bar{r}')i\omega\mu G_1 dS' + P\int[(\hat{n}' \times \bar{E}_1(\bar{r}')) \times \nabla' G_1 + \hat{n}' \cdot \bar{E}_1(\bar{r}')\nabla' G_1]dS'\right\} = \bar{E}^{inc}(\bar{r}) \tag{4.11}$$

$$\frac{\bar{H}_1(\bar{r})}{2} - \left\{\iint (-i\omega)\hat{n}' \times \bar{E}_1(\bar{r}')\varepsilon_1 G_1 dS' + P\int[(\hat{n}' \times \bar{H}_1(\bar{r}')) \times \nabla' G_1 + \hat{n}' \cdot \bar{H}_1(\bar{r}')\nabla' G_1]dS'\right\} = \bar{H}^{inc}(\bar{r}) \tag{4.12}$$

$$-\frac{\overline{E}_2(\overline{r})}{2}-\left\{\iint (i\omega)\hat{n}'\times\overline{H}_2(\overline{r}')\mu G_2 dS'+P\int[(\hat{n}'\times\overline{E}_2(\overline{r}'))\times\nabla' G_2+\hat{n}'\cdot\overline{E}_2(\overline{r}')\nabla' G_2]dS'\right\}=0 \quad (4.13)$$

$$-\frac{\overline{H}_2(\overline{r})}{2}-\left\{\iint -\hat{n}'\times\overline{E}_2(\overline{r}')i\omega\varepsilon_2 G_2 dS'+P\int[(\hat{n}'\times\overline{H}_2(\overline{r}'))\times\nabla' G_2+\hat{n}'\cdot\overline{H}_2(\overline{r}')\nabla' G_2]dS'\right\}=0 \quad (4.14)$$

where the integral $P\int$ denotes a Cauchy integral and G_1 and G_2 are the 3-dimensional Green's functions of free space and the lower dielectric medium, respectively. They are given by

$$G_{1,2}=\frac{\exp(ik_{1,2}R)}{4\pi R} \quad (4.15)$$

where $R=\{(x-x')^2+(y-y')^2+[f(x,y)-f(x',y')]^2\}^{1/2}$ and k_2 is the wavenumber of the lower medium. The unit normal vector $\hat{n}'$ refers to primed coordinate and points away from the second medium. Applying the boundary conditions,

$\hat{n}\times\overline{E}_1(\overline{r})=\hat{n}\times\overline{E}_2(\overline{r})=\hat{n}\times\overline{E}(\overline{r})$, $\hat{n}\times\overline{H}_1(\overline{r})=\hat{n}\times\overline{H}_2(\overline{r})=\hat{n}\times\overline{H}(\overline{r})$,

$\hat{n}\cdot\overline{E}_2(\overline{r})=\frac{\varepsilon_1}{\varepsilon_2}\hat{n}\cdot\overline{E}_1(\overline{r})=\frac{\varepsilon_1}{\varepsilon_2}\hat{n}\cdot\overline{E}(\overline{r})$, and $\hat{n}\cdot\overline{H}_1(\overline{r})=\hat{n}\cdot\overline{H}_2(\overline{r})=\hat{n}\cdot\overline{H}(\overline{r})$, we have

$$\frac{\hat{n}\times\overline{H}(\overline{r})}{2}-\hat{n}\times\left\{\iint(-i\omega)\hat{n}'\times\overline{E}(\overline{r}')\varepsilon_1 G_1 dS'+P\int[(\hat{n}'\times\overline{H}(\overline{r}'))\times\nabla' G_1+\hat{n}'\cdot\overline{H}(\overline{r}')\nabla' G_1]dS'\right\}$$
$$=\hat{n}\times\overline{H}^{inc}(\overline{r}) \quad (4.16)$$

$$\frac{\hat{n}\cdot\overline{E}(\overline{r})}{2}-\hat{n}\cdot\left\{\iint\hat{n}'\times\overline{H}(\overline{r}')i\omega\mu G_1 dS'+P\int[(\hat{n}'\times\overline{E}(\overline{r}'))\times\nabla' G_1+\hat{n}'\cdot\overline{E}(\overline{r}')\nabla' G_1]dS'\right\}=\hat{n}\cdot\overline{E}^{inc}(\overline{r}) \quad (4.17)$$

$$-\frac{\hat{n}\times\overline{E}(\overline{r})}{2}-\hat{n}\times\left\{\int(i\omega)\hat{n}'\times\overline{H}(\overline{r}')\mu G_2 dS'+P\int[(\hat{n}'\times\overline{E}(\overline{r}'))\times\nabla' G_2+\hat{n}'\cdot\overline{E}(\overline{r}')\frac{\varepsilon_1}{\varepsilon_2}\nabla' G_2]dS'\right\}=0 \quad (4.18)$$

$$-\frac{\hat{n}\cdot\overline{H}(\overline{r})}{2}-\hat{n}\cdot\left\{\iint-\hat{n}'\times\overline{E}(\overline{r}')i\omega\varepsilon_2 G_2 dS'+P\int[(\hat{n}'\times\overline{H}(\overline{r}'))\times\nabla' G_2+\hat{n}'\cdot\overline{H}(\overline{r}')\nabla' G_2]dS'\right\}=0 \quad (4.19)$$

We change equations (16) and (18) into scalar equations by projecting the vector into x and y directions, respectively. The method of moments (MoM) is used to discretize the integral equation. The resulting matrix equations are

$$\sum_{n=1}^{N}[Z_{mn}^{p1}I_n^{(1)} + Z_{mn}^{p2}I_n^{(2)} + Z_{mn}^{p3}I_n^{(3)} + Z_{mn}^{p4}I_n^{(4)} + Z_{mn}^{p5}I_n^{(5)} + Z_{mn}^{p6}I_n^{(6)}] = I_m^{(p)inc} \tag{4.20}$$

for $p = 1,2,3$ which correspond the surface integral equation when approaching the surface from free space and for $p = 4,5,6$ when approaching the surface from the lower medium. The quantities of $I_m^{(p)inc}$ are zero for $p = 4,5,6$.

Where

$$I_n^{(1)} = F_x(\bar{r}) = S_{xy}(\bar{r}_n)[\hat{n}\times\bar{H}(\bar{r}_n)]\cdot\hat{x} \tag{4.21}$$

$$I_n^{(2)} = F_y(\bar{r}) = S_{xy}(\bar{r}_n)[\hat{n}\times\bar{H}(\bar{r}_n)]\cdot\hat{y} \tag{4.22}$$

$$I_n^{(3)} = I_n(\bar{r}) = S_{xy}(\bar{r}_n)\hat{n}\cdot\bar{E}(\bar{r}_n) \tag{4.23}$$

$$I_n^{(4)} = I_x(\bar{r}) = S_{xy}(\bar{r}_n)[\hat{n}\times\bar{E}(\bar{r}_n)]\cdot\hat{x} \tag{4.24}$$

$$I_n^{(5)} = I_y(\bar{r}) = S_{xy}(\bar{r}_n)[\hat{n}\times\bar{E}(\bar{r}_n)]\cdot\hat{y} \tag{4.25}$$

$$I_n^{(6)} = F_n(\bar{r}) = S_{xy}(r_n)\hat{n}\cdot\bar{H}(\bar{r}_n) \tag{4.26}$$

are surface unknowns and $S_{xy} = \left\{1+\left[\frac{\partial f(x,y)}{\partial x}\right]^2 + \left[\frac{\partial f(x,y)}{\partial y}\right]^2\right\}^{1/2}$. The Z_{mn}^{pq} are the impedance elements and are determined by the free space Green's function and the dielectric medium Green's function. The parameter N is the number of points we use to discretize the rough surface.

In the past, we have used the method called the sparse-matrix canonical grid (SMCG) to solve large matrix equations. The computational complexity is of the order $O(N\log N)$ [Pak, 1997], where N is the number of grid points. We used the SMCG to solve the problem of wave scattering from dielectric rough surface with relative permittivity up to 7 [Pak, 1997]. The rough surface was sampled by taking 8 points per

free space wavelength. We call such a sampling a single coarse grid (SCG). If the lower medium has a high permittivity, say $17+2i$, the sampling frequency needs to be higher than that of coarse grid. We call this a single dense grid (SDG). The computational operations of SMCG is O($N_{sdg}\log N_{sdg}$), where N_{sdg} is the number of grid points on the dense grid. Next, we describe the PBTG that is as accurate as SDG and yet can reduce the computational steps to O($N_{scg}\log N_{scg}$), where N_{scg} is the number of grid points on the coarse grid.

4.3 Physics-Based Two-Grid Method

In this section, we describe the physics-based two-grid method. We assume that the upper medium is the free space and the lower medium is lossy with large permittivity.

$$\varepsilon_2 = \varepsilon_2'(1+i\tan\delta) \tag{4.27}$$

where $\tan\delta$ stands for loss tangent. Let λ_1 and λ_2 represent the wavelength of the wave in the free space and the lower medium, respectively, and

$$n_2 = \text{int}\,eger(\sqrt{\varepsilon_2'}) \tag{4.28}$$

Then, the relationship between λ_1 and λ_2 can be expressed approximately by

$$\lambda_2 \approx \frac{\lambda_1}{n_2} \tag{4.29}$$

The number of sampling points needed in the lower medium should be n_2 times that of the free space.

In the physics-based two-grid method, we use two grids with samplings per wavelength of n_{scg} (coarse grid) and n_{sdg} (dense grid), respectively. Let N_{sdg} and N_{scg} be respectively the total number of points on the dense grid and the coarse grid.

$$N_{sdg} = (n_{sdg}\frac{L_x}{\lambda_1})(n_{sdg}\frac{L_y}{\lambda_1}) \tag{4.30}$$

$$N_{scg} = (n_{scg}\frac{L_x}{\lambda_1})(n_{scg}\frac{L_y}{\lambda_1}) \tag{4.31}$$

For example $n_{scg} = 8$ and $n_{sdg} = 8n_2$. We first re-write equation (20) using the dense grid.

$$\sum_{n=1}^{N_{sdg}}[Z_{mn}^{p1}I_n^{(1)} + Z_{mn}^{p2}I_n^{(2)} + Z_{mn}^{p3}I_n^{(3)} + Z_{mn}^{p4}I_n^{(4)} + Z_{mn}^{p5}I_n^{(5)} + Z_{mn}^{p6}I_n^{(6)}] = I_m^{(p)inc} \tag{4.32}$$

The Roman numeral subscripts m, n denote indexing with the dense grid. Note that in the method of PBTG, the surface fields on the dense grid are calculated. To reduce the calculation, we make the following three observations.

1) The Green's function in the lower region is heavily attenuative. A medium with a large real part of dielectric constant is normally associated with a large imaginary part at high frequency because of Kramer-Kronig's relation. Let k_2" be the imaginary part of k_2. If $k_2''r > C$, where C is a constant, then the field interaction between the mth and the nth point is vanishingly small. We can define a distance limit as dictated by dissipative loss:

$$r_t = \frac{C}{k_2''} \tag{4.33}$$

outside of which the lower medium Green's function can be set equal to zero. Based on comparisons with the results from SMCG, C is fixed at 1.5 in this paper.

Based on this observation, we calculate the left-hand sides of (32) for $p = 4,5,6$ as follows by approximating

$$Z_{mn}^{pq} \approx \tilde{Z}_{mn}^{pq} = \begin{cases} Z_{mn}^{pq} & r_{mn} \le r_t \\ 0 & r_{mn} \ge r_t \end{cases} \tag{4.34}$$

where r_{mn} is the distance between the mth point and the nth point on the dense grid. Thus $\tilde{Z}_{mn}^{pq}$ $(p = 4,5,6)$ are sparse matrices and Equation (32) for $p = 4,5,6$ becomes

$$\sum_{n=1}^{N_{sdg}}[\tilde{Z}_{mn}^{p1}I_n^{(1)} + \tilde{Z}_{mn}^{p2}I_n^{(2)} + \tilde{Z}_{mn}^{p3}I_n^{(3)} + \tilde{Z}_{mn}^{p4}I_n^{(4)} + \tilde{Z}_{mn}^{p5}I_n^{(5)} + \tilde{Z}_{mn}^{p6}I_n^{(6)}] = 0 \tag{4.35}$$

2) For non-near field interaction, Green's function for the upper medium is slowly varying on the dense grid. Thus when performing matrix and column vector multiplication on the dense grid as indicated in (32), the Green's function of the upper medium is essentially constant over an area of $n_2 \times n_2$ points on the dense grid. Thus we can write

$$\sum_{l=1}^{n_2^2} Z^{pq}_{(m+l')(n+l)} I^{(q)}_{n+l} = Z^{pq}_{m_{mp}n_{mp}} \sum_{l=1}^{n_2^2} I^{(q)}_{n+l} = n_2^2 Z^{pq}_{m_{mp}n_{mp}} \left(\frac{1}{n_2^2} \sum_{l=1}^{n_2^2} I^{(q)}_{n+l}\right) \tag{4.36}$$

where $l' = 1, 2, \ldots, n_2^2$ and the points with indexes m_{mp} and n_{mp} are the central point of the n_2^2 dense grid points of $m+1, m+2, \ldots, m+n_2^2$ and $n+1, n+2, \ldots, n+n_2^2$, respectively. What is performed in (36) is that the surface fields on the dense grid are first averaged before multiplied by the upper medium Green's function.

3) The slowly varying nature of Green's function of the upper medium only applies to non-near field interaction. For near field interaction, Green's functions G_1 and G_2 have similar rate of variation. Thus we separate out a distance, say 1λ, outside of which G_2 is much more rapidly varying than G_1.

Based on the observations above, we decompose the upper medium Green's function into near field and non-near field interactions

$$\sum_{n=1}^{N_{sdg}} Z^{pq}_{mn} I^{(q)}_n = \sum_{n=1}^{N_{sdg}} Z^{pq(s)}_{mn} I^{(q)}_n + \sum_{n=1}^{N_{sdg}} Z^{pq(ns)}_{mn} I^{(q)}_n \tag{4.37}$$

where $Z^{pq(s)}_{mn}$ and $Z^{pq(ns)}_{mn}$ are determined by

$$Z^{pq(s)}_{mn} = \begin{cases} Z^{pq}_{mn} & r_{mn} \le r_f \\ 0 & r_{mn} \ge r_f \end{cases} \tag{4.38}$$

$$Z^{pq(ns)}_{mn} = \begin{cases} 0 & r_{mn} \le r_f \\ Z^{pq}_{mn} & r_{mn} \ge r_f \end{cases} \tag{4.39}$$

Thus r_f is the distance outside which the Green's function of the lower medium is fast varying compared with that of free space Green's function.

Let $\tilde{m}$ and $\tilde{n}$ denote the coarse grid indices. The coarse grid has surface unknowns $\tilde{I}_{\tilde{n}}^{(q)}$, which are averages of the dense grid surface unknowns. Thus if $\bar{r}_{\tilde{n}}$ is centered in the group of the n_2^2 dense grid points of $n+1$, $n+2$, ..., $n+n_2^2$, we have

$$\tilde{I}_{\tilde{n}}^{(q)} = \frac{I_{n+1}^{(q)} + I_{n+2}^{(q)} + \cdots + I_{n+n_2^2}^{(q)}}{n_2^2} \tag{4.40}$$

The Green's function of the upper medium on the coarse grid is represented by $\tilde{Z}_{\tilde{m}\tilde{n}}^{pq}$. Then Equation (32) for $p = 1,2,3$ becomes

$$\sum_{q=1}^{6}\sum_{n=1}^{N_{sdg}} Z_{mn}^{pq(s)} I_n^{(q)} + \sum_{q=1}^{6}[\sum_{\tilde{n}=1}^{N_{scg}} \tilde{Z}_{\tilde{m}\tilde{n}}^{pq(ns)} \tilde{I}_{\tilde{n}}^{(q)}]_{\text{int } p} = I_m^{(p)inc} \tag{4.41}$$

Note in Equation (41) that $\sum_{n=1}^{N_{sdg}} Z_{mn}^{pq(s)} I_n^{(q)}$ includes N_{sdg} values of $m = 1, 2, \bullet\bullet\bullet, N_{sdg}$ on the dense grid, while $\sum_{\tilde{n}=1}^{N_{scg}} \tilde{Z}_{\tilde{m}\tilde{n}}^{pq(ns)} \tilde{I}_{\tilde{n}}^{(q)}$ only has N_{scg} values of $\tilde{m} = 1, 2, \bullet\bullet\bullet, N_{scg}$ on the coarse grid. Thus we first compute $\sum_{\tilde{n}=1}^{N_{scg}} \tilde{Z}_{\tilde{m}\tilde{n}}^{pq(ns)} \tilde{I}_{\tilde{n}}^{(q)}$. Then we use linear interpolation of $\sum_{\tilde{n}=1}^{N_{scg}} \tilde{Z}_{\tilde{m}\tilde{n}}^{pq(ns)} \tilde{I}_{\tilde{n}}^{(q)}$ on the coarse grid to find N_{sdg} values on the dense grid. In Equation (41), we use subscript intp to represent that interpolation. Thus the computational steps for matrix-vector multiplication are associated with the number of surface unknowns on the coarse grid. The algorithm is pictorially described in Figure 1. Note that the surface field is obtained with the dense grid but the CPU time depends on the coarse grid. The PBTG is also used in conjunction with the SMCG that was previously used in computing scattering from 2-dimensional rough surfaces. The computational complexity of the combined algorithm of PBTG/SMCG is $O(N_{scg}log(N_{scg}))$.

4.4 Bistatic Scattering Coefficient and Emissivity

The numerical simulation results are presented in terms of the bistatic scattering coefficients normalized by the incident power. For an incident wave with a polarization β, we have

$$\gamma_{\alpha\beta}(\theta_s,\phi_s;\theta_i,\varphi_i)=\frac{\left|E_\alpha^s\right|^2}{2\eta_1 P_\beta^{inc}} \tag{4.42}$$

The incident power is

$$P_\beta^{inc}=\frac{2\pi^2}{\eta}\int_{k_\rho<k} dk_x dk_y \left|E(k_x,k_y)\right|^2 \frac{k_z}{k} \tag{4.43}$$

where $k_\rho=\sqrt{k_x^2+k_y^2}$.

The horizontal and vertical polarized scattered components of E_α^s are, respectively,

$$E_h^s=\frac{ik}{4\pi}\int_{ds'} dx'dy'\exp(-ik\beta')\{I_x(x',y')\cos\theta_s\cos\phi_s+I_y(x',y')\cos\theta_s\sin\varphi_s$$
$$-I_x(x',y')\frac{\partial f(x',y')}{\partial x'}\sin\theta_s-I_y(x',y')\frac{\partial f(x',y')}{\partial y'}\sin\theta_s-\eta[F_x(x',y')\sin\phi_s-F_y(x',y')\cos\phi_s]\} \tag{4.44}$$

$$E_v^s=\frac{ik}{4\pi}\int_{ds'} dx'dy'\exp(-ik\beta')\{I_x(x',y')\sin\phi_s-I_y(x',y')\cos\phi_s+\eta[F_x(x',y')\cos\theta_s\cos\varphi_s$$
$$+F_y(x',y')\cos\theta_s\sin\phi_s-F_x(x',y')\frac{\partial f(x',y')}{\partial x'}\sin\theta_s-F_y(x',y')\frac{\partial f(x',y')}{\partial y'}\sin\theta_s]\} \tag{4.45}$$

where $\beta'=x'\sin\theta_s\cos\phi_s+y'\sin\theta_s\sin\phi_s+f(x',y')\cos\theta_s$.

For scattering by a dielectric surface, the emissivity of the rough surface at incident angle (θ_i,ϕ_i) (observation angle in emission because of reciprocity) is

$$e_\beta(\theta_i,\phi_i)=1-\frac{1}{4\pi}\iint[\gamma_{h\beta}(\theta_s,\phi_s;\theta_i,\varphi_i)+\gamma_{v\beta}(\theta_s,\phi_s;\theta_i,\varphi_i)]\sin\theta_s d\theta_s d\phi_s \tag{4.46}$$

Thus the emissivity is a measure of energy conservation in a scattering calculation. A rigorous derivation of this result can be found from [Greffet, 1998]. Because of reciprocity, emissivity is the same as absorptivity, the amount of power absorbed by the dielectric in a scattering problem. In passive remote sensing, the brightness temperature T_B of the medium is measured at observation angle (θ_i, ϕ_i). The brightness temperature is

$$T_B(\theta_i, \phi_i) = e_\beta(\theta_i, \phi_i)T \tag{4.47}$$

where T is the physical temperature of the medium in degrees Kelvin. The brightness temperature is commonly measured by the instrument mounted on satellites and aircrafts. The brightness temperature will be measured in the new generation of remote sensing satellites of EOS, ADEOS II, and WINDSAT etc. The brightness temperatures can be measured to an accuracy of 1 degree K. For example for the case of T = 300K, an error of calculation in the emissivity of 0.03 gives an error of 9K in brightness temperature and will not be acceptable. It is important that the scattering calculation obey energy conservation to less than 0.01, so that the error in brightness temperature is limited to less than 3 degrees K.

4.5 Numerical Results and Discussion

In this section, we illustrate the numerical simulation results of wave scattering from 2-D lossy dielectric rough surface (3-D scattering problem). Simulations are based on Gaussian random rough surfaces with Gaussian correlation functions. All the cases are computed with the relative dielectric constants of 17+i2 and 4.06+i0.3, surface area of 8 free space wavelengths by 8 free space wavelengths, rms height from 0.05 to 0.3 wavelengths, and correlation length of 1.0 wavelength.

The results of three methods will be shown: (i) single coarse grid of 8 points per free space wavelength with SMCG (SCG/SMCG), (ii) single dense gird of 16 points per free space wavelength with SMCG (SDG/SMCG), and (iii) PBTG/SMCG. Based on the

experience of 1-D dielectric rough surfaces[Li, 1999], the sampling density of 16 points per wavelength for the permittivity of 17+i2.0 gives convergent results. Thus we regard (ii) as accurate results. We will show that (iii) is as accurate as (ii) and takes much less CPU time. First, we compare the bistatic scattering coefficients for one realization based on different methods. Next, the emissivities and CPU are compared. The results show that the dense grid is required for the case with large dielectric constant. Then the variation of brightness temperatures with observation angles is illustrated and compared with the second order small perturbation method. Finally, the brightness temperature as a function of rms height is shown for different observation angles. We use T = 300 Kelvin as the physical temperature. All the numerical results were computed on a DEC ALPHA workstation.

a) Comparisons of bistatic scattering coefficients computed by various methods.

In Figures 2a and 2b, the comparisons of bistatic scattering coefficients in the plane of incidence $\varphi_i = 0^o$, $\varphi_s = 0^o$ and 180^o of a single realization of rough surface obtained by the SCG/SMCG, SDG/SMCG, and PBTG/SMCG are shown. Figure 2a is for co-polarization and 2b for cross-polarization. The incidence wave is TE wave with the incidence angle of 10 degrees, and the rms height is 0.3 free space wavelength. The relative permittivity of lower medium is 17+i2. There are some small differences among three results. That means it is not strictly necessary to use dense grid for the calculation of the bistatic scattering coefficients for this case of TE incidence. But the PBTG/SMCG can give better results than the SCG/SMCG. In Figures 3a and 3b, the results are shown for TM wave incidence. It is seen that the coarse grid leads to a larger error for TM wave than for TE wave. Comparing the results of Figures 2 and 3 indicates that the PBTG/SMCG can give better results than the SCG/SMCG particularly for cross-polarization component.

b) Comparisons of emissivities and CPU requirements from various methods.

In TABLE I, the emissivities obtained by various methods are shown for one realization. The input parameters of rough surface are the same as before. The difference of emissivities between the SDG/SMCG and the SCG/SMCG for TE wave incidence is 0.0447. It will lead to a difference of 13.41 Kelvin degrees in brightness temperature and is unacceptable in passive remote sensing applications. The emissivities obtained by the PBTG/SMCG are also shown. The difference between the SDG/SMCG and the PBTG/SMCG is only 0.003316. That will give a small difference of 0.99 Kelvin in brightness temperature. The emissivities for TM wave incidence are also shown in TABLE I. It is seen that the PBTG/SMCG can give almost the same results as the SDG/SMCG while the SCG/SMCG cannot. The CPU requirements for various methods are also shown in TABLE I. It is clear that the SDG/SMCG requires the most CPU. On the other hand the PBTG/SMCG is five times faster than the SDG/SMCG and takes even less CPU than the SCG/SMCG. The fact that the PBTG/SMCG requires less CPU than SCG/SMCG is because the former requires less number of conjugate gradient iterations. Thus PBTG/SMCG can obtain the accurate results and require much less CPU than that of the single dense grid.

c) Variation of brightness temperature with observation angles and comparison with results from the second order small perturbation method.

The brightness temperature results based on averaging over 5 realizations are shown in Figures 4a and 4b for horizontal and vertical polarization, respectively. The rough surface is with rms height of 0.3 wavelengths and correlation length of 1.0 wavelength. The observation angles are varied from 10 degrees to 50 degrees. The relative permittivities is 17.0 + i2.0. We note that in the simulation of emissivity in passive remote sensing, only a small number of realizations are required. This is because in passive remote sensing an integration of scattered angles is used and that has built in smoothing. For the case of

permittivity of 17+i2 at the observation angle of 10 degrees, the horizontal emissivity averaged over 10 realizations is 0.699 and is 0.701 for averaging over 5 realizations. The difference between them is 0.002. That means that averaging over 5 realizations can give accurate results. Figure 4a is for TE wave and 4b for TM wave. The brightness temperature shown in solid line is from the second order small perturbation method (SPM) [Yueh, 1994], in dash-dot line is from flat surface, and in circle is from numerical simulation results. It is shown that surface roughness increases the brightness temperature over flat surface for horizontal polarization. It can increase or decrease the brightness temperature for vertical polarization depending on observation angles. Although it is known that the SPM cannot give the correct results of emissivities for moderate to large rms slope, nevertheless the SPM is often used beyond the limit of validity because the results satisfy energy conservation. Thus it is useful to demonstrate the difference between the SPM and numerical simulations. For TE wave, the numerical results show that the brightness temperature decreases with observation angles. On the other hand the SPM results show that brightness temperature increases with observation angles. That means that the SPM cannot give the correct result for the brightness temperature for this case. The brightness temperature for the permittivity of 4.06+i0.3 is also plotted in the figures. Similar features are exhibited in this case. It can be seen that surface roughness has a larger influence in brightness temperature for large permittivity than for the small permittivity. For horizontal polarization, more energy is reflected with the increase of incident angles. Thus the brightness temperature decreases with the observation angles. For vertical polarization, more energy is transmitted into lower medium with the increase of incident angles if angle is less than the Brewster angle. Thus the brightness temperature increases with the observation angles.

d) Variation of brightness temperatures with rms height and comparison with that from the second order small perturbation method.

The brightness temperatures as functions of rms height are plotted in Figure 5a for horizontal polarization and in Figure 5b for vertical polarization for the observation angles of 10, 30, and 50 degrees, respectively. The correlation length is 1 wavelength and the permittivity is 17+2i. We also show the results from the second order SPM. The numerical results are averaged over 5 realizations. For the small rms height, the two results are in good agreement. It illustrates that the algorithm can give the correct emissivity calculations. For the case of flat surface, one needs to use many angles in integrating near the specular direction to give correct emissivity. With the increase of rms height, the differences between them get large, especially for the observation angles of 10 and 50 degrees. Because the numerical results and SPM results cross each other around the observation angle of 30 degrees as shown in Figure 4, the differences between them is small. For the rms height of 0.3 wavelength, the difference between SPM and numerical simulation in horizontal polarization can be as large as 30 Kelvin degrees in the brightness temperatures at the observation angle of 50 degrees. Thus the SPM results have to be modified in emissivity calculation for the moderate to large rms height/large slope. Another feature shown in the figures is that the surface roughness increases the brightness temperature for all the cases except for the vertical polarization at observation angle of 50 degrees. The reason is that the observation angle of 50 degrees is close to the Brewster angle. At the Brewster angle, the emissivity of flat surface is the maximum for vertical polarization. Thus surface roughness will lead to decrease the emissivity.

e) Comparisons with empirical formula.

In passive remote sensing with soil, an empirical formula, which has been used for many years, is as follows [Wang, 1983]

$$T_{Bv}(\theta_i,\varphi_i) = \{1-[r_{v0}(\theta_i,\varphi_i)(1-Q)+r_{h0}(\theta_i,\varphi_i)Q]e^{-H\cos^2\theta_i}\}T \tag{4.48}$$

$$T_{Bh}(\theta_i,\varphi_i) = \{1-[r_{h0}(\theta_i,\varphi_i)(1-Q)+r_{v0}(\theta_i,\varphi_i)Q]e^{-H\cos^2\theta_i}\}T \tag{4.49}$$

where T_{Bv} and T_{Bh} are brightness temperatures for vertical and horizontal polarizations, respectively, T is physical temperature of dielectric medium, and Q and H are empirical constants that are used to fit the data. The parameters r_{v0} and r_{h0} are the flat surface Fresnel reflectivity of vertical and horizontal polarized waves, respectively. The empirical parameters Q represents coupling between polarizations and H represents depletion of reflectivity. Both are assumed to be constants.

In Table II, we tabulate the brightness temperatures of figure 4 based on numerical simulations for the permittivity of 17+i2.0 and also use the simulated results to compute Q and H parameters from (48) and (49). The table shows that Q and H are actually functions of observation angles. In the original proposal, H is supposed to be $4k^2h^2$ where h is the rms height. For this case, $4k^2h^2 = 14.19$. From the table, H is much smaller. The table shows that Q and H are empirical parameters that are deprived of physical meaning.

4.6 Conclusions

In this paper, we have extended the PBTG method from 1-D dielectric rough surfaces to 2-D dielectric rough surfaces and combined it with the SMCG. The method saves both CPU and memory while satisfying the accuracy requirement for wave scattering from lossy dielectric rough surface with large permittivity. We have shown that the PBTG/SMCG gives accurate results for the emissivities. The computational complexity and the memory requirements of the present algorithm are $O(N_{scg}log(N_{scg}))$ and $O(N_{scg})$, respectively, where N_{scg} is the number of grid points for the coarse grid. The method can be used for extensive calculations of emissivities of rough surfaces of soils, ocean and snow/ground interfaces.

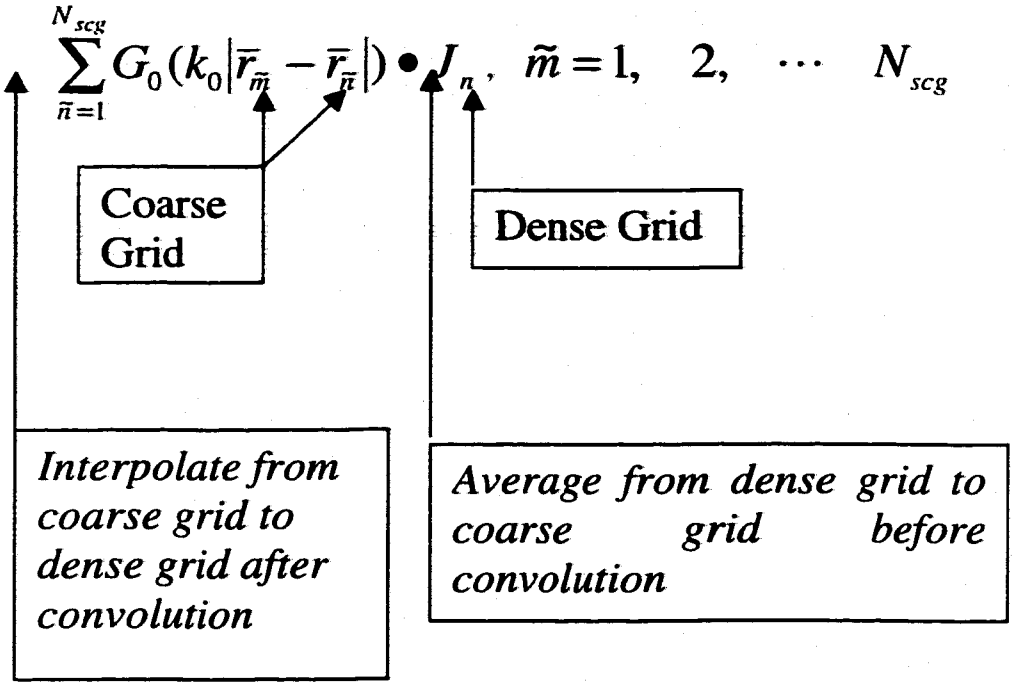

Figure 4.1 Illustration of physics-based two-grid method

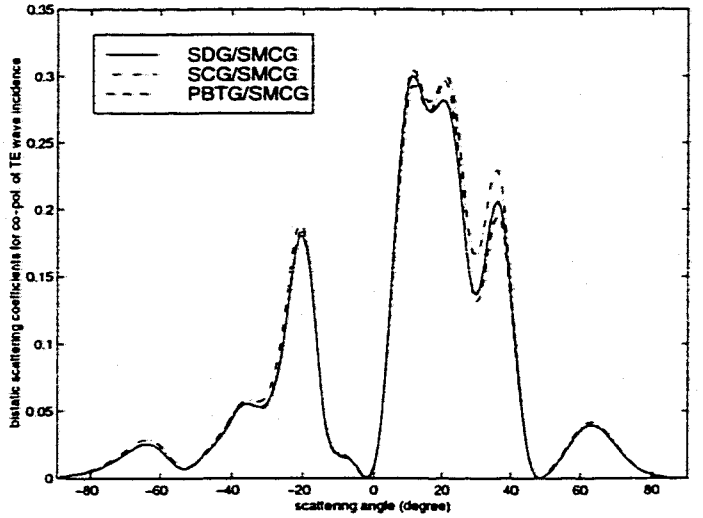

(a)

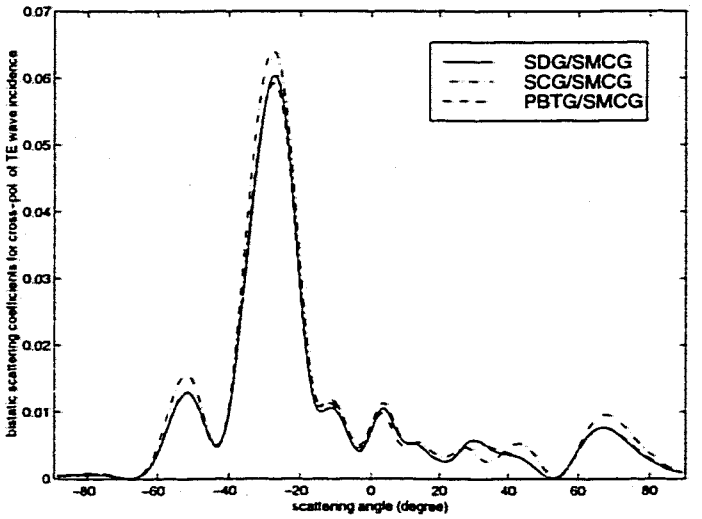

(b)

Figure 4.2 Comparison of the bistatic scattering coefficients between the SDG/SMCG, SCG/SMCG, and PBTG/SMCG for the TE wave incidence. The case is with rms height of 0.3 wavelengths, correlation lengths of 1 wavelength, surface lengths of 8 by 8 wavelengths, and relative permittivity of 17 + 2i at incidence angle of 10 degrees. a). co-polarization b). cross-polarization.

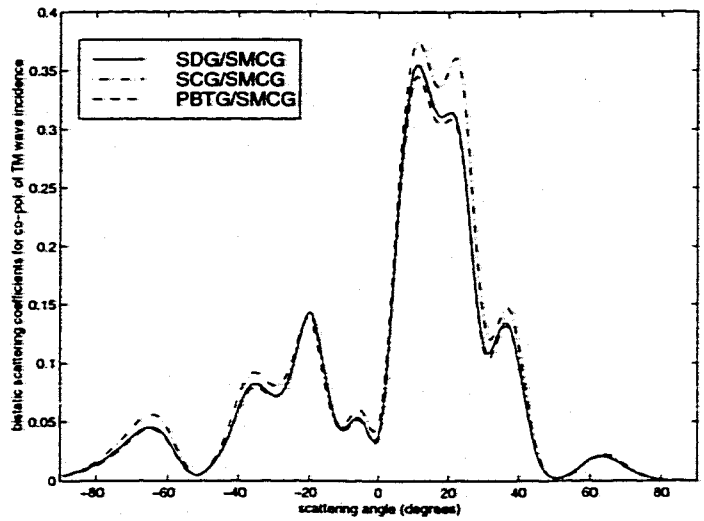

(a)

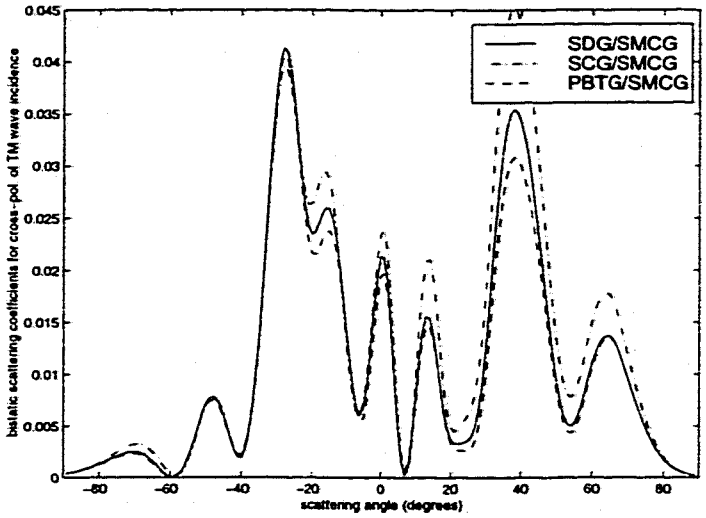

(b)

Figure 4.3 Same as Figures 2 except for TM wave incidence.

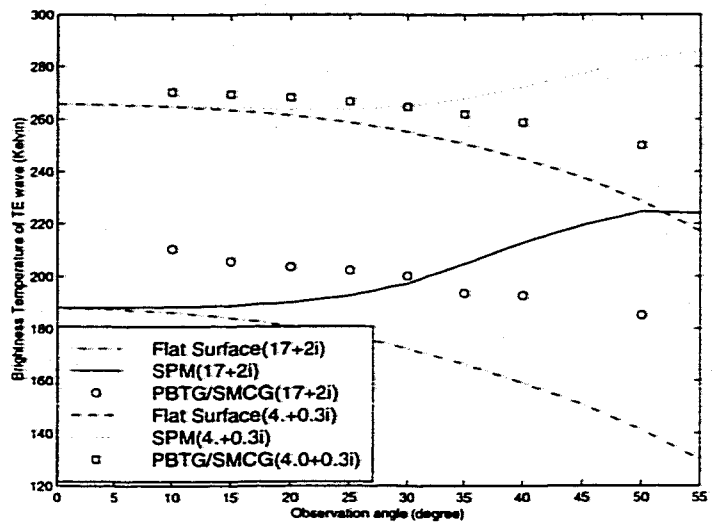

(a)

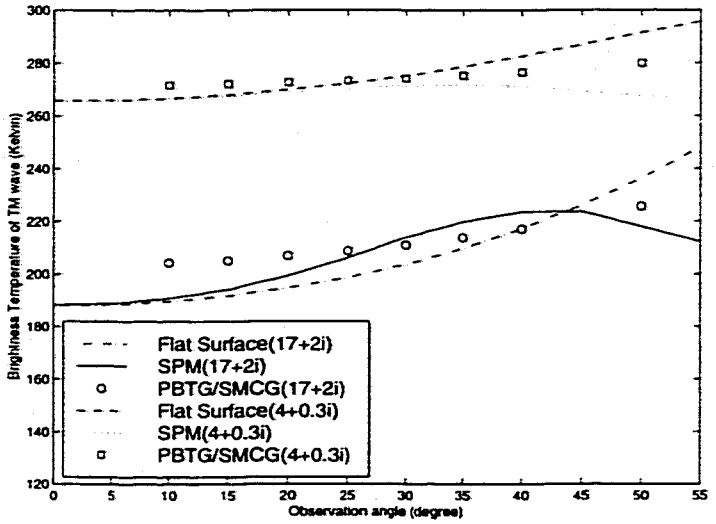

(b)

Figure 4.4 The brightness temperature of Monte Carlo simulation averaged over 5 realizations as a function of observation angles and comparisons with that from the second order small perturbation method and flat surface. The case is with rms height of 0.3 wavelengths, correlation lengths of 1.0 wavelength, relative permittivities of 17+i2.0 and 4.06+i0.3, and physical temperature of 300 Kelvin degrees. a). TE wave b). TM wave.

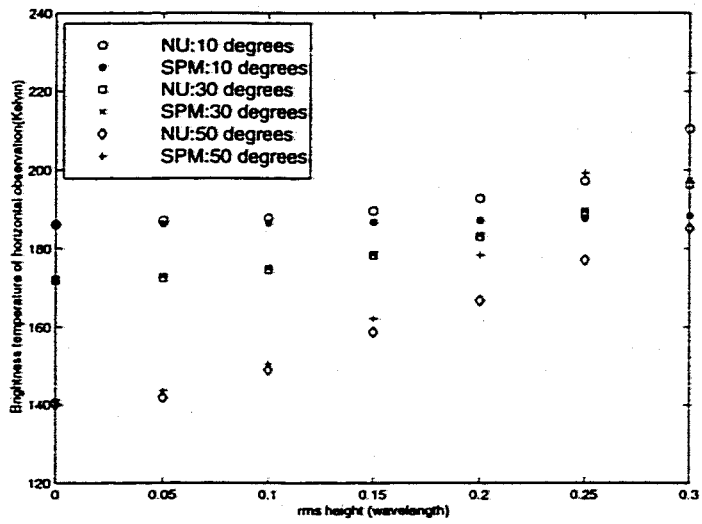

(a)

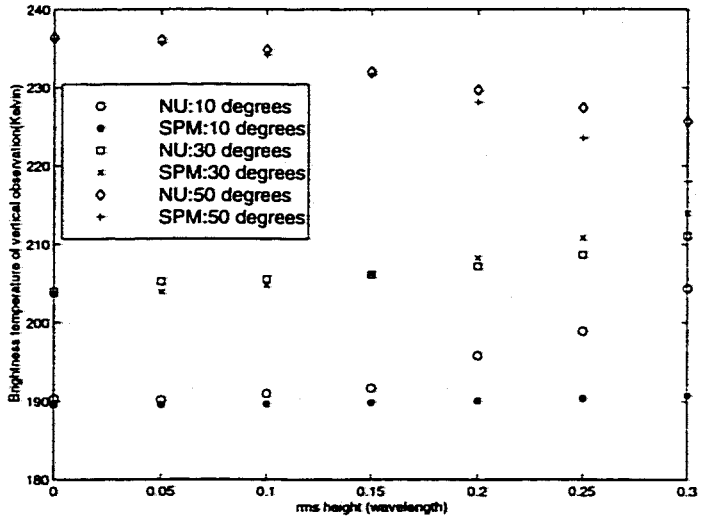

(b)

Figure 4.5 The brightness temperature of Monte Carlo simulation averaged over 5 realizations as a function of rms heights and comparisons with that from the second order small perturbation method. The rms height of zero means flat surface. The case is with correlation lengths of 1.0 wavelength, relative permittivity of 17 + 2i, and physical temperature of 300 Kelvin degrees at observation angles of 10, 30, and 50 degrees. a). TE wave b). TM wave.

Table 4.1 Comparison of emissivities and cpu based on different methods

Method	Incidence Wave	CPU time (hours)	Emissivity	Difference of emissivity*	Difference of Brightness Temperature
SDG/SMCG	TE	45.05	0.6612		
SCG/SMCG	TE	9.11	0.6165	-0.044	13.4
PBTG/SMCG	TE	8.48	0.6645	0.0033	0.99
SDG/SMCG	TM	48.83	0.6690		
SCG/SMCG	TM	10.16	0.6224	-0.046	13.97
PBTG/SMCG	TM	8.68	0.6729	0.0039	1.17

The difference of emissivity means the emissivity minus the emissivity of corresponding SDG/SMCG.

Table 4.2 The Brightness Temperatures of Fig. 4

Observation angle (degrees)		Flat Surface	SPM	PBTG/SMCG	Q*	H*
10	TE	186.2	188.4	210.4	1.5997	1.1971
	TM	189.6	190.7	204.4		
15	TE	184.1	188.9	205.7	0.5362	0.1825
	TM	191.7	194.3	205.2		
20	TE	181.1	190.1	203.7	0.3592	0.1907
	TM	194.7	199.3	206.9		
25	TE	177.2	192.8	202.3	0.3198	0.2081
	TM	198.7	205.8	208.8		
30	TE	172.3	197.7	200.2	0.2943	0.2284
	TM	203.7	213.9	211.1		
35	TE	166.3	204.5	193.6	0.2287	0.2242
	TM	209.8	221.1	213.9		
40	TE	159.2	212.3	192.7	0.2519	0.2759
	TM	217.3	224.4	217.2		
50	TE	141.1	225.3	185.1	0.2497	0.3927
	TM	236.3	218.2	225.7		

* Parameters Q and H are computed from the brightness temperatures from the numerical simulation results.

Chapter 5

Application of Physics-based Two-Grid Method and Sparse Matrix Canonical Grid Method for Numerical Simulations of Emissivities of Soils with Rough Surfaces at Microwave Frequencies

5.1 Introduction

The surface roughness, soil moisture, soil type, and physical temperature determine the thermal emission of soils with rough surfaces. The measurements of brightness temperature can provide information about soil moisture content. Soil moisture is an important parameter that affects global climate change. Thus the brightness temperatures of soils will be measured by the new generations of satellites such as ADEOS II and EOS-PM. Scattering by random rough surfaces has been studied by the analytic methods such as Kirchhoff method and the small perturbation method and expressed in terms of rough surface parameters such as rms height and correlation length [Tsang, 1985]. However, both methods have restricted domain of validity. For example, to match the experimental data of the same soil surface at L and C bands, the different rms heights and correlation lengths are used [Mo, 1987]. Another common approach is to use empirical formulas such as the h and Q empirical parameters [Wang, 1983].

Microwave interactions with rough surfaces of soils are governed exactly by Maxwell's equations. Thus it is desirable to solve exactly the 3-dimensional Maxwell's

equations with 2-dimensional random rough surfaces. In the past, numerical simulations are mainly used to compare or validate analytic results. However in this paper, we show that full 3-D simulations can be performed readily with the use of fast computational methods. Because the method is fast, 3-D simulation results can now be computed extensively for practical applications. The most common method that has been used in numerical simulations is the surface integral equation method and its solution by the method of moments (MoM). Most of Monte Carlo simulations have been applied to calculate the bistatic scattering coefficients in active remote sensing. There have been no numerical simulations studying emissivity of soils with 2-dimensional rough surfaces. There are several fast computational methods proposed [Rino, 1992; Tsang, 1995; Michielssen, 1996; Kapp, 1996; Chou, 1998; Donohue, 1998] for 2-D problem with 1-D rough surfaces. But to date, the methods that have been applied to 3 dimensional simulations are the sparse matrix canonical grid method (SMCG) [Tsang, 1994; Johnson, 1996; Pak, 1995; Pak, 1997] and the fast multipole method (FMM) [Jandhyala, 1998 a & b]. The computational complexity of SMCG is of O(NlogN) and the computational complexity of FMM is of O(N), Where N is the number of sampling points on the computational grid.

Another major difficulty of performing numerical simulations of emissivity is that the wet soils are with large permittivity that requires a large number of sampling points per square wavelength. In this paper, numerical simulations of emissivity of wet soils with 2-dimensional rough surfaces are studied based on the physics-based two-grid method (PBTG) [Tsang, 1997; Li, 1999] in conjunction with the sparse matrix canonical grid method (SMCG). In PBTG, two grids are used: a dense grid and a coarse grid. The coarse grid is that of the usual 64 points per square wavelength. The dense grid ranges from 256 points per square wavelength or higher depending on the relative permittivity of the lossy dielectric medium. The surface fields are calculated on the dense grid. In the formulation of the surface integral equations, two Green's functions are used to convolve with the surface fields, the free space Green's function and the Green's function of the lossy

dielectric medium. Because of Kramer-Kronig relation, a large real part of dielectric constant is usually associated with a large imaginary part at microwave frequency. The PBTG is based on two observations. (1) the Green's function of the lossy dielectric is attenuative which makes it space limited, and (2) the Green's function of free-space is slowly varying on the dense grid making it spatial frequency limited. The first observation results in a sparse matrix for the Green's function of the lossy dielectric. When this Green's function is convolved with the surface fields on the dense grid, it will be just the product of a sparse matrix and a column vector. The second observation allows us, when using the free-space Green's function to convolve with the surface fields of dense grid, to first average the values of surface unknowns on the dense grid and then place them on the coarse grid. Thus the PBTG speeds up the CPU and yet preserves the accuracy of the solution. The computational complexity of the present algorithm is of O(NlogN), where N is the number of sampling points on the coarse grid. The simulation results can give the emissivity as a result of 3-D solution of Maxwell equations. In this paper, we report and show extensive illustrations and tabulations of the results of emissivities for rough soils with Gaussian spectrum at L and C bands. The same physical roughness parameters are used at L and C bands. The results are important to better understand the effects of surface roughness on the microwave thermal emission of soils.

The paper is arranged in the following, In Section II, the formulation of the problem of wave impinging upon a 2-D dielectric surface (3-D scattering problem) is given in terms of surface integral equations. Then the surface integral equations are converted into a matrix equation using a dense grid discretization. In Section III, we describe the physics-based two-grid algorithm and combine it with the sparse matrix canonical grid method. In section IV, the tapered plane incident wave is described. The mathematical expressions of the bistatic scattering coefficients and the emissivity are given in Section V. In Section VI, the numerical results are illustrated.

5.2 Formulation and Single Grid Implementation

Consider an electromagnetic wave, $\overline{E}_i(\overline{r})$ and $\overline{H}_i(\overline{r})$, with a time dependence of $e^{-i\omega t}$, impinging upon a 2-D dielectric rough surface with a random height profile of $z = f(x, y)$. The surface fields satisfy the Stratton-Chu integral equations[Pak, 1997]:

$$\frac{\overline{E}(\overline{r})}{2} - \left\{\int \hat{n}\times\overline{H}(\overline{r}')i\omega\mu G_0 dS' + P\int[(\hat{n}\times\overline{E}(\overline{r}'))\times\nabla' G_0 + \hat{n}'\cdot\overline{E}(\overline{r}')\nabla' G_0]dS'\right\} = \overline{E}^{inc}(\overline{r}) \qquad (5.1)$$

$$\frac{\overline{H}(\overline{r})}{2} - \left\{\int (-i\omega)\hat{n}\times\overline{E}(\overline{r}')\varepsilon_0 G_0 dS' + P\int[(\hat{n}\times\overline{H}(\overline{r}'))\times\nabla' G_0 + \hat{n}'\cdot\overline{H}(\overline{r}')\nabla' G_0]dS'\right\} = \overline{H}^{inc}(\overline{r}) \qquad (5.2)$$

$$-\frac{\overline{E}_1(\overline{r})}{2} - \left\{\int (i\omega)\hat{n}\times\overline{H}_1(\overline{r}')\mu G_1 dS' + P\int[(\hat{n}\times\overline{E}_1(\overline{r}'))\times\nabla' G_1 + \hat{n}'\cdot\overline{E}_1(\overline{r}')\nabla' G_1]dS'\right\} = 0 \qquad (5.3)$$

$$-\frac{\overline{H}_1(\overline{r})}{2} - \left\{\int -\hat{n}\times\overline{E}_1(\overline{r}')i\omega\varepsilon_1 G_1 dS' + P\int[(\hat{n}\times\overline{H}_1(\overline{r}'))\times\nabla' G_1 + \hat{n}'\cdot\overline{H}_1(\overline{r}')\nabla' G_1]dS'\right\} = 0 \qquad (5.4)$$

Where $\overline{r}'$ denote a source point and $\overline{r}$ denote a field point on the rough surface. The integral $P\int$ denotes a Cauchy integral and G_0 and G_1 are the 3-dimensional Green's functions of free space and the lower dielectric medium, respectively. The unit normal vector $\hat{n}'$ refers to primed coordinate and points away from the second medium. Using unit normal vector of $\hat{n}$ cross the above four equations, respectively, and then adding equation (1) and (3) and equation (2) and (4), respectively, we derive the following two vector equations.

$$-\hat{n}\times\left\{\int \hat{n}\times\overline{H}(\overline{r}')i\omega\mu(G_0 + G_1)dS' + P\int[(\hat{n}\times\overline{E}(\overline{r}'))\times\nabla'(G_0 + G_1) + \hat{n}'\cdot\overline{E}(\overline{r}')\nabla'(G_0 + \frac{\varepsilon_0}{\varepsilon_1}G_1)]dS'\right\}$$
$$= \hat{n}\times\overline{E}^{inc}(\overline{r}) \qquad (5.5)$$

$$\hat{n}\times\left\{\int (-i\omega)\hat{n}\times\overline{E}(\overline{r}')(\varepsilon_0 G_0 + \varepsilon_1 G_1)dS' + P\int[(\hat{n}\times\overline{H}(\overline{r}'))\times\nabla'(G_0 + G_1) + \hat{n}'\cdot\overline{H}(\overline{r}')\nabla'(G_0 + G_1)]dS'\right\}$$
$$= -\hat{n}\times\overline{H}^{inc}(\overline{r}) \qquad (5.6)$$

We have used the boundary conditions in deriving above two equations. Now we project equation (5) and (6) into the directions of $\hat{x}$, $\hat{y}$, and equation (1) and (4) into the

direction of $\hat{n}$, respectively. The six scalar integral equations are obtained because there are six unknowns of each sampling point. The method of moments (MoM) is used to discretize the scalar integral equation. The resulting matrix equations are

$$\sum_{n=1}^{N}\sum_{q=1}^{6} Z_{mn}^{pq} I_n^{(q)} = I_m^{(p)inc} \tag{5.7}$$

Where Z_{mn}^{pq} are the impedance element given by the free space Green's function and the dielectric medium Green's function, $I_n^{(q)}$ are unknown surface fields needed to be solved, and $I_m^{(p)inc}$ are given by the incident fields. The parameter N is the number of points we use to sample the rough surface.

To solve equation (7), the surface fields can be obtained. Traditionally, the matrix equation is solved by matrix inversion or Gaussian elimination methods, which require $O(N^3)$ operations and $O(N^2)$ memory. Because of large CPU and memory requirements, the iterative techniques are used to save CPU. The CPU requirement for iterative techniques is mainly determined by the matrix-vector multiplication time. Typical iterative techniques such as conjugate gradient method need $O(N^2)$ operations and $O(N^2)$ memory. To reduce CPU and memory requirements, several methods are developed to facilitate the matrix-vector multiplication such as the FMM and the SMCG. The computational complexities are of the orders of $O(N)$ for the FMM[Jandhyala, 1998 a & b] and $O(N \log N)$ for the SMCG[Tsang, 1994; Johnson, 1996; Pak, 1995; Pak, 1997]. When using the methods to solve the problem of wave scattering from dielectric rough surfaces with modest permittivity, usually eight points per free space wavelength are used to sample the rough surface. We call such a sampling a single coarse grid (SCG). The total number of sampling points of SCG is N_{scg}. If the lower medium has a high relative permittivity, say $17+2i$, the sampling frequency needs to be higher than that of coarse grid. We call this a single dense grid (SDG). Thus the computational operations of the SMCG is $O(N_{sdg} \log N_{sdg})$, where N_{sdg} is the number of grid points on the dense

grid. In the next section, we describe the PBTG that is as accurate as SDG and yet can reduce the computational steps to O($N_{scg} \log N_{scg}$).

5.3 Physics-Based Two-Grid Method

Assume that the upper medium is the free space and the lower medium is lossy with large permittivity ε_1. The wavelength λ_1 in the medium is approximately n_1 times shorter than the wavelength λ in the free space. Where n_1 is of the nearest integer of $real(\sqrt{\varepsilon_1})$. Thus the number of sampling points needed in the lower medium should be n_1 times that of the free space.

In the physics-based two-grid method, we use two grids with sampling points per wavelength of n_{scg} (coarse grid) and n_{sdg} (dense grid), respectively. Let N_{sdg} and N_{scg} be respectively the total number of points on the dense grid and the coarse grid.

$$N_{sdg} = (n_{sdg} \frac{L_x}{\lambda})(n_{sdg} \frac{L_y}{\lambda}) \tag{5.8}$$

$$N_{scg} = (n_{scg} \frac{L_x}{\lambda})(n_{scg} \frac{L_y}{\lambda}) \tag{5.9}$$

Where L_x and L_y are the surface lengths in the directions of x and y. For example $n_{scg} = 8$ and $n_{sdg} = 8n_1$. We first re-write equation (7) using the dense grid.

$$\sum_{n=1}^{N_{sdg}} \sum_{q=1}^{6} Z_{mn}^{pq} I_n^{(q)} = I_m^{(p)inc} \tag{5.10}$$

The Roman numeral subscripts m, n denote indexing with the dense grid. Note that in the method of the PBTG, the surface fields on the dense grid are calculated. To reduce the calculation, the real part of products of distance and Green's functions of free space and medium are plotted in figure 1. The reason for that is that the field received at observed

point from all points at distance r is proportional to the products. The following observations are made from the figure.

1) The Green's function in the lossy medium is heavily attenuative. This is a space-limited property of the dielectric medium Green's function. A medium with a large real part of dielectric constant is associated with a large imaginary part at microwave frequency because of Kramer-Kronig's relation. Let $k_1^{''}$ be the imaginary part of k_1. If $k_1^{''} r > C$, where C is a constant, then the field interaction between the mth and the nth point is vanishingly small. We can define a distance limit as dictated by dissipative loss:

$$r_l = \frac{C}{k_1^{''}} \tag{5.11}$$

outside of which the lower medium Green's function can be set equal to zero. Thus we can approximate the elements of Z_{mn}^{pq} as follows

$$Z_{mn}^{pq} \approx Z_{mn}^{pq(s)} + Z_{mn}^{pq(ns)} \tag{5.12}$$

The element of $Z_{mn}^{pq(s)}$ is original when $r_{mn} \le r_l$ and zero when $r_{mn} > r_l$. The element of $Z_{mn}^{pq(ns)}$ is determined only by the terms including the free space Green's function when $r_{mn} > r_l$ and zero when $r_{mn} \le r_l$. Where r_{mn} is the distance between the mth point and the nth point on the dense grid. The elements of $Z_{mn}^{pq(s)}$ compose sparse matrices and the left side of equation (10) becomes

$$\sum_{n=1}^{N_{wg}} Z_{mn}^{pq} I_n^{(q)} \approx \sum_{n=1}^{N_{wg}} Z_{mn}^{pq(s)} I_n^{(q)} + \sum_{n=1}^{N_{wg}} Z_{mn}^{pq(ns)} I_n^{(q)} \tag{5.13}$$

2) Green's function of free space is slowly varying on the dense grid. This is a spatial frequency-limited property of the free space Green's function on the dense grid. Thus when performing matrix and column vector multiplication of the last term on the dense grid as indicated in (13), the Green's function of free space is essentially constant over an area of $n_1 \times n_1$ points on the dense grid. Thus we can write

$$\sum_{l=1}^{n_1^2} Z^{pq(ns)}_{(m+l')(n+l)} I^{(q)}_{n+l} \approx Z^{pq(ns)}_{m_{mp}n_{np}} \sum_{l=1}^{n_1^2} I^{(q)}_{n+l} = n_1^2 Z^{pq(ns)}_{m_{mp}n_{np}} \left(\frac{1}{n_1^2} \sum_{l=1}^{n_1^2} I^{(q)}_{n+l}\right) \tag{5.14}$$

Where $l' = 1, 2, \ldots, n_1^2$ and the points with indexes m_{mp} and n_{mp} are the central point of the n_1^2 dense grid points of $m+1, m+2, \ldots, m+n_1^2$ and $n+1, n+2, \ldots, n+n_1^2$, respectively. What is performed in (14) is that the surface fields on the dense grid are first averaged before multiplied by the free space Green's function on the coarse grid.

Let $\tilde{m}$ and $\tilde{n}$ denote the coarse grid indices. The coarse grid has surface unknowns $\tilde{I}^{(q)}_{\tilde{n}}$, which are averages of the dense grid surface unknowns. Thus if $\bar{r}_{\tilde{n}}$ is centered in the group of the n_1^2 dense grid points of $n+1, n+2, \ldots, n+n_1^2$, we have

$$\tilde{I}^{(q)}_{\tilde{n}} = \frac{I^{(q)}_{n+1} + I^{(q)}_{n+2} + \cdots + I^{(q)}_{n+n_1^2}}{n_1^2} \tag{5.15}$$

Assume that the Green's function of the free space on the coarse grid is represented by $\tilde{Z}^{pq}_{\tilde{m}\tilde{n}}$.

Then equation (10) becomes

$$\sum_{q=1}^{6} \sum_{n=1}^{N_{sdg}} Z^{pq(s)}_{mn} I^{(q)}_{n} + \sum_{q=1}^{6} \left[\sum_{\tilde{n}=1}^{N_{scg}} \tilde{Z}^{pq(ns)}_{\tilde{m}\tilde{n}} \tilde{I}^{(q)}_{\tilde{n}}\right]_{\text{int}\,p} = I^{(p)inc}_{m} \tag{5.16}$$

Note in equation (16) that $\sum_{n=1}^{N_{sdg}} Z^{pq(s)}_{mn} I^{(q)}_{n}$ includes N_{sdg} values of $m = 1, 2, \bullet\bullet\bullet, N_{sdg}$ on the dense grid, while $\sum_{\tilde{n}=1}^{N_{scg}} \tilde{Z}^{pq(ns)}_{\tilde{m}\tilde{n}} \tilde{I}^{(q)}_{\tilde{n}}$ only has N_{scg} values of $\tilde{m} = 1, 2, \bullet\bullet\bullet, N_{scg}$ on the coarse grid. Thus we first compute $\sum_{\tilde{n}=1}^{N_{scg}} \tilde{Z}^{pq(ns)}_{\tilde{m}\tilde{n}} \tilde{I}^{(q)}_{\tilde{n}}$ on the coarse grid. Then we use linear interpolation of $\sum_{\tilde{n}=1}^{N_{scg}} \tilde{Z}^{pq(ns)}_{\tilde{m}\tilde{n}} \tilde{I}^{(q)}_{\tilde{n}}$ on the coarse grid to find N_{sdg} values on the dense grid. In equation (16), we use subscript intp to represent that interpolation. Thus the computational steps for matrix-vector multiplication are associated with the number of

surface unknowns on the coarse grid. The algorithm is pictorially described in Figure 2. Note that the surface field is obtained with the dense grid but the CPU time depends on the coarse grid. The PBTG is also used in conjunction with the SMCG that was previously used in computing scattering from 2-dimensional rough surfaces. The computational complexity of the combined algorithm of PBTG/SMCG is $O(N_{scg}log(N_{scg}))$ for non-near field interactions and $O(N_{sdg})$ for near field interactions.

5.4 Incident fields

Because of limitations of numerical simulations, the finite surface area has to be used. To avoid edge effects, the incident field is tapered so that the illuminated rough surface can be confined to the surface area $L_x \times L_y$ [Pak, 1997]. The direction of incident wave is $\hat{k}_i = \sin\theta_i \cos\phi_i \hat{x} + \sin\theta_i \sin\phi_i \hat{y} - \cos\theta_i \hat{z}$.

The incident fields are given as

$$\overline{E}_i(\overline{r}) = \int_{-\infty}^{+\infty} dk_x \int_{-\infty}^{+\infty} dk_y \exp(ik_x x + ik_y y - ik_z z) E(k_x, k_y) \hat{e}(-k_z) \tag{5.17}$$

$$\overline{H}_i(\overline{r}) = -\frac{1}{\eta} \int_{-\infty}^{+\infty} dk_x \int_{-\infty}^{+\infty} dk_y \exp(ik_x x + ik_y y - ik_z z) E(k_x, k_y) \hat{h}(-k_z) \tag{5.18}$$

For TE wave incidence

$$\hat{e}(-k_z) = \frac{1}{k_\rho}(\hat{x}k_y - \hat{y}k_x) \tag{5.19}$$

$$\hat{h}(-k_z) = \frac{k_z}{kk_\rho}(\hat{x}k_x + \hat{y}k_y) + \frac{k_\rho}{k}\hat{z} \tag{5.20}$$

and for TM wave incidence

$$\hat{h}(-k_z) = -\frac{1}{k_\rho}(\hat{x}k_y - \hat{y}k_x) \tag{5.21}$$

$$\hat{e}(-k_z) = \frac{k_z}{kk_\rho}(\hat{x}k_x + \hat{y}k_y) + \frac{k_\rho}{k}\hat{z} \tag{5.22}$$

with $k_z = \sqrt{k^2 - k_\rho^2}$ and $k_\rho = \sqrt{k_x^2 + k_y^2}$. In the above k and η are the wavenumber and wave impedance of free space, respectively. The spectrum of the incident wave, $E(k_x, k_y)$, is given as

$$E(k_x, k_y) =$$

$$\frac{1}{4\pi^2}\int_{-\infty}^{\infty} dx \int_{-\infty}^{\infty} dy \exp(-ik_x x - ik_y y)\exp[i(k_{ix}x + k_{iy}y)(1+w)]\exp(-t) \tag{5.23}$$

where $t = t_x + t_y = (x^2 + y^2)/g^2$ and

$$t_x = \frac{(\cos\theta_i \cos\phi_i x + \cos\theta_i \sin\phi_i y)^2}{g^2 \cos^2\theta_i} \tag{5.24}$$

$$t_y = \frac{(-\sin\phi_i x + \cos\phi_i y)^2}{g^2} \tag{5.25}$$

$$w = \frac{1}{k_1^2}\left(\frac{2t_x - 1}{g^2\cos^2\theta_i} + \frac{2t_y - 1}{g^2}\right) \tag{5.26}$$

The parameter g controls the tapering of the incident wave.

5.5 Bistatic Scattering Coefficient and Emissivity

The numerical simulation results are presented in terms of the bistatic scattering coefficients normalized by the incident power. For an incident wave with a polarization β, we have

$$\gamma_{\alpha\beta}(\theta_s,\phi_s;\theta_i,\varphi_i)=\frac{\left|E_\alpha^s\right|^2}{2\eta_1 P_\beta^{inc}} \tag{5.27}$$

The incident power is

$$P_\beta^{inc}=\frac{2\pi^2}{\eta}\int_{k_\rho<k} dk_x dk_y \left|E(k_x,k_y)\right|^2 \frac{k_z}{k} \tag{5.28}$$

The electric field of E_α^s is α component of the scattered fields.

For scattering by a dielectric surface, the emissivity of the rough surface at incident angle (θ_i,ϕ_i) (observation angle in emission because of reciprocity) is

$$e_\beta(\theta_i,\phi_i)=1-\frac{1}{4\pi}\iint[\gamma_{h\beta}(\theta_s,\phi_s;\theta_i,\varphi_i)+\gamma_{v\beta}(\theta_s,\phi_s;\theta_i,\varphi_i)]\sin\theta_s d\theta_s d\phi_s \tag{5.29}$$

Thus the emissivity is a measure of energy conservation in a scattering calculation. Because of reciprocity, emissivity is the same as absorptivity, the amount of power absorbed by the dielectric in a scattering problem. In passive remote sensing, the brightness temperature T_B of the medium is measured at observation angle (θ_i,ϕ_i). The brightness temperature is

$$T_B(\theta_i,\phi_i)=e_\beta(\theta_i,\phi_i)T \tag{5.30}$$

where T is the physical temperature of the medium in degrees Kelvin. The brightness temperature will be measured in the new generation of remote sensing satellites of EOS, ADEOS II, and WINDSAT etc. The brightness temperatures can be measured to an accuracy of 1 degree K. For example for the case of T = 300K, an error of calculation in the emissivity of 0.03 gives an error of 9K in brightness temperature and will not be acceptable. It is important that the scattering calculation obey energy conservation to less than 0.01, so that the error in brightness temperature is limited to less than 3 degrees K. Also, the difference in brightness temperature of a flat surface and a rough surface can be only a few degrees K. Thus accuracy is required to study the effect of roughness.

5.6 Numerical Results and Discussion

In this section, we illustrate the numerical simulation results of emissivities of wet soils with 2-D rough surface (3-D problem). Simulations are based on Gaussian random rough surfaces with Gaussian correlation functions. Surface area is taken as 64 square wavelengths. The permittivities of wet soil by weight of the soil moisture at L band (1.4 GHz) [Tsang, 1982] are listed in Table I. The permittivities of soil by the soil moisture in volumetric water contents (cm^3/cm^3) [Wang, 1980; Wang, 1983] for L and C bands are given in Table II. C band is at 5 GHz. All the cases are computed at the observation angle of 50 degrees. In Tables III to VII, emissivities calculated are tabulated for interested readers. We also illustrate the brightness temperatures in Figures 3 to 7. The physical temperature is taken as 300 Kelvin for all cases.

a) Variation of brightness temperatures at L band of wet soil with the soil moisture and correlation length at fixed rms height.

In Figures 3 and 4, we plot the brightness temperatures as a function of soil moistures by weight at L band for horizontal and vertical polarizations, respectively. The corresponding permittivities are taken from Table I. The rms height is fixed at 0.1 wavelength and the correlation lengths are varied from 0.33 to 1.0 wavelengths. It is shown that brightness temperature decreases with the increase of soil moistures for both horizontal and vertical polarizations. For horizontal polarization, soils with largest correlation length of 1.0 wavelength have the smallest brightness temperature and vice visa. For vertical polarization, this feature is not exhibited. The surface roughness has a larger influence in brightness temperature for horizontal polarization than the vertical. The brightness temperature in vertical polarization is mainly determined by the rms height for this case. With the increase of soil moisture, the differences in brightness temperatures between different correlation lengths increase. For horizontal polarization, the biggest difference in brightness temperature increases from 12.7 Kelvin degrees for 5% of soil moisture to 18.6 Kelvin degrees for 25% of soil moisture. It increases from

1.86 Kelvin degrees to 6.72 Kelvin degrees for the corresponding vertical polarization. This shows that the effects of surface roughness become larger for large soil moisture than small one.

b) Variation of brightness temperature at L band with the soil moistures for the rough surfaces with the fixed rms slope and different rms height.

In Figure 5, the brightness temperatures are plotted as a function of soil moisture in both horizontal and vertical polarizations. Two sets of simulation results are used. One is with rms height of 0.1 wavelength and correlation length of 0.33 wavelength. The other is with rms height of 0.3 wavelength and correlation length of 1.0 wavelength. The rms slopes for these two cases are the same. It can be seen that the increase of rms height decreases the difference in brightness temperature between horizontal and vertical polarizations. As scattering by rough surface increases, there is "mixing" of polarizations. The roughness effect is more pronounced for horizontal polarization.

c) Variation of brightness temperatures with the soil moistures at both L and C bands using the same physical roughness parameters.

The brightness temperatures in passive microwave remote sensing are measured at L and C bands. So it is useful to compare the brightness temperatures of soils at L and C bands using the same physical parameters of roughness and soil moisture. In Figure 6, we plot the brightness temperatures as a function of soil moisture in volumetric water content at both L and C bands. The corresponding permittivities are taken from Table II. The physical parameters are that the rms height is 2.45 cm and correlation length is 8.0 cm. We can see that the brightness temperatures are higher at C band than at L band for horizontal polarization and lower at C band than at L band for vertical polarization. Since the permittivities between L and C bands are comparable, the results indicate that roughness has a larger effect on C band than at L band. In Figure 7, the results are shown with different rough surface parameters. The rms height is 0.73 cm and correlation length is 3.5 cm in this figure. Comparing the results of figures 6 and 7 indicates that as

roughness decreases, the brightness temperatures of L and C bands are closer to each other.

d) Comparisons with empirical formula.

In passive remote sensing with soil, an empirical formula, which has been used for many years, is as follows [Wang, 1983]

$$T_{Bv}(\theta_i,\varphi_i) = \{1-[r_{v0}(\theta_i,\varphi_i)(1-Q)+r_{h0}(\theta_i,\varphi_i)Q]e^{-H\cos^2\theta_i}\}T \tag{5.31}$$

$$T_{Bh}(\theta_i,\varphi_i) = \{1-[r_{h0}(\theta_i,\varphi_i)(1-Q)+r_{v0}(\theta_i,\varphi_i)Q]e^{-H\cos^2\theta_i}\}T \tag{5.32}$$

where T_{Bv} and T_{Bh} are brightness temperatures for vertical and horizontal polarizations, respectively, T is physical temperature of dielectric medium, and Q and H are empirical constants that are used to fit the data. The parameters r_{v0} and r_{h0} are the flat surface Fresnel reflectivity of vertical and horizontal polarized waves, respectively. The empirical parameter Q represents coupling between polarizations and H represents depletion of reflectivity. Both are assumed to be constants.

In Tables VIII and VIIII, we tabulate the values of Q and H computed from (31) and (32) by using the brightness temperatures of figures 6 and 7 based on numerical simulations. The table shows that parameters of Q and H are actually the functions of soil moistures and surface roughness parameters. In the original proposal, H is supposed to be $4k^2h^2$ where h is the rms height. The table expresses that Q and H are empirical parameters that are deprived of physical meaning.

5.7 Conclusions

In this paper, we have made numerical simulations of emissivities of soil with rough surfaces by using physics-based two-grid method combined with sparse matrix canonical grid method (PBTG-SMCG). The advantage of this approach is that unlike analytic approximations such as Kirchhoff method and the small perturbation method, this method solves the 3-dimensional Maxwell equations numerically. The use of fast numerical method presented in the paper shows that numerical simulations of emissivities can be calculated with modest CPU. Thus the results of extensive numerical simulations can be directly applied to passive microwave remote sensing of soil moisture. With solutions of 3-D Maxwell equations, we will study other aspects of rough surface of soils such as moisture profiles and non-Gaussian rough surface profiles.

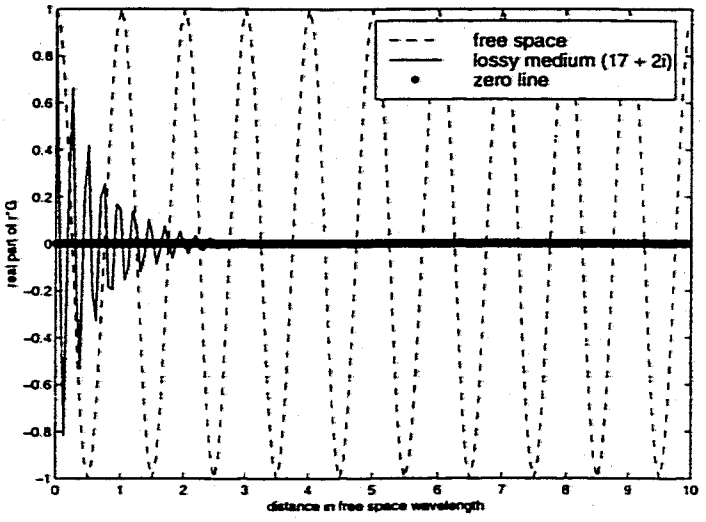

Figure 5.1. The variation of $r*G$ of free space and lossy medium with relative permittivity of 17 + i2.0 as a function of distance.

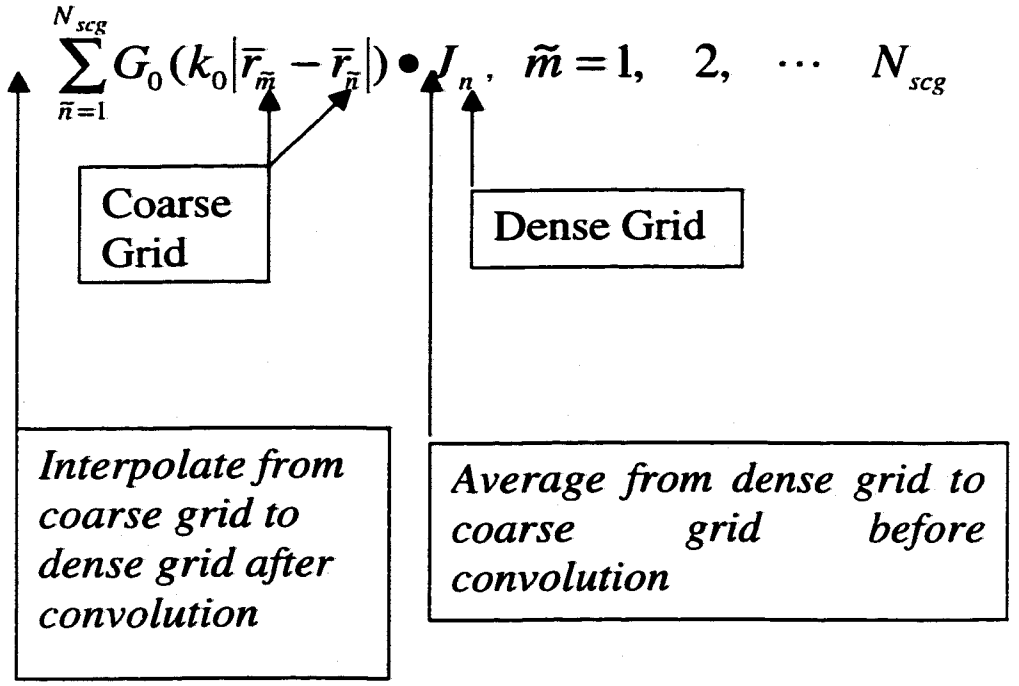

Figure 5.2. Illustration of physics-based two-grid method in using the spatial frequency limited property of the free space green's function on a dense grid of surface fields.

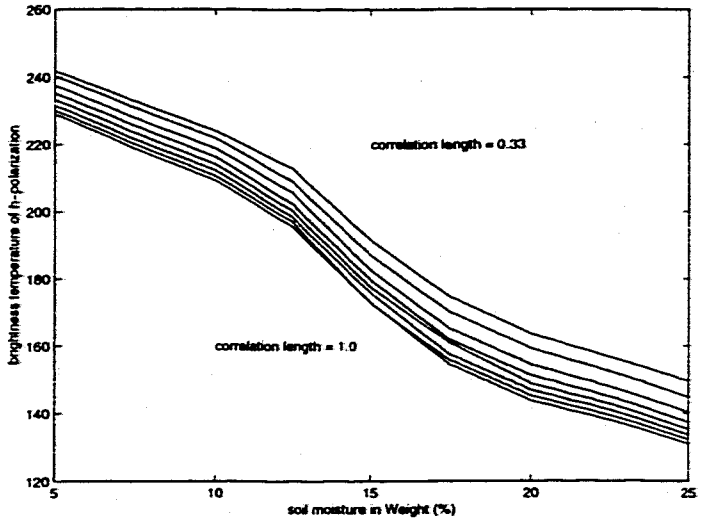

Figure 5.3. The variation of brightness temperatures at L band with the soil moistures in weight. The rough surface is with rms height of 0.1 wavelength and correlation lengths from 0.33 to 1.0 wavelength. The observation angle is at 50 degrees. Horizontal polarization

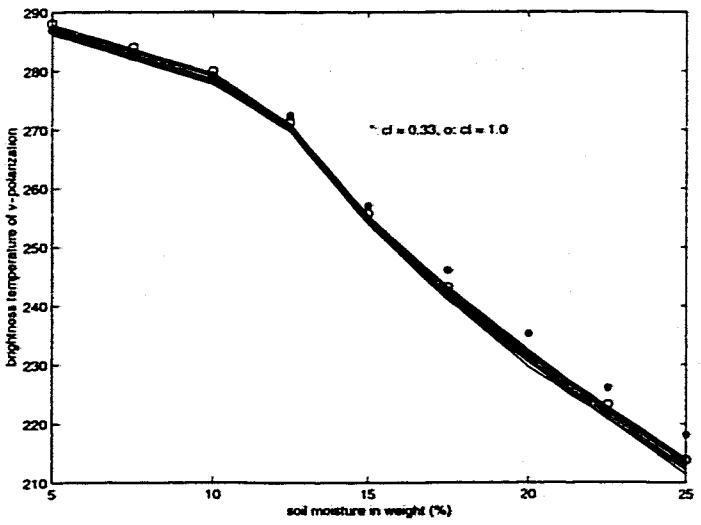

Figure 5.4. Same as figure 5.3 except vertical polarization

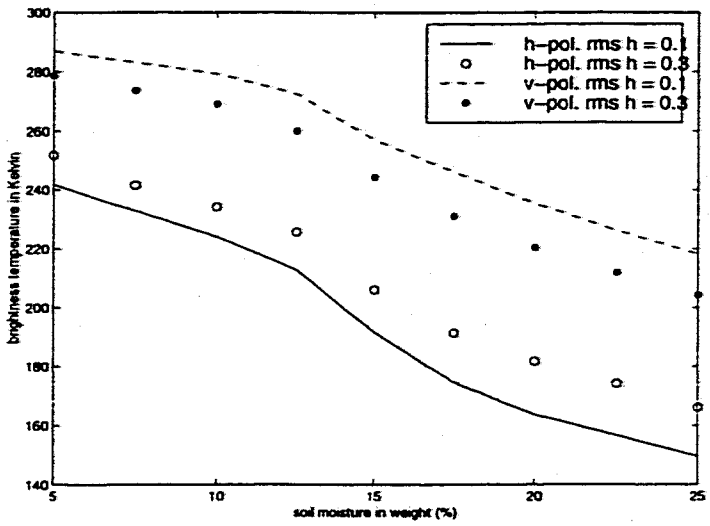

Figure 5.5. The variation of brightness temperatures with the soil moistures in weight. The rough surfaces are with rms height of 0.1 and 0.3 wavelength and correlation lengths of 0.33 and 1.0 wavelength, respectively. The two surfaces have the same rms slope. The observation angle is at 50 degrees.

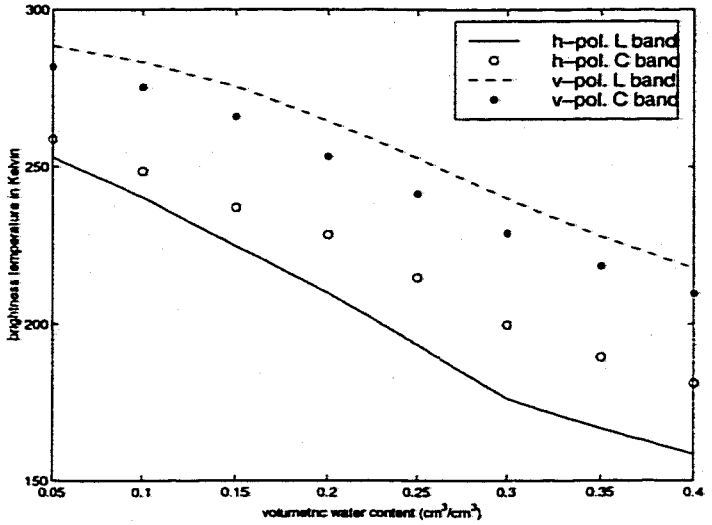

Figure 5.6. The variation of brightness temperatures with the soil moistures in volumetric water content at L and C bands using the permittivities in TABLE II. The physical rough surface parameters are with rms height of 2.45 cm and correlation length of 8.0 cm. The observation angle is at 50 degrees.

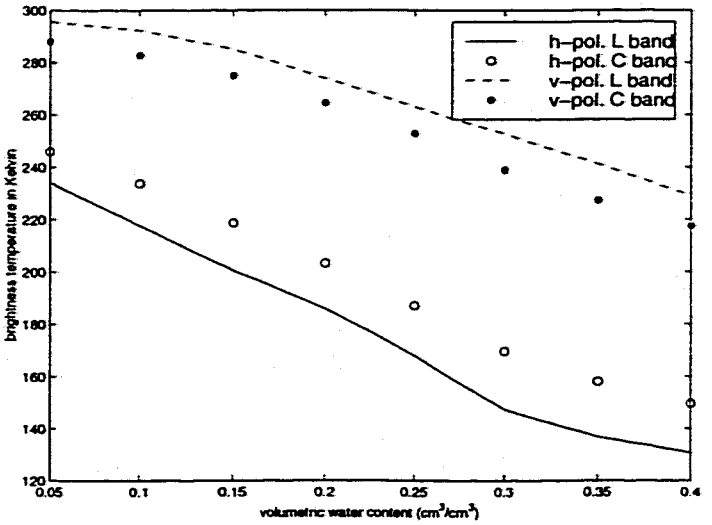

Figure 5.7. Same as figure 5.6 except the physical rough surface parameters are with rms height of 0.73 cm and correlation length of 3.5cm.

Table 5.1. Relative permittivities of soil moistures in weight at L band

Moisture (%)	5	7.5	10.0	12.5	15.0	17.5	20.0	22.5	15.0
Permittivity	4.06 + i0.30	4.81 + i0.45	5.56 + i0.60	7.35 + i0.87	10.8 + i1.33	14.25 + i1.79	17.7 + i2.26	21.15 + i2.72	24.6 + i3.18

Table 5.2. Relative permittivities of soil moistures in volumetric water content (cm^3/cm^3) at L and C bands

Moisture	0.05	0.10	0.15	0.20	0.25	0.30	0.35	0.40
Permittivity at L band	3.66 + i0.15	4.66 + i0.29	6.26 + i0.52	8.45 + i0.85	11.3 + i1.27	15.2 + i1.82	19.2 + i2.41	23.1 + i3.04
Permittivity at C band	3.62 + i0.19	4.52 + i0.44	5.94 + i0.85	7.90 + i1.42	10.4 + i2.17	13.9 + i3.22	17.4 + i4.30	20.8 + i5.30

Table 5.3. Emissivities of wet soil of horizontal component

Moisture (%)	Correlation Length (in wavelengths) horizontal polarization							
	0.33	0.4	0.5	0.6	0.7	0.8	0.9	1.0
5.00	0.8060	0.8011	0.7918	0.7841	0.7777	0.7720	0.7671	0.7636
7.50	0.7758	0.7693	0.7591	0.7514	0.7442	0.7377	0.7330	0.7286
10.0	0.7464	0.7393	0.7290	0.7205	0.7132	0.7072	0.7017	0.6973
12.5	0.7092	0.6964	0.6855	0.6743	0.6676	0.6614	0.6569	0.6520
15.0	0.6385	0.6236	0.6088	0.5990	0.5919	0.5862	0.5758	0.5766
17.5	0.5819	0.5668	0.5504	0.5393	0.5365	0.5248	0.5193	0.5149
20.0	0.5453	0.5309	0.5149	0.5042	0.4961	0.4896	0.4840	0.4792
22.5	0.5220	0.5077	0.4925	0.4827	0.4755	0.4695	0.4642	0.4596
25.0	0.4986	0.4826	0.4678	0.4577	0.4508	0.4454	0.4409	0.4366

rms height = 0.1 wavelength, observation angle = 50 degrees.

Table 5.4. Emissivities of wet soil of vertical component

Moisture (%)	Correlation Length (in wavelengths) vertical polarization							
	0.33	0.4	0.5	0.6	0.7	0.8	0.9	1.0
5.00	0.9565	0.9545	0.9541	0.9550	0.9563	0.9578	0.9592	0.9603
7.50	0.9437	0.9410	0.9400	0.9408	0.9423	0.9439	0.9454	0.9468
10.0	0.9308	0.9276	0.9261	0.9268	0.9284	0.9302	0.9318	0.9333
12.5	0.9081	0.9024	0.8995	0.8995	0.9006	0.9018	0.9031	0.9043
15.0	0.8568	0.8508	0.8469	0.8468	0.8480	0.8493	0.8510	0.8524
17.5	0.8202	0.8104	0.8036	0.8041	0.8054	0.8073	0.8091	0.8107
20.0	0.7841	0.7744	0.7684	0.7655	0.7696	0.7716	0.7734	0.7714
22.5	0.7535	0.7412	0.7361	0.7363	0.7382	0.7402	0.7423	0.7440
25.0	0.7272	0.7123	0.7048	0.7073	0.7092	0.7113	0.7134	0.7130

rms height = 0.1 wavelength, observation angle = 50 degrees.

Table 5.5. Emissivities of wet soil

Emissivity	Soil Moisture in Weight (%)								
	5.00	7.50	10.0	12.5	15.0	17.5	20.0	22.5	25.0
h (case1)	0.8060	0.7758	0.7464	0.7092	0.6385	0.5819	0.5453	0.5220	0.4986
h (case2)	0.8392	0.8053	0.7946	0.7519	0.6868	0.6376	0.6054	0.5804	0.5535
h (case3)	0.8107	0.7820	0.7686	0.7252	0.6593	0.6110	0.5802	0.5653	0.5333
v case1)	0.9565	0.9437	0.9308	0.9081	0.8568	0.8202	0.7841	0.7535	0.7272
v (case2)	0.9289	0.9123	0.8990	0.8667	0.8143	0.7698	0.7345	0.7064	0.6806
v (case3)	0.9302	0.9154	0.9052	0.8758	0.8266	0.7840	0.7503	0.7227	0.6961

Case1: rms height = 0.1 wavelength, correlation length = 0.333 wavelength, observation angle = 50 degrees
Case2: rms height = 0.3 wavelength, correlation length = 1.000 wavelength, observation angle = 50 degrees
Case3: rms height = 0.3 wavelength, correlation length = 1.000 wavelength, observation angle = 55 degrees

Table 5.6. Emissivities of wet soil at L and C band

Emissivity	Volumetric Water Content (cm^3/cm^3)							
	0.05	0.10	0.15	0.20	0.25	0.30	0.35	0.40
h (L band)	0.8434	0.8008	0.7490	0.6996	0.6446	0.5868	0.5553	0.5278
h (C band)	0.8626	0.8285	0.7900	0.7613	0.7160	0.6658	0.6313	0.6032
v(L band)	0.9615	0.9444	0.9181	0.8817	0.8424	0.7995	0.7593	0.7256
v(C band)	0.9393	0.9178	0.8867	0.8441	0.8045	0.7630	0.7284	0.6989

rms height = 2.45 cm, correlation length = 8.0 cm, observation angle = 50 degrees; L band: f = 1.4 GHz, C band: f = 5.0 GHz

Table 5.7. Emissivities of wet soil at L and C band

Emissivity	Volumetric Water Content (cm^3/cm^3)							
	0.05	0.10	0.15	0.20	0.25	0.30	0.35	0.40
h(L band)	0.7807	0.7258	0.6684	0.6198	0.5597	0.4915	0.4560	0.4354
h(C band)	0.8202	0.7793	0.7290	0.6778	0.6234	0.5656	0.5272	0.4990
v(L band)	0.9854	0.9747	0.9503	0.9132	0.8766	0.8426	0.8042	0.7633
v(C band)	0.9604	0.9430	0.9169	0.8820	0.8427	0.7968	0.7581	0.7254

rms height = 0.73 cm, correlation length = 3.5 cm, observation angle = 50 degrees; L band: f = 1.4 GHz, C band: f = 5.0 GHz

Table 5.8. Empirical parameters of Q and H

Q and H	Volumetric Water Content (cm^3/cm^3)							
	0.05	0.10	0.15	0.20	0.25	0.30	0.35	0.40
Q(L band)	0.1304	0.1242	0.1190	0.1292	0.1258	0.1144	0.1305	0.1407
H(L band)	0.4661	0.4450	0.4337	0.4189	0.3718	0.3273	0.3289	0.3148
Q(C band)	0.2644	0.2675	0.2793	0.3248	0.3255	0.3157	0.3173	0.3200
H(C band)	0.4013	0.3956	0.4246	0.4812	0.4520	0.4284	0.4233	0.4084

rms height = 2.45 cm, correlation length = 8.0 cm, observation angle = 50 degrees; L band: f = 1.4 GHz, C band: f = 5.0 GHz

Table 5.9. Empirical parameters of Q and H

Q and H	Volumetric Water Content (cm^3/cm^3)							
	0.05	0.10	0.15	0.20	0.25	0.30	0.35	0.40
Q(L band)	-0.0344	-0.0541	-0.0545	-0.0356	-0.0457	0.0866	-0.0844	-0.0549
H(L band)	0.0271	0.0538	0.1051	0.1547	0.1437	0.1297	0.1441	0.1436
Q(C band)	0.1111	0.1106	0.1085	0.1127	0.1115	0.1074	0.1107	0.1169
H(C band)	0.1541	0.1769	0.2044	0.2165	0.1919	0.1622	0.1573	0.1529

rms height = 0.73 cm, correlation length = 3.5 cm, observation angle = 50 degrees; L band: f = 1.4 GHz, C band: f = 5.0 GHz

Chapter 6

Wave Scattering from Lossy Dielectric Random Rough Surfaces Using the Physics-Based Two-Grid Method in Conjunction with the Multilevel Fast Multipole Method

6.1 Introduction

Monte-Carlo simulations have been extensively used recently to study the wave scattering from random rough surfaces [Axline, 1978; Thorsos, 1988; Holliday, 1996; Kapp, 1996; Donhue, 1998; Chou, 1998; Michielssen, 1996 a & b; Liu, 1994; Tsang, 1995; Chan, 1998] because the analytic approximations are limited in validity. Monte-Carlo simulations can be used to deal with wave scattering from random rough surfaces with arbitrary profiles [Holliday, 1996; Kapp, 1996; Donhue, 1998; Chou, 1998; Michielssen, 1996 a & b; Liu, 1994; Tsang, 1995; Chan, 1998]. Most of the fast computational methods use iterative moment method solutions and facilitate computation by either reducing the number of iteration [Holliday, 1996; Kapp, 1996; Chou, 1998] or reducing computational steps of the matrix-vector multiply [Chou, 1998; Michielssen, 1996 a & b; Liu, 1994; Tsang, 1995; Chan, 1998].

The methods proposed by Michielssen, the fast multipole method (FMM), and the banded-matrix iterative approach/canonical grid method (BMIA/CAG) are examples for the second purpose. The algorithm proposed by Michielssen uses a recursive formula with a computational complexity of $O(N \log^2 N)$ [Michielssen, 1996] for a quasi-planar surface. The banded-matrix iterative approach/canonical grid method (BMIA/CAG) [Tsang, 1995; Chan, 1998] permits the solution of large-scale random rough surface problems. The essence of the method consists of decomposing the interaction into near and non-near field interactions. The non-near field interactions are then expanded on a canonical grid of a horizontal surface by Taylor series. The coefficients of Taylor expansion on a canonical grid of flat surface are composed of Topelitz matrices thus Fast Fourier Transform (FFT) can be used to facilitate matrix vector convolution. The computational complexity and the memory requirements for BMIA/CAG are $O(N\ log(N))$ and $O(N)$, respectively. The BMIA/CAG is also applied to dielectric rough surface [Chan, 1998]. The idea of the FMM is to reduce the number of scattering centers. If a scattering object is discretized into N segments and the interactions among them are computed directly, N^2 operations are required. Instead of calculating them directly, the FMM divides the segments into groups according to the distances among them. The scattered field of each segment within a group is translated to group center by aggregation. The interactions among the elements of neighboring groups are calculated as before. For the interactions of the elements of non-near groups, only the interactions of group centers are calculated. Thus, the number of scattering centers is reduced. After each group center receives all the scattered fields from other non-near group centers, it redistributes these fields to the subscatterers belonging to the group. In this way, the single level FMM can reduce the computational complexity to $O(N^{1.5})$. For the multilevel FMM, the multi-sized groups are formed. The small sized group is used to calculate the interactions among the near elements and large sized group is used to calculate the interactions among far away elements. With the aid of interpolation and anterpolation, the computational complexity of the multilevel FMM is O(NlogN) for the arbitrary shape of surfaces. For the quasi-planar scatterer such as rough surfaces, the angular spectral

representation of Green's function can be calculated on the steepest descent path of flat surface. The number of angles required to sample integrand along this path is independent of group sizes. Thus a linear algorithm can be achieved by the multilevel steepest descent path fast multipole method (SDFMM).

To study wave scattering from lossy medium with large permittivity, a dense grid of many points per wavelength is required because of the large spatial variation of medium's Green's function and surface fields. Dense grid means more number of surface unknowns. A physics-based two-grid (PBTG) method was developed for dealing with this problem [Tsang, 1997]. The PBTG is based on the properties that lossy medium Green's function is attenuative. Therefore it is space-limited. Free space Green's function is slowly varying on the dense gird making it spatial frequency-limited. It has been shown that the PBTG makes CPU and memory requirements depend on the coarse grid for non-near field interactions and on the dense grid for near-field interactions. The PBTG can also be used in conjunction with other fast computational methods. We have combined the PBTG with the banded-matrix iterative approach (BMIA) [Li, 1999]. In this paper we combine it with the multilevel steepest descent path fast multipole method (MLSDFMM). Using the proposed algorithm of the PBTG-FMM, we study the wave scattering from Gaussian and non-Gaussian random rough surfaces. The CPU requirement is also illustrated.

The paper is arranged in the following. We illustrate the single grid method in section 2. In section 3, we derive the formulations of the PBTG. We show the multilevel steepest descent path fast multipole method in section 4 and illustrate the computational complexity of the combined algorithm of the PBTG with the MLSDFMM in section 5. In section 6, we give the formulations of the bistatic scattering coefficients and emissivity. In section 7, we apply the algorithm to the Gaussian rough surfaces and discuss the

accuracy issue of the algorithm. In section 8, we give the modified power-law spectrum. In section 9, we discuss the numerical results and give conclusion in section 10.

6.2 Formulation of Single Grid

Consider a tapered plane wave of $\psi_{inc}(\bar{r})$ incident on a random dielectric rough surface of $z = f(x)$, the surface fields satisfy the following surface integral equations [Chan, 1998]:

$$\frac{1}{2}\psi(\bar{r}') - \int_s [\psi(\bar{r})\frac{\partial G(\bar{r},\bar{r}')}{\partial \hat{n}} - G(\bar{r},\bar{r}')\frac{\partial \psi(\bar{r})}{\partial \hat{n}}]ds = \psi_{inc}(\bar{r}') \tag{6.1}$$

$$\frac{1}{2}\psi_1(\bar{r}') + \int_s [\psi_1(\bar{r})\frac{\partial G_1(\bar{r},\bar{r}')}{\partial \hat{n}} - G_1(\bar{r},\bar{r}')\frac{\partial \psi_1(\bar{r})}{\partial \hat{n}}]ds = 0 \tag{6.2}$$

Where $G(\bar{r},\bar{r}')$ and $G_1(\bar{r},\bar{r}')$ are the 2-dimensional Green's functions of free space and medium, respectively. Functions $\psi(\bar{r})$ and $\psi_1(\bar{r})$ are the surface fields which are associated by boundary conditions.

$$\psi_1(\bar{r}) = \psi(\bar{r}) \qquad \text{and} \qquad \frac{\partial \psi_1(\bar{r})}{\partial \hat{n}} = \rho\frac{\partial \psi(\bar{r})}{\partial \hat{n}} \tag{6.3}$$

where ρ equals μ_1/μ and $\varepsilon_1/\varepsilon$ for TE and TM polarization, respectively. Using the method of moment (MoM), the integral equations can be cast into the matrix equation:

$$\sum_{j=1}^{N} a_{ij}u(x_j) + \sum_{j=1}^{N} b_{ij}\psi(x_j) = \psi_{inc}(x_i) \tag{6.4}$$

$$\sum_{j=1}^{N} a_{ij}^{(1)}\rho u(x_j) + \sum_{j=1}^{N} b_{ij}^{(1)}\psi(x_j) = 0 \tag{6.5}$$

where $u(x) = \sqrt{1+[f'(x)]^2}\,\partial\psi/\partial n$. Quantity N is the number of sampling points on the surfaces. The matrix elements a_{ij}, b_{ij}, $a_{ij}^{(1)}$, and $b_{ij}^{(1)}$ are determined by the Green's functions.

$$a_{ij} = G(\bar{r}_i, \bar{r}_j) \tag{6.6}$$

$$b_{ij} = -\frac{\partial G(\bar{r}_i, \bar{r}_j)}{\partial \hat{n}} + \frac{1}{2}\delta_{ij} \tag{6.7}$$

$$a_{ij}^{(1)} = G_1(\bar{r}_i, \bar{r}_j) \tag{6.8}$$

$$b_{ij}^{(1)} = -\frac{\partial G_1(\bar{r}_i, \bar{r}_j)}{\partial \hat{n}} - \frac{1}{2}\delta_{ij} \tag{6.9}$$

Where

$$\delta_{ij} = \begin{cases} 1 & i = j \\ 0 & i \neq j \end{cases}$$

To solve the matrix equations (4) and (5) using the conjugate gradient method, the CPU requirement is determined by the computational steps of the matrix-vector multiplication. Therefor it depends on the number of sampling points. For the wave scattering for perfectly conducting rough surfaces, only free space Green's function is used. The number of sampling is usually 10 points per free space wavelength. We call it single coarse grid in this paper. But for the wave scattering from dielectric rough surfaces with large permittivity, the wavelength of medium is much shorter than that of free space. Thus Green's function of G_1 has rapid spatial variation on the rough surfaces. A dense grid of many points per wavelength, say 30 to 50 points per wavelength, is required for accurate results. Dense grid means more CPU and memory requirements. In the following, the PBTG will be introduced. We will show that the PBTG makes the CPU requirement only depend on the coarse grid for the non-near field interactions.

6.3 Physics-Based Two-Grid Method

The physics-based two-grid method is applied to the lossy medium with large permittivity. We let Roman numeral subscripts i, j denote indexing with the dense grid and $\tilde{i}$, $\tilde{j}$ with the coarse grid. Assume that the upper medium is the free space and the lower medium is lossy with the relative complex permittivity of ϵ_l. From Kramer-Kronig relation, a medium with a large real part of dielectric constant is normally associated with a large imaginary part at microwave frequency, such as wet soil and ocean. It is observed that the Green's function of the lossy medium is heavily attenuative and the Green's function of free space is slowly varying compared with Green's function of the lossy medium.

Based on the first observation, we can define a distance limit r_t as determined by the complex permittivity of lower medium. Outside of which the field interaction between the *ith* and the *jth* point is vanishingly small and the lower medium Green's function can be set equal to zero. Therefore we can approximate

$$a_{ij}^{(1)} \approx \tilde{a}_{ij}^{(1)} = \begin{cases} a_{ij}^{(1)} & r_{ij} \le r_t \\ 0 & r_{ij} \ge r_t \end{cases} \tag{6.10}$$

$$b_{ij}^{(1)} \approx \tilde{b}_{ij}^{(1)} = \begin{cases} b_{ij}^{(1)} & r_{ij} \le r_t \\ 0 & r_{ij} \ge r_t \end{cases} \tag{6.11}$$

where r_{ij} is the distance between the *ith* point and the *jth* point on the dense grid. Thus $\tilde{a}_{ij}^{(1)}$ and $\tilde{b}_{ij}^{(1)}$ are banded matrices and Equation (5) becomes

$$\sum_{j=1}^{N} \tilde{a}_{ij}^{(1)} \rho u(x_j) + \sum_{j=1}^{N} \tilde{b}_{ij}^{(1)} \psi(x_j) = 0 \tag{6.12}$$

Based on the second observations above, we decompose the upper medium Green's function into near field and non-near field interactions

$$\sum_{j=1}^{N} a_{ij} u(x_j) = \sum_{j=1}^{N} a_{ij}^{s} u_j + \sum_{j=1}^{N} a_{ij}^{ns} u_j \tag{6.13}$$

$$\sum_{j=1}^{N} b_{ij}\psi(x_j) = \sum_{j=1}^{N} b_{ij}^{s}\psi_j + \sum_{j=1}^{N} b_{ij}^{ns}\psi_j \tag{6.14}$$

where a_{ij}^{s} , b_{ij}^{s}, a_{ij}^{ns} , and b_{ij}^{ns} are determined by

$$a_{ij}^{s} = \begin{cases} a_{ij} & r_{ij} \le r_f \\ 0 & r_{ij} > r_f \end{cases} \tag{6.15}$$

$$b_{ij}^{s} = \begin{cases} b_{ij} & r_{ij} \le r_f \\ 0 & r_{ij} > r_f \end{cases} \tag{6.16}$$

$$a_{ij}^{ns} = \begin{cases} 0 & r_{ij} \le r_f \\ a_{ij} & r_{ij} > r_f \end{cases} \tag{6.17}$$

$$b_{ij}^{ns} = \begin{cases} 0 & r_{ij} \le r_f \\ b_{ij} & r_{ij} > r_f \end{cases} \tag{6.18}$$

For non-near field interactions, Green's function of free space is slowly varying on the dense grid. We can use the coarse grid to sample it. Assume the number of sampling points on the coarse grid is less than that on the dense grid by a factor of n_1, where $n_1 = \text{int}eger(real(\sqrt{\varepsilon_1}))$. Thus the $\tilde{i}\,th$ point on the coarse grid corresponds to n_1 points of $\tilde{i}_1$, $\tilde{i}_2$,..., $\tilde{i}_{n_1}$ on the dense grid. The $\tilde{i}_p th$ ($p = 1,2,...n_1$) point is the ith dense grid point where i is given by $i = (\tilde{i} - 1)n_1 + p$. When we calculate the convolution of a_{ij}^{ns} and surface fields of u_j on the dense grid, the following approximation can be made.

$$\sum_{j=1}^{N} a_{ij}^{ns} u(x_j) = \sum_{\tilde{j}=1}^{N/n_1} \sum_{q=1}^{n1} a_{\tilde{i}_p \tilde{j}_q}^{ns} u(x_{\tilde{j}_q}) \approx \sum_{\tilde{j}=1}^{N/n_1} a_{\tilde{i}_p \tilde{j}}^{ns} \sum_{q=1}^{n_1} u(x_{\tilde{j}_q}) \tag{6.19}$$

Because the Green's function of the free space is essentially constant over an interval of n_1 points. Furthermore, the elements $a_{\tilde{i}_p \tilde{j}}^{ns}$ of $p = 1,2,\cdots,n_1$ can be found by interpolating from the coarse grid to the dense grid.

$$a_{\tilde{i}_p \tilde{j}}^{ns} = \sum_{\tau=-T}^{T} In(\tilde{i}_p, \tilde{i} + \tau) a_{(\tilde{i}+\tau)\tilde{j}}^{ns} \tag{6.20}$$

Where $In(\tilde{i}_p, \tilde{i}+\tau)$ is the interpolation operator and T is the number of points of the coarse grid we use to interpolate. Then

$$\sum_{j=1}^{N} a_{ij}^{ns} u(x_j) = \sum_{\tilde{j}=1}^{N/n_1} \sum_{\tau=-T}^{T} In(\tilde{i}_p, \tilde{i}+\tau) a_{(\tilde{i}+\tau)\tilde{j}}^{ns} \sum_{q=1}^{n_1} u(x_{\tilde{j}_q}) = \sum_{\tau=-T}^{T} In(\tilde{i}_p, \tilde{i}+\tau) g_{\tilde{i}+\tau} \tag{6.21}$$

Where

$$g_{\tilde{i}+\tau} = \sum_{\tilde{j}=1}^{N/n_1} a_{(\tilde{i}+\tau)\tilde{j}}^{ns} \sum_{q=1}^{n_1} u(x_{\tilde{j}_q}) \tag{6.22}$$

What is done in here is that the surface fields on the dense grid are first averaged before convolved by the free space Green's function on the coarse grid. Then we use interpolation to find N values on the dense grid. Similarly, we can obtain:

$$\sum_{j=1}^{N} b_{ij}^{ns} \psi(x_j) = \sum_{\tau=-T}^{T} In(\tilde{i}_p, \tilde{i}+\tau) h_{\tilde{i}+\tau} \tag{6.23}$$

Where

$$h_{\tilde{i}+\tau} = \sum_{\tilde{j}=1}^{N/n_1} b_{(\tilde{i}+\tau)\tilde{j}}^{ns} \sum_{q=1}^{n_1} \psi(x_{\tilde{j}_q}) \tag{6.24}$$

Thus, the equation (4) can be rewritten as

$$[\sum_{j=1}^{N} a_{ij}^{s} u(x_j) + \sum_{j=1}^{N} b_{ij}^{s} \psi(x_j)] + \sum_{\tau=-T}^{T} In(\tilde{i}_p, \tilde{i}+\tau) g_{\tilde{i}+\tau} + \sum_{\tau=-T}^{T} In(\tilde{i}_p, \tilde{i}+\tau) h_{\tilde{i}+\tau} = \psi_{inc}(x_i) \tag{6.25}$$

We can write the equations (12) and (25) as the following matrix equations.

$$\overline{\overline{Z}}_{A,sdg}^{(1)} \cdot \overline{u}_{sdg} + \overline{\overline{Z}}_{B,sdg}^{(1)} \cdot \overline{\psi}_{sdg} = \overline{0}_{sdg} \tag{6.26}$$

$$\overline{\overline{Z}}_{A,sdg} \cdot \overline{u}_{sdg} + \overline{\overline{Z}}_{B,sdg} \cdot \overline{\psi}_{sdg} + \overline{\overline{\tilde{Z}}}_{A,scg} \cdot \overline{\tilde{u}}_{scg} \Big|_{interpol} + \overline{\overline{\tilde{Z}}}_{B,scg} \cdot \overline{\tilde{\psi}}_{scg} \Big|_{interpol} = \overline{\psi}_{inc,sdg} \tag{6.27}$$

Instead of solving equations (4) and (5) directly, we can solve equations (26) and (27). Note that the elements of $\tilde{a}_{ij}^{(1)}$, $\tilde{b}_{ij}^{(1)}$, a_{ij}^{s}, and b_{ij}^{s} compose of only banded matrices and the computational steps for them are only proportional to the number of surface unknowns on

the dense grid. The main CPU requirements are to calculate the values of $g_{\tilde{i}}$ and $h_{\tilde{i}}$ with $\tilde{i}$ from 1 to N/n_1. It takes approximately $(N/n_1)^2$ operations for multiplying them directly and is only dependent on the number of surface unknowns on the coarse grid. It has been shown [Tsang, 1997; Li, 1999] that the PBTG can give the accurate results as the dense grid but with CPU requirement on the coarse gird. The computational steps can be further reduced using the BMIA and the FMM. We have illustrated the PBTG-BMIA in [Li, 1999]. In the following section, we will illustrate how to combine the PBTG with the multilevel steepest descent path FMM.

6.4 Multilevel Steepest Descent Path Fast Multipole Method

Using the iterative techniques to solve the surface integral equations, the computational steps are determined by the number of sampling points. The idea of the fast multipole method (FMM) is to reduce the number of scattering centers by grouping subscatterers together [Michielssen, 1996b; Liu, 1994]. Only interactions of group centers are calculated for non-near field interactions. For the multi-level FMM [Liu, 1994], the different group sizes are used according to the distances of the groups. The larger the distance of groups is, the larger the group size. For general FMM, the number of plane waves required to calculate the scattered fields is increased with the group size [Liu, 1994], which leads to an O($N \log N$) algorithm. For the wave scattering from random rough surfaces, using the quasi-planar property of the surface, it can be shown that the number of plane waves required is independent of group size, which leads to a linear algorithm. We will illustrate that in the following.

Two-dimensional Green's function is the zeroth order Hankel function of the first kind. The angular spectral representation of $H_0^{(1)}(k\rho)$ is:

$$H_0^{(1)}(k\rho_{ij}) = \frac{1}{\pi}\int_{\Gamma} d\alpha \exp[ik\sin\alpha|x_i - x_j| + ik\cos\alpha(z_i - z_j)] \tag{6.28}$$

The integral path Γ is shown in figure 1. For the non-near field interactions, the horizontal distance is much larger than the vertical distance because the rough surface is a quasi-planar surface. The numerical calculation of $H_0^{(1)}(k\rho)$ can be efficiently performed by deforming the original integral path to the steepest descent path of flat surface [Michielssen, 1996b]. The steepest descent path of flat surface is given by

$\sin\alpha'\cosh\alpha'' = 1$

where $\alpha = \alpha' + i\alpha''$. It is also shown in figure 1. Hankel function of $H_0^{(1)}(k\rho)$ then can be expressed as:

$$H_0^{(1)}(k\rho_{ij}) = \int_{SDP} d\alpha \exp[ik\sin\alpha|x_i - x_j| + ik\cos\alpha(z_i - z_j)]$$

$$= \sum_{\bar{q}=1}^{Q} \Delta\alpha_{\bar{q}} \exp[ik\sin\alpha_{\bar{q}}(x_i - x_j) + ik\cos\alpha_{\bar{q}}(z_i - z_j)] \quad \text{for } x_i > x_j \tag{6.29}$$

The integer number of Q is the number of angles we need to discretize the integral. It will be shown later that the value of Q is independent of group size for the interactions of two group elements. Assume that *ith* element belongs to the group I with the center of (x_I, z_I) and *jth* element belongs to the group J with the center of (x_J, z_J). Then, above equation can be rewritten as

$$H_0^{(1)}(k\rho_{ij}) = \sum_{\bar{q}=1}^{Q} \exp[ik\sin\alpha_{\bar{q}}(x_i - x_I) + ik\cos\alpha_{\bar{q}}(z_i - z_I)]$$

$$\cdot \Delta\alpha_{\bar{q}} \exp[ik\sin\alpha_{\bar{q}}(x_I - x_J) + ik\cos\alpha_{\bar{q}}(z_I - z_J)]$$

$$\cdot \exp[ik\sin\alpha_{\bar{q}}(x_J - x_j) + ik\cos\alpha_{\bar{q}}(z_J - z_j)]$$

$$= \sum_{\bar{q}=1}^{Q} V_{Ii}(\alpha_{\bar{q}}) T_{IJ}(\alpha_{\bar{q}}) W_{Jj}(\alpha_{\bar{q}}) \tag{6.30}$$

The above equation illustrates that when calculating the interaction of between *ith* and *jth* elements, first the surface field at *jth* point can be translated into its group center, then it is transferred from the *Jth* group center to the *Ith*, the center of group I redistributes the receiving field to its *ith* element.

For the multilevel FMM, multi-sized groups are formed. At the lowest level, the N elements are decomposed into L groups. Each group includes M elements where $N = ML$. Then each two subgroups at the level form an upper level group (large group) until the highest level. The interactions of groups at each level are calculated only for the non-near groups at this level inside the neighboring groups of upper level. Thus, the impedance matrix can be written as the sum of the following matrices.

$$\overline{\overline{Z}} = \overline{\overline{Z}}^{(0)} + \overline{\overline{Z}}^{(1)} + \cdots + \overline{\overline{Z}}^{(n)} + \cdots + \overline{\overline{Z}}^{(\tilde{p})} \tag{6.31}$$

Where matrix $\overline{\overline{Z}}^{(n)}$ only includes the elements that would be computed at *nth* levels.

The procedure of the MLFMM is composed of three steps. First, the surface fields at each element are translated to the group centers at each level. When transferring the field from the lower level group center to the upper level group center, an interpolation is required to find the values of the fields from the coarse angles to the fine angles. Second, the interactions of group centers at each level are calculated. Only those of the non-near groups inside the neighboring groups of upper level are calculated at each level. Last, the receiving fields at each group center are distributed to its subgroup centers/elements. The last step is performed from the highest level to the lowest level with anterpolation.

The number of computational steps for the first step is

$$N_1 = 2[QN + \sum_{n=2}^{p} Q\frac{L}{2^{(n-2)}}] + 2\sum_{n=2}^{p} QQ_1\frac{L}{2^{(n-2)}} \approx 2QN + 4Q(Q_1+1)\frac{N}{M} \tag{6.32}$$

Where the first term is from aggregating the surface fields to group centers and second one is from interpolating the fields from the coarse angles to the dense angles for all the levels. The integer Q_1 is the number of operations used to interpolate for a single angle.

The number of computational steps for the second step is

$$N_2 = \sum_{n=1}^{p} 3\frac{L}{2^{(n-1)}}Q \approx 6\frac{Q}{M}N \tag{6.33}$$

And the number of computational steps for the last one is

$$N_3 = 2[QN + \sum_{n=2}^{p} Q\frac{L}{2^{(n-2)}}] + 2\sum_{n=2}^{p} QQ_1\frac{L}{2^{(n-2)}} \approx 2QN + 4Q(Q_1+1)\frac{N}{M} \tag{6.34}$$

The first term is for disaggregating and the second is for anterpolating.

Thus, total number of computational steps for the matrix-vector multiply is

$$N_{total} = M(3N - 2M) + 2Q[2 + \frac{4Q_1+7}{M}]N \tag{6.35}$$

Where the first term is from near field interactions and last one is from non-near field interactions. As long as Q is constant, the computation steps will increase only with linear N.

In the following, we will prove that parameter Q is a constant for the problem of rough surface scattering. From equation (29),

$$H_0^{(1)}(k\rho) = \frac{1}{\pi}\int_0^{\pi} d\alpha'(1 - ictg\alpha' cth\alpha'')\exp(ik|x| + ikz\cos\alpha'\cosh\alpha'')$$
$$\exp(-k|x|\cos\alpha'\sinh\alpha'' + kz\sin\alpha'\sinh\alpha'') \tag{6.36}$$

It can be seen that the magnitude of the integrand could be exponentially increased with the angle α' away from $\frac{\pi}{2}$ for z not equal to zero because the steepest path is only for flat surface. But for $|x| >> |z|$, the main contributions to the integral comes from the angles around $\frac{\pi}{2}$ because the function of $\exp(-k|x|\cos\alpha'\sinh\alpha'')$ is fast decaying away from the $\frac{\pi}{2}$. At the angles of around $\frac{\pi}{2}$, α'' is close to zero that keeps the magnitude of integrand is not very large for z not equal to zero.

To discuss the integral limits and sampling rate for numerically calculating the above integral for large x, we make the following approximation. In the proximity of $\frac{\pi}{2}$, we have

$\cos\alpha' \approx (\frac{\pi}{2}-\alpha')$ and

$\sinh\alpha'' \approx \alpha'' \approx (\frac{\pi}{2}-\alpha')$

Thus equation (36) can be approximately rewritten as

$$H_0^{(1)}(k\rho) \approx \frac{1}{\pi}\int_0^{\pi} d\alpha'(1-ictg\alpha' cth\alpha'')\exp(ik|x|+ikz\cos\alpha'\cosh\alpha'')$$

$$\exp(-k|x|(\frac{\pi}{2}-\alpha')^2+kz\sin\alpha'\sinh\alpha'') \qquad (6.37)$$

When x is large, the integral limits and sampling rate of the above integral are mainly controlled by the term of $\exp[-k|x|(\frac{\pi}{2}-\alpha')^2]$. We give a small quantity and assume that if the magnitude of the integrand is less than the quantity, there is negligible contribution to the final value of integral from that part. Then we can find that the integral limits are from $\frac{\pi}{2}-BW$ to $\frac{\pi}{2}+BW$. The parameter BW is given by

$$BW = \frac{C_0}{\sqrt{|x|}} \qquad (6.38)$$

and C_0 is a constant.

From the sampling theorem, we know that to sample a banded-limited function, the sampling frequency has to be larger than the bandwidth of function. The Fourier

spectrum of function of $\exp[-k|x|(\frac{\pi}{2}-\alpha')^2]$ is $\sqrt{\frac{\pi}{k|x|}}\exp[-\frac{\omega^2}{4k|x|}]$. Thus the sampling interval has to be:

$$d\alpha' = \frac{C_1}{\sqrt{|x|}} \tag{6.39}$$

and C_1 is a constant.

Thus we can see for the fixed large value of x, the integral of equation (37) can be calculated numerically by using a constant number of sampling points.

To apply equation (37) to the multi-level fast multipole method, the equation has to be held for the interactions of all the elements among two groups. Thus the sampling frequency and integral limits have to be set for all the elements. Assume that the nearest and farthest horizontal distances of the two separated groups are $x_{\min}$ and $x_{\max}$, respectively. The integral limits have to be taken as

$$BW = \frac{C_0}{\sqrt{x_{\min}}} \tag{6.40}$$

so that all the important contributions are included when calculating integral numerically. The sampling interval has to be taken as

$$d\alpha' = \frac{C_1}{\sqrt{x_{\max}}} \tag{6.41}$$

so that the fastest variations of integrand can be caught. Thus the number of sampling points required for calculating interactions among two group's elements is

$$Q = \frac{2BW}{d\alpha'} = C\sqrt{\frac{x_{\max}}{x_{\min}}} \tag{6.42}$$

When using the multi-level fast multipole method to compute the interactions among the subscatterers, the interactions are computed grouply. The interactions of near subscatterers are computed by small group size and those of far-away subscatterers are

computed by large group size. The ratio of x_{max} and x_{min} is approximately a constant. Thus the number of sampling points is not increased with the group size. It leads to a linear algorithm for the multi-level SDFMM.

6.5 Computational Complexity of the Combined Algorithm of the PBTG with the MLFMM.

To combine the PBTG with the MLFMM, the near field interactions have to be calculated directly on the dense grid and non-near field interactions are calculated on the coarse grid through the MLFMM.

In equation (26), the number of computational steps for $\overline{\overline{Z}}^{(1)}_{A,sdg} \cdot \overline{u}_{sdg}$ and $\overline{\overline{Z}}^{(1)}_{B,sdg} \cdot \overline{\psi}_{sdg}$ is $2M_1 N_{sdg}$. Where M_1 is determined by the permittivity of lossy medium and the number of sampling points per wavelength on the dense grid and is a constant for a given case because no non-near field interactions are calculated through it. In the equation (27), the MLSDFMM is used. We treat the matrices $\overline{\overline{Z}}_{A,sdg}$ and $\overline{\overline{Z}}_{B,sdg}$ as $\overline{\overline{Z}}^{(0)}$ in equation (31) and $\tilde{\overline{\overline{Z}}}_{A,scg}$ and $\tilde{\overline{\overline{Z}}}_{B,scg}$ as $\overline{\overline{Z}}^{(1)} + \cdots + \overline{\overline{Z}}^{(n)} + \cdots + \overline{\overline{Z}}^{(\tilde{P})}$. Thus the number of computational steps for this part is $2M_{sdg}(3N_{sdg} - 2M_{sdg}) + 4Q[2 + \frac{4Q_1 + 7}{M_{scg}}]N_{scg}$ plus the number of operations used to interpolate from coarse grid to dense grid, which is proportional to N_{sdg}. The total number of operations for the PBTG-MLSDFMM is $2M_1 N_{sdg}$ + $2M_{sdg}(3N_{sdg} - 2M_{sdg}) + 4Q[2 + \frac{4Q_1 + 7}{M_{scg}}]N_{scg}$ + $Q_2 N_{sdg}$. Thus the computational complexity of the PBTG-MLSDFMM is $O(N_{sdg} + N_{scg})$.

6.6 Bistatic Scattering Coefficients and Emissivity

Numerical simulation results will be presented in terms of the normalized bistatic scattering coefficients and emissivties or brightness temperatures. The bistatic scattering coefficients are defined as

$$\sigma(\theta_s,\theta_i)=\frac{\left|\int_{-\infty}^{\infty} dx[ik\psi(x)(\frac{df}{dx}\sin\theta_s-\cos\theta_s)-u(x)]\exp(-ik\alpha(\theta_s,x))\right|^2}{4\pi g^2\int_{-k}^{k} dk_x k_z \exp[-(k_x-k\sin\theta_i)^2 g^2/2]} \tag{6.43}$$

In (43), $\alpha(\theta_s, x) = \sin\theta_s\, x + \cos\theta_s\, f(x)$, and $k_z=\sqrt{k^2-k_x^2}$. The bistatic scattering coefficient is a measure of the scattering from incident angle θ_i into scattered angle θ_s. For scattering by a perfectly conducting surface, the energy conservation test is that $\int\sigma(\theta_s,\theta_i)d\theta_s=1$. For scattering by a dielectric surface, the sum of scattering power and the absorptivity of the rough surface at the incident angle θ_i, which is the amount of power absorbed by the dielectric in a scattering problem, should be equal to one. The absorptivity can be calculated by integrating the normal total Poynting vector over the surface profile.

Because of reciprocity, emissivity is the same as absorptivity. Thus it can be calculated by either

$$e(\theta_i)=1-\int d\theta_s\sigma(\theta_s,\theta_i) \quad \text{or} \tag{6.44}$$

$$e(\theta_i)=absorptivity \tag{6.45}$$

In passive remote sensing, the brightness temperature T_B of the medium is measured at the observation angle of θ_i. The brightness temperature is defined as

$$T_B(\theta_i)=e(\theta_i)T \tag{6.46}$$

where T is the physical temperature of the medium in Kelvin degrees.

6.7 Applications to Gaussian Rough Surfaces

In this section, we focus on the accuracy issue of the proposed algorithm for the energy conservation and compare the results and CPU requirements between the PBTG-MLSDFMM and the BMIA with the single dense grid. We use 10 points per wavelength as the coarse grid and 30 points per wavelength as the dense grid. We also plot the results from the PBTG-BMIA. All the results are run on Pentium II with 450 MHz and 256 Mbytes.

In figure 2, the bistatic scattering coefficients computed from the BMIA, PBTG-FMM, and PBTG-BMIA are shown for one realization. The relative permittivity of lower medium is 25+2i and rms height and correlation length is 0.3 and 0.5 wavelengths. We use 30 points per wavelength as dense grid and the surface length is 128 wavelengths with 7,680 surface unknowns. The incident angle is 30 degrees. Figure (a) is for TE wave incidence and (b) is for TM. We think the results from the BMIA with 30 points per wavelength as the accurate one. The three results are in good agreement. The CPU required for the BMIA, PBTG-FMM, and PBTG-BMIA are 372, 163, and 157 seconds for TE wave and 123, 49, and 48 seconds for TM wave, respectively. Thus the PBTG can save CPU compared with the single dense grid.

In figure 3, the relative error of energy conservation check is plotted as a function of the relative permittivity of the lower medium. The results are from the PBTG-MLSDFMM. The relative permittivities of the lower medium are changed according to the soil moistures from 5 to 30 percent in weight. The correlation length is 1.0 wavelength in this case and other parameters are same as in figure 2. The energy conservation is within 1% for all the cases.

In figure 4, the CPU per iteration in conjugate gradient method is plotted against the number of surface unknowns for three methods. The dense grid is fixed at 30 points per wavelength and we change the surface length. It is shown that the PBTG-BMIA and PBTG-MLSDFMM have almost same performance for the cases we compute although the first algorithm is an O($N \log N$) algorithm and the latter is a linear algorithm. Both of them take less CPU than the BMIA with the dense grid.

6.8 Spectral Density of Rough Surfaces

To investigate the wave scattering from random rough surfaces, another problem is how to describe the statistical property of rough surfaces. Two functions are needed to define a random rough surface. One is height probability distribution function and the other is surface correlation function or surface roughness spectral density (which is defined as a Fourier transform of a correlation function for stationary surfaces) [Kuga, 1993]. It is usually assumed that height distribution functions are Gaussian and surface correlation functions are changed according to the requirements. There are two types of correlation functions often used [Kuga, 1993], Gaussian and exponential correlation functions. The spectral densities of the Gaussian and exponential are given, respectively, by

$$W(k) = \frac{h^2 l}{\sqrt{4\pi}} \exp(-\frac{k^2 l^2}{4}) \tag{6.47}$$

$$W(k) = \frac{h^2 l}{\pi} \frac{1}{1+k^2 l^2} \tag{6.48}$$

Where h is rms height, l is correlation length, and k is surface wavenumber. It has been found that the surfaces with Gaussian spectral density are far away from real natural rough surfaces such as soil and ocean and the surfaces with exponential correlation function are without rms slope, which is required for numerical simulations of wave

scattering from random rough surfaces. The third type of surface roughness spectrum, power-law spectral density, is proposed as the following [Chen, 1990; Kuga, 1993].

$$W(k)=\frac{h^2 l}{\sqrt{4\pi}}[1+\pi[\frac{(2n-3)!!}{(2n-2)!!}]^2\frac{k^2l^2}{4}]^{-n} \tag{6.49}$$

$$(2n-2)!!=2\times4\times\cdots\times(2n-2)$$

$$(2n-3)!!=1\times3\times\cdots\times(2n-3)$$

$$(-1)!!=1$$

The above spectrum becomes Gaussian spectrum when power index of n goes to infinite and is very similar to the spectrum with exponential correlation function when n is one. The parameters h and l are supposed to be rms height and correlation length in the above spectrum. But if we compare the power-law spectrum with power index of one with the spectrum of exponential correlation function, we can find that the real correlation length of power-law spectrum is actually $\sqrt{\pi}l/2$. It can be seen by rewriting the power-law spectrum with the power of 1 as:

$$W(k)=\frac{h^2(\sqrt{\pi}l/2)}{\pi}\frac{1}{1+k^2(\sqrt{\pi}l/2)^2} \tag{6.50}$$

Thus, a coefficient varying with the power index is needed and introduced to overcome this problem. The modified power-law spectrum is as the following:

$$W(k)=\frac{h^2 l}{\sqrt{4\pi}}\frac{1}{b_p}[1+(\frac{a_p}{b_p})^2\frac{k^2l^2}{4}]^{-p} \tag{6.51}$$

$$a_p=\frac{\Gamma(p-0.5)}{\Gamma(p)}$$

Where Γ is the Gamma function and $b_1=\sqrt{\pi}/2$, $b_2=0.95$, $b_3=0.97$, $b_4=0.98$,..., and $b_\infty=1.0$ are determined numerically, and h is rms height and l is correlation length. The modified power-law spectrum becomes Gaussian spectrum when power index of n goes to infinite and is the spectrum of exponential correlation function when n is one. The important feature of the proposed spectrum is that it gives various spectrums but with

fixed rms height and correlation length, which are physical parameters usually used to describe the rough surfaces. In the following section, we will describe the numerical results of wave scattering from the random rough surfaces with the power-law spectrum.

6.9 Numerical Results of the Bistatic Scattering Coefficients and the Brightness Temperatures

In this section, we show some numerical results of the bistatic scattering coefficients and the brightness temperatures from wet soil with the power law spectrum. The rms height and correlation length is fixed at 0.3 and 1.0 wavelength, respectively. The surface length is 64 wavelengths and the dense grid is 30 points per wavelength. The simulation was performed by the PBTG-MLSDFMM.

In figure 5, the comparisons of the bistatic scattering coefficients between the surfaces of power law spectrum with the different power index are shown. The relative permittivity of the lower medium is 17.7+i2.26 and incident angle is 30 degrees. Figure (a) is for TE wave incidence and (b) is for TM. For the scattering angle less than 0 degree, the surface with the power index of 2 has the strongest scattering and the Gaussian surface has the weakest. For the scattering angle larger than 0 degree, the situation is opposite.

In figure 6, we plot the brightness temperatures as a function of the observation angles. The physical temperature is 300K and the other parameters are same as figure 5. The emissivity is calculated by equation (45). Figure (a) is for horizontal polarization and (b) is for vertical polarization. For the same roughness parameters of rms height and correlation length, the differences in brightness temperature for the various spectrums can be as large as 15K. For the horizontal polarization, this difference is almost same for the observation angles between 10 and 50 degrees. For the vertical polarization, the

difference has the largest value at the observation angle of 10 degrees and the smallest value at the observation angle of 50 degrees. In general, the surfaces with the less number of the power index have the large brightness temperature.

In figure 7, the brightness temperatures are illustrated as a function of the soil moistures. The observation angle is fixed at 30 degrees and the other parameters are same as the previous figure. Again, for the horizontal polarization, the differences of the brightness temperatures among the different spectrums are essentially same for the soil moistures between 5 and 30 percent. For the vertical polarization, this difference is increased with the increasing of the soil moistures.

6.10 Conclusion

In this paper, we have shown that the PBTG developed by us can be used in combination with the multilevel steepest-descent path fast multipole method. The PBTG-MLSDFMM algorithm has a computational complexity of $O(N)$ for near field interactions and $O(N/n_1)$ for non-near field interactions. A modified power-law spectrum is also proposed and it is shown that the Gaussian and exponential spectrums are special cases of the proposed spectrum. The initial numerical results show that the surface roughness spectrum has some influences on the brightness temperatures.

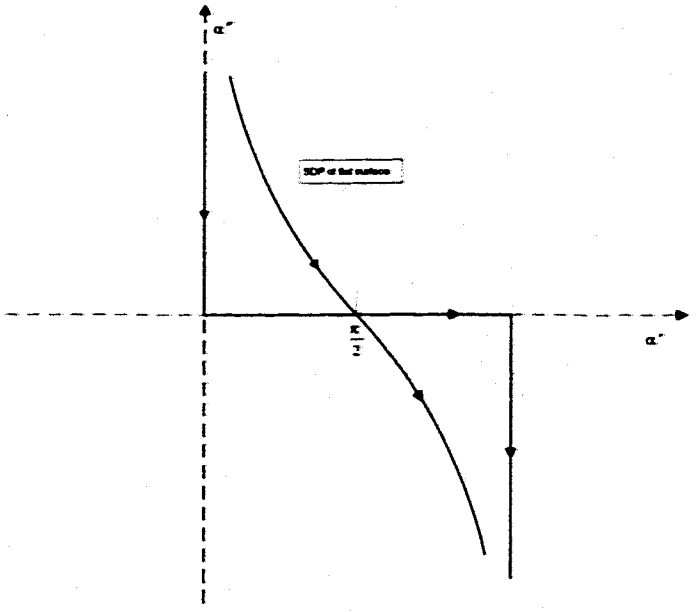

Figure 6.1 Integration paths of the zeroth order Hankel function of the first kind on the complex angle plane.

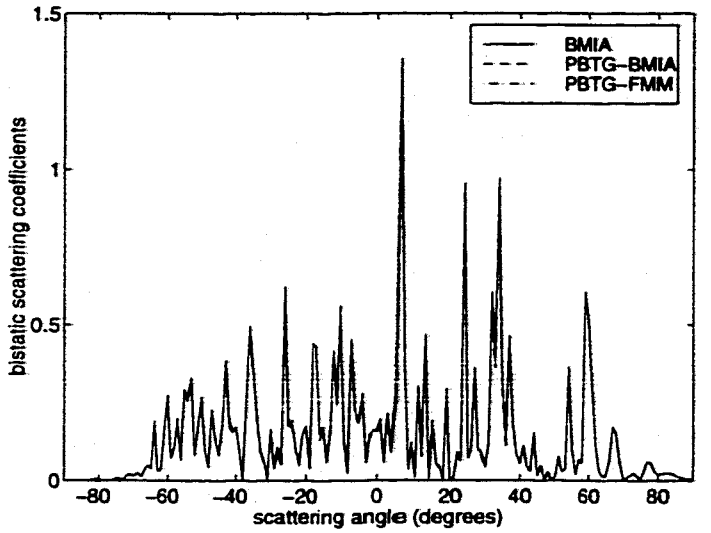

(a)

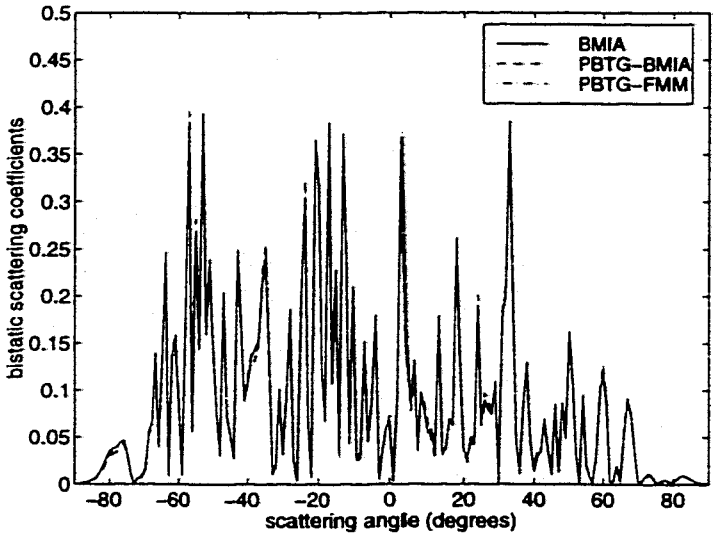

(b)

Figure 6.2. Comparison of the bistatic scattering coefficients computed by the PBTG-FMM, PBTG-BMIA, and BMIA. The rms height is 0.3 wavelength, correlation length is 0.5 wavelength, incidence angle is 30 degrees, permittivity is 25+2i, and surface length is 128 wavelengths. (a) TE wave incidence; (b) TM wave incidence.

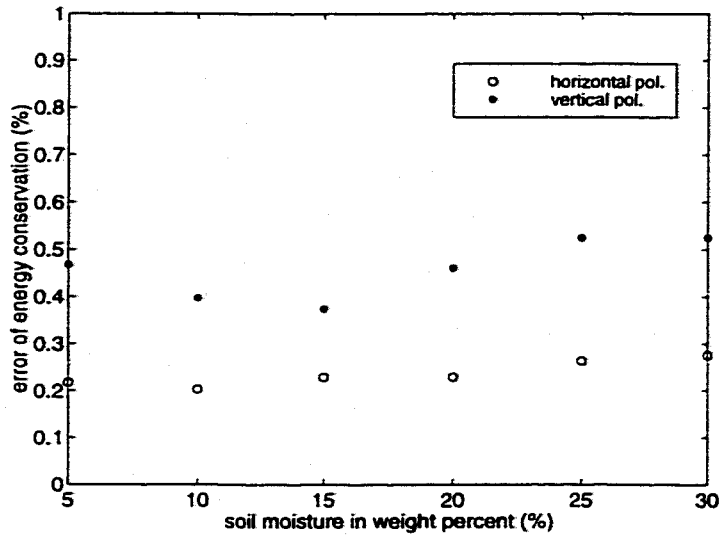

Figure 6.3 Error of the energy conservation check as a function of soil moisture.

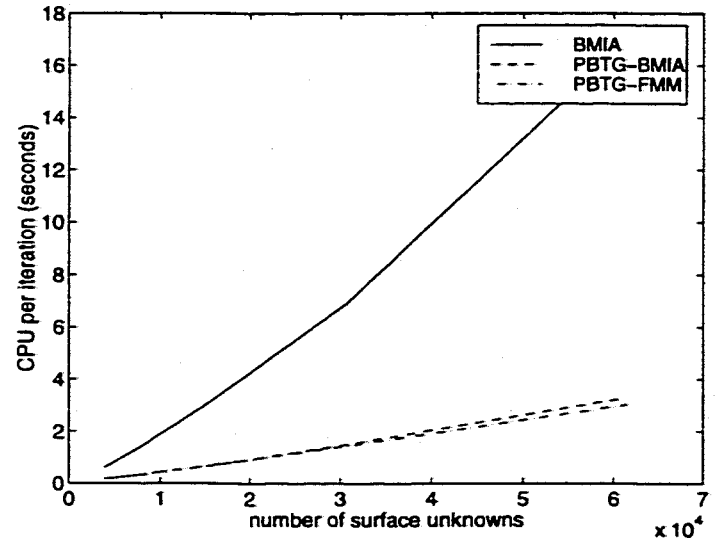

Figure 6.4 Comparisons of CPU time per iteration in the conjugate gradient method required by the PBTG-FMM, PBTG-BMIA, and BMIA. N is the number of surface unknowns.

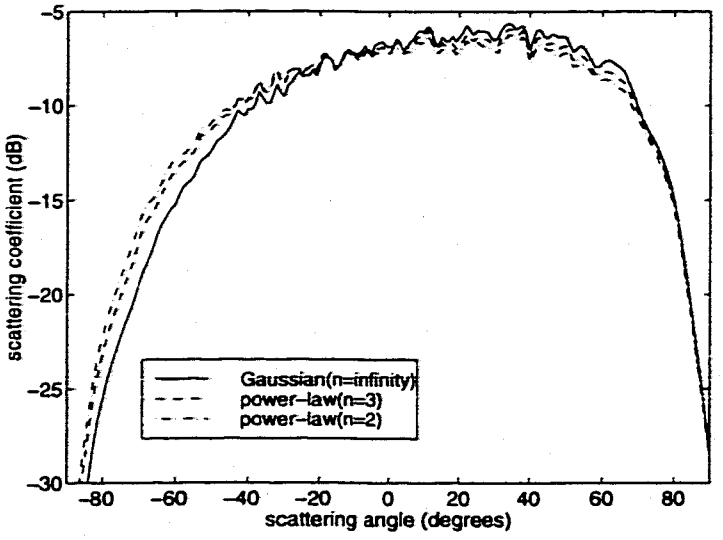

(a)

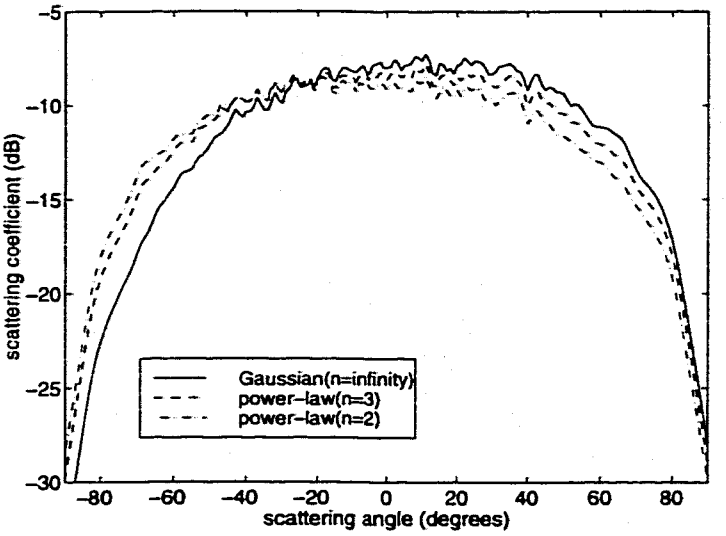

(b)

Figure 6.5 Comparisons of the bistatic scattering coefficients from various spectrums but with fixed rms height of 0.3 wavelength and correlation length of 1.0 wavelength at the incidence angle of 30 degrees. The relative permittivity is 17.7+i2.26. (a) TE wave; (b) TM wave.

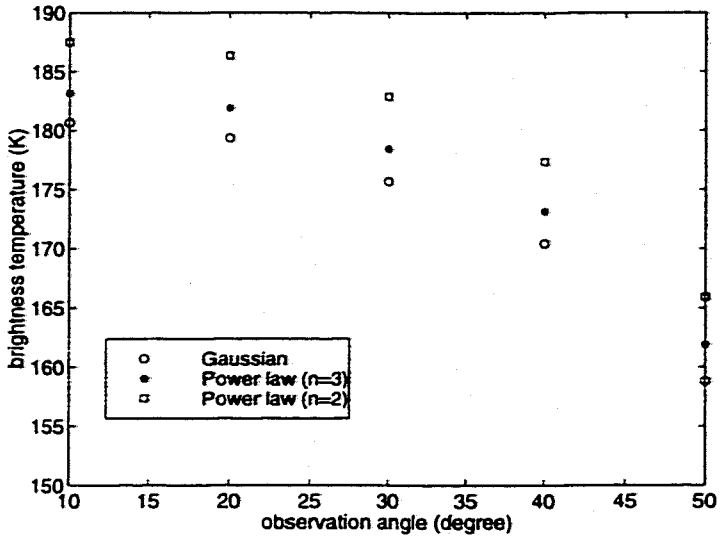

(a)

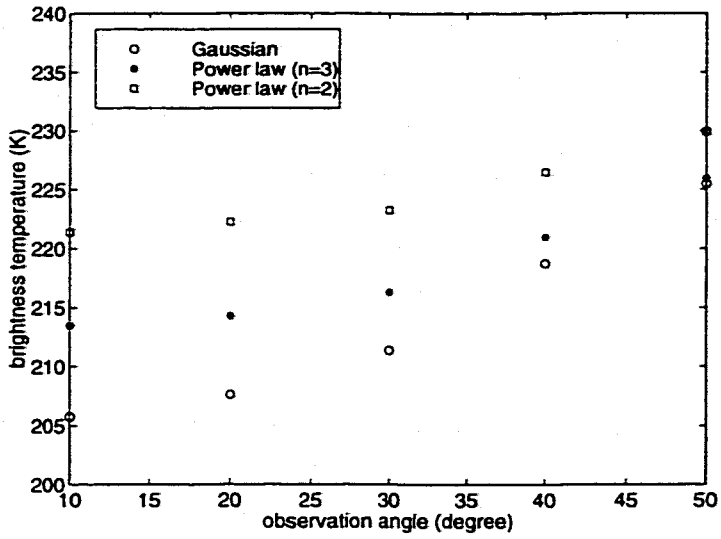

(b)

Figure 6.6 Brightness temperature of rough surface as a function of observation angles and comparisons between various spectrums. The rms height is 0.3 wavelength and correlation length is 1.0 wavelength. The relative permittivity is 17.7+i2.26.

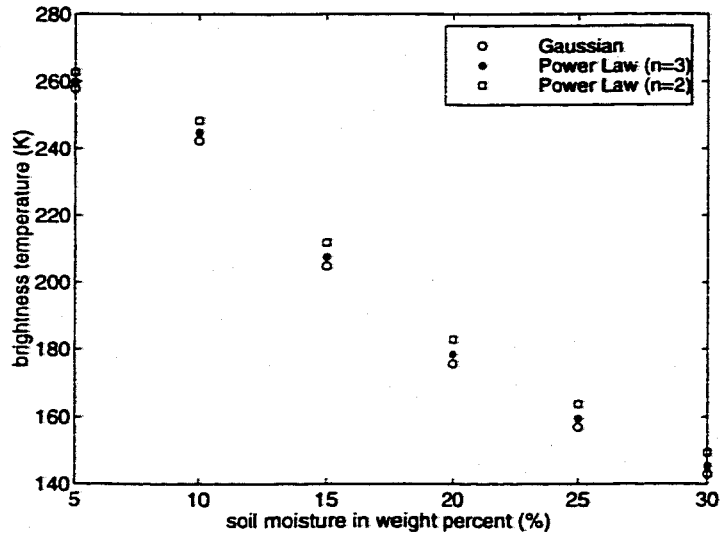

(a)

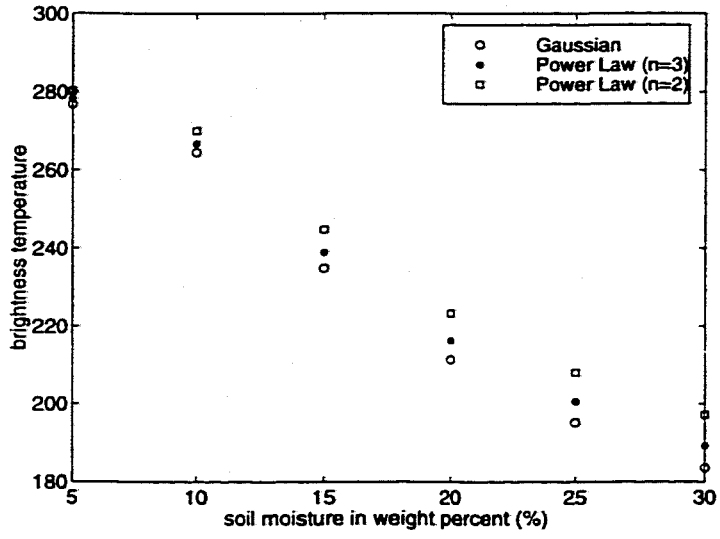

(b)

Figure 6.7 Brightness temperature of rough surface as a function of soil moistures and comparisons between various spectrums. The rms height is 0.3 wavelength and correlation length is 1.0 wavelength. The observation angle is 30 degrees.

Chapter 7

Summary

The physics-based two-grid (PBTG) method was developed for numerically simulating wave scattering from random lossy dielectric rough surfaces with large permittivity in this dissertation. For the wave scattering from random lossy dielectric rough surfaces with large permittivity, we showed that the dense grid is required for the accurate results and the coarse grid can not give those results with required accuracy, especially for the calculation of emissivity. The reason for that is that wavenumber in the medium is much larger than the free-space wavenumber, there can be rapid spatial variations of the dielectric medium Green's function and surface fields. But single dense grid has large CPU and memory requirements. We showed that the PBTG developed in this dissertation gives the accurate results as compared with the single dense grid and takes less CPU as compared with the single coarse grid. We have shown that the calculation of emissivity based on the PBTG can be accurate to within 0.01, which corresponds to a brightness temperature difference of about 3 degrees. The another advantage of the PBTG is that it can be used for both 1-dimensional and 2-dimensional rough surfaces and can be used in conjunction with other fast computational methods. We have combined the PBTG with the BMIA/CAG and steepest descent path FMM for 1-dimensional rough surfaces and with the SMCG for 2-dimensional rough surfaces of 3-dimensional scattering problem. Need to be mentioned in here, the surface fields are calculated on the dense grid in the PBTG. The coarse grid is only used to facilitate matrix-vector multiplication above rough surfaces.

In Chapter 2, first we show that the both surface fields and bistatic scattering coefficients computed by the single coarse grid have big differences with those computed

by the single dense grid for 1-dimensional rough surfaces. It illustrates that the single dense gird is required. Then we describe the physics-based two-grid method (PBTG) for solving the problem of scattering of waves by lossy dielectric surfaces for TE wave incidence. The numerical results showed that the PBTG gives the same accurate results as the single dense grid and takes the same CPU as the coarse grid.

In Chapter 3, the PBTG method was combined with the BMIA/CAG method and steepest descent path FMM for improving of CPU and memory requirements. The algorithms are used to study bistatic scattering coefficients and emissivity for TE and TM cases and apply to low grazing angle scattering. We used it to treat a rough surface with a large surface length since the edge effects have to be avoided for low-grazing angle incidence. Using this approach, we illustrated numerical results of TE and TM wave scattering up to surface length of 500 wavelengths with 30,000 surface unknowns.

In Chapter 4, the PBTG was extended to 2-dimensional random rough surface (3-D scattering problem) and combined with the sparse matrix canonical grid method (SMCG) for improving CPU and memory requirements. The algorithm was used to study the bistatic scattering coefficients and emissivity for wave scattering from 2-D dielectric rough surface with high permittivity. The approach is denoted as PBTG/SMCG. Using this approach, we illustrate numerical results of wave scattering from 2-Dimensional rough surface with permittivity as high as 17 + 2i. Also the numerical results of emissivity are compared with that of approximately analytic solutions of the second order small perturbation method (SPM). It was found that the SPM did not give correct emissivity for the rough surfaces with medium rms slopes.

In Chapter 5, the thermal emission of wet soil with surface roughness using the PBTG/SMCG was extensively studied. The thermal emission of soils with rough surfaces is determined by the surface roughness, soil moisture, soil type, and physical temperature. The simulation results gave the emissivity as a result of 3-D solution of Maxwell

equations. In this Chapter, we reported and showed extensive illustrations and tabulations of the results of emissivities for rough soils with Gaussian spectrum at L and C bands. The same physical roughness parameters are used at L and C bands. The results are important to better understand the effects of surface roughness on the microwave thermal emission of soils.

In Chapter 6, we combined the PBTG with the steepest descent path FMM. We use the steepest-descent path fast multipole method to compute the non-near field interactions on the coarse grid. The computational complexity and memory requirement are proportional to the number of sampling points on the coarse grid for non-near field interactions and on the dense grid for the near field interactions. We also compared the performance between the PBTG-BMIA/CAG and the PBTG-FMM in this chapter. Although the latter algorithm is linear and the first one is O(NlogN), we found the two approaches have almost same CPU requirements for the surface unknowns less than 60,000. Using the proposed algorithm of the PBTG-FMM, the wave scattering from Gaussian and non-Gaussian random rough surfaces was studied. A modified power-law spectrum was proposed to generate random rough surfaces. The feature of the proposed spectrum is that it can become Gaussian spectrum and the spectrum of exponential correlation function by properly choosing the power index and with fixed rms height and correlation length.

Although the PBTG was developed for the wave scattering from lossy dielectric rough surfaces with large permittivity, the approach also can be extended to treat the fine structure of perfectly electric conducting rough surfaces such as fractal surfaces. For the fractal surfaces, a very dense grid is required to describe small structure of surface profile. We can use dense grid to compute the near field interactions and coarse grid to compute non-near field interactions. Due to the spatial frequency limited property of free space Green's function, the fast variation of surface fields could be smoothed after convolution with the free space Green's function. Thus only coarse grid is required for non-near field interactions. Another possible extension of the PBTG is to simulate wave

scattering from lossy layered medium with surface roughness. In this case, the lossy medium Green's function is replaced by the layered medium Green's function directly. The approach can be implemented for both 1-dimensional and 2-dimensional cases.

BIBLIOGRAPHY

[1] Adamas, R. J. and G. S. Brown, "Use of Fast Multipole Method with Method of Ordered Multipole Interactions," *Electronics Letters*, vol.34, no.23; pp.2219-2220, Nov. 1998.

[2] Anastassiu, H. T., M. Smelyanskiy, S. Bindiganavale, and J. L. Volakis, "Scattering from Relatively Flat Surfaces Using the Adaptive Integral Method," *Radio Science*, vol. 33, no. 1, pp.7-16, January-February 1998.

[3] Axline, R. M. and A. K. Fung, "Numerical computation of scattering from a perfectly conducting random surface," *IEEE Trans. Antennas Propagation*, vol. 26, no. 3, pp. 482-488, May 1978.

[4] Bass, F. G., and I. M. Fuks, *Wave Scattering from Statistically Rough Surfaces*, translated by C. B. Vesecky and J. F. Vesecky, Oxford, UK: Pergamon Press, 1979.

[5] Beckmann, P., and A. Spizzichno, *The Scattering of Electromagnetic Waves from rough Surfaces*, New York: MacMillan, 1963.

[6] Brandt, Achi, "Multilevel Computations of the Integral Transforms and Particle Interactions with Oscillatory Kernels," *Computer Phys. Communications*, vol. 65, no. 1-3, pp. 24-38, April 1991.

[7] Briggs, W. L., *A Multigrid Tutorial*, SIAM, Philadelphia, Pennsylvania, 1987.

[8] Bucci, O. M., C. Gennarelli, and C. Savarese, "Fast and Accurate Near-Field-Far-Field Transformation by Sampling Interpolation of Plane-Polar Measurements," *IEEE Trans. Antennas Propagation*, vol. 39, no. 1, pp. 48-55, January 1991a.

[9] Bucci, O. M., C. Gennarelli, and C. Savarese, "Optimal Interpolation of Radiated Fields Over a Sphere," *IEEE Trans. Antennas Propagation*, vol. 39, no. 11, pp. 1633-1643, November 1991b.

[10] Burkholder, R. J. and D. H. Kwon, "High-frequency asymptotic acceleration of the Fast Multipole Method," *Radio Science*, vol. 31, no. 5, pp. 1199-1206, September-October 1996.

[11] Catedra, M. F., R. P. Torres, J. Basterrechea, and E. Gago, *The CG-FFT Method: The Application of Signal Processing Techniques to Electromagnetics*, Nowwood, Massachusetts: Artech House, 1994.

[12] Chan, C. H., and R. Mittra, "Some Recent Development in Iterative Techniques for Solving Electromagnetic Boundary Value Problems," *Radio Science*, vol. 22, no. 6, pp. 929-934, November 1987.

[13] Chan, C. H., S. H. Lou, and L. Tsang, "Electromagnetic scattering of waves by random rough surface: A finite-difference time-domain approach," *Microwave and Optical Technology Letters*, vol.4, no. 9, August, 1991.

[14] Chan, C. H., L. Li, and L. Tsang, "A banded matrix iteration approach to Monte Carlo simulation of large-scale random rough surface scattering: penetrable case," in *Proc. 9th Annu. Rev. Progress Appl. Computat. Electromagn. Symp.*, pp. 391-397, Monterey, March 1993.

[15] Chan, C. H. and L. Tsang, "A Sparse-Matrix Canonical-Grid Method for Scattering by Many Scatterers," *Microwave Optical Tech. Letters*, vol. 8, no. 2, pp. 114-118, February 1995.

[16] Chan, C. H., L. Tsang and Q. Li, "Monte-Carlo simulations of large-scale one-dimensional random rough surface scattering at near grazing incidence: penetrable case," *IEEE Trans. Antennas Propagation*, vol. 46, no. 1, pp. 142-149, January 1998.

[17] Chen, J. S., and A. Ishimaru, "Numerical simulation of the second order Kirchhoff approximation from very rough surfaces and study of backscattering enhancement," *J. Acoustical Soc. Am.*, vol. 88, pp. 1846-1850, October 1990.

[18] Chen, K. S. and A. K. Fung, "A Comparison of Backscattering Models for Rough Surfaces," *IEEE Trans. Geosciences Remote Sensing*, vol. 33, no. 1, pp. 195-199, January 1995.

[19] Chen, R., and J. C. West, "Analysis of scattering from rough surface at large incidence angles using a periodic-surface moment method," *IEEE Trans. Geosciences Remote Sensing*, vol. 33, no. 5, pp. 1206-1213, September 1995.

[20] Chew, W. C., *Waves and Fields in Inhomogeneous Media*, New York: Van Nostrand Reinhold, 1990.

[21] Chew, W. C., J.-M. Jin, C.-C. Lu, E. Michielssen, and J. M. Song, "Fast Solution Methods in Electromagnetics," *IEEE Trans. Antennas Propagation*, vol. 45, no. 3, pp. 533-543, March 1997a.

[22] Chew, W. C., S. Koc, J. M. Song, C. C. Lu, and E. Michielssen, "A Succinct Way to Diagonalize the Translation Matrix in Three Dimensions," *Microwave & Optical Tech. Letters*, vol. 15, no. 3, pp. 144-146, June 1997b.

[23] Chou, H. T., and J. T. Johnson, "A novel acceleration algorithm for the computation of scattering from rough surfaces with the forward-backward method," *Radio Science*, vol.33, no.5, pp.1277-87, October 1998.

[24] Coifman, R., V. Rokhlin, and S. Wandzura, "The Fast Multipole Method for the Wave Equation: A pedestrian Prescription," *IEEE Antennas Propagation Magazine*, vol. 35, no. 3, pp. 7-12, June 1993.

[25] Depine, R. A., "Scattering of Light from One-dimensional random Rough Surfaces: A New Antispecular Effect in the Oblique Incidence," *J. Optical Soc. Am. A*, vol.10, no. 5, pp. 920-927, May 1993.

[26] Devayya, R., and D. J. Wingham, "The numerical calculation of rough surface scattering by the conjugate gradient method," *IEEE Trans. Geosciences Remote Sensing*, vol. 30, pp. 645-648, 1992.

[27] Donohue, D. J., H. C. Ku, and D. R. Thompson, "Application of Iterative Moment-Method Solutions to Ocean Surface Radar Scattering," *IEEE Trans. Antennas Propagation*, vol. 46, no. 1, pp.121-132, January 1998.

[28] Engheta, N., W. D. Murphy, V. Rokhlin, and M. S. Vassilious, "The Fast Multipole Method (FMM) for Electromagnetic Scattering Problems," *IEEE Trans. Antennas Propagation*, vol. 40, no. 6, pp.634-641, June 1992.

[29] Ericson, E. A. and D. R. Lyzenga, "Performance of a numerical iterative solution of the surface current integral equation for surfaces containing small radii of curvature," *Radio Science*, vol. 33, no. 2, pp. 205-217, March-April 1998.

[30] Franceschetti, G., A. Iodice, M. Migliaccio, and D. Riccio, "Scattering from natural rough surfaces modeled by fractional browning motion two-dimensinal process," *IEEE Trans. Antennas Propagation*, vol. 47, no. 9, pp.1405-1415, September 1999.

[31] Fung, A. K., Z. Li, and K. S. Chen, "Backscattering from a Randomly Rough Dielectric Surface," *IEEE Trans. Geoscience Remote Sensing*, vol. 30, no. 2, pp. 356-369, March 1992.

[32] Fung, A. K., *Microwave Scattering and Emission Models and Their Applications*, Norwood, Massachusetts: Artech House, 1994.

[33] Greffet, J. J., and M. Nieto-Vesperinas, "Field theory for generalized bidirectional reflectivity: derivation of Helmholtz's reciprocity principle and Kirchhoff's law," *J. Optic. Soc. Am. A*, vol.15, no.10, pp. 2735-44, October 1998.

[34] Harrington, R. F., *Field Computation by Moment Method*, New York: Macmillan, 1968.

[35] Holliday, D., L. L. DeRaad, Jr., and G. J. St-Cyr, "Forward-backward: A new method for computing low-grazing angle scattering," *IEEE Trans. Antennas Propagation*, vol. 44, pp. 722-729, May 1996.

[36] Holliday, D., L. L. DeRaad, Jr., and G. J. St-Cyr, "Forward-backward method for scattering from imperfect conductors," *IEEE Trans. Antennas Propagation*, vol. 46, pp. 101-107, January 1998.

[37] Irisov, V. G., "Small slope expansion for Electromagnetic-wave Diffraction on a rough surface," *Waves in Random Media*, vol. 4, pp.441-452, 1994.

[38] Irisov, V. G., "Small slope expansion for thermal and reflected radiation from a rough surface," *Waves in Random Media*, vol. 7, pp.1-10, 1997.

[39] Ishimaru, A., *Wave Propagation and Scattering in Random Media*, New York: Academic Press, 1978.

[40] Ishimaru, A. and J. S. Chen, "Scattering from Very Rough Surfaces Based on the Modified Second Order Kirchhoff Approximation with Angular and Propagation Shadowing," *J. Acoustical Soc. Am. A*, vol.88, no. 4, pp. 1877-1883, October 1990.

[41] Ishimaru, A., *Electromagnetic Wave Propagation, radiation, and Scattering*, Englewood Cliffs, New Jersey: Prentice-Hall, 1991.

[42] Jandhyala, V., E. Michielssen, S. Balasubramaniam, and W. C. Chew, "A Combined Steepest Descent-Fast Multipole Algorithm for the Fast Analysis of Three-dimensional Scattering by Rough Surfaces," *IEEE Trans. Geosciences Remote Sensing*, vol. 36, pp. 738-748, May 1998a.

[43] Jandhyala, V., B. Shanker, E. Michielssen, W. C. Chew, "A Fast Algorithm for the Analysis of Scattering by Dielectric Rough Surfaces," *J. Opt. Soc. Am. A*, vol.15, no.7, pp. 1877-85, July 1998b.

[44] Johnson, J. T., L. Tsang, R. Shin, K. Pak, C. H. Chan, A. Ishimaru, and Y. Kuga, "Backscattering Enhancement of Electromagnetic Waves from Two-dimensional Perfectly Conducting Random Rough Surfaces: A Comparison of Monte Carlo Simulations with Experimental Data," *IEEE Trans. Antennas Propagation*, vol. 44, pp. 748-756, 1996.

[45] Johnson, J. T., R. T. Shin, J. C. Eidson, L. Tsang, and J. A. Kong, "A Method of Moments Model for VHF Propagation," *IEEE Trans. Antennas Propagation*, vol. 45, pp. 115-125, January 1997.

[46] Johnson, J. T., "A Numerical Study of Low-Grazing Angle Backscatter from Ocean-Like Impedance Surfaces with the Canonical Grid Method," *IEEE Trans. Antennas Propagation*, vol. 46, no. 1, pp. 114-120, January 1998.

[47] Johnson, J. T., R. T. Shin, J. A. Kong, and L. Tsang, "A Numerical Study of Ocean Polarimetric Thermal Emission," *IEEE Trans. Geoscience Remote Sensing*, vol. 37, no. 1, pp. 8-20, January 1999.

[48] Kapp, D. A., and G. S. Brown, "A New Numerical Method for Rough Surface Scattering Calculations," *IEEE Trans. Antennas Propagation*, vol. 44, pp. 711-721, May 1996.

[49] Kim, Y., E. Rodriguez, and S. Durden, "A numerical assessment of rough surface scattering theories: Vertical polarization," *Radio Science,* vol. 27, no. 4, pp. 515-527, July 1992.

[50] Kong, J. A., *Electromagnetic Wave Theory*, New York: John Wiley & Sons, 1986.

[51] Kuga, Y., J. S. Colburn, and P. Phu, "Millimeter-wave Scattering from One-Dimensional Surfaces of Different Surface Correlation Functions," *Waves in Random Media*, vol. 3, pp. 101-110, 1993.

[52] Li, L., C. H. Chan, and L. Tsang, "Numerical simulation of conical diffraction of tapered electromagnetic waves from random rough surfaces and applications to passive remote sensing," *Radio Science*, vol. 29, no. 3, pp. 587-598, May-June 1994.

[53] Li, Q., C. H. Chan, and L. Tsang, "Monte-Carlo Simulations of Wave Scattering from Lossy Dielectric Random Rough Surfaces Using the Physics-Based Two-Gird Method and Canonical Grid Method," *IEEE Trans. Antennas Propagation,* vol. 47, no. 4, pp. 752-763, April 1999.

[54] Li, Q., L. Tsang, K. Pak, and C. H. Chan, "Bistatic Scattering and Emissivities of Random Rough Dielectric Lossy Surfaces with the Physics-Based Two-Grid Method in Conjunction with the Sparse-Matrix Canonical Grid Method," to be appeared in *IEEE Trans. Antennas Propagation*, January 2000.

[55] Lin, C.-M., and C. H. Chan, "Monte Carlo Simulations for the Electromagnetic Scattering of Rough Surfaces by the Combined Wavelet Transform and Banded-Matrix Iterative Approach/Canonical Grid Method," *Microwave Optical Tech. Letters*, vol. 19, no. 4, pp. 274-279, November 1998.

[56] Lou, S. H., L. Tsang, C. H. Chan, and A. Ishimaru, "Monte Carlo Simulations of Scattering Waves by a Random Rough Surfaces with the Finite Element Method and the Finite Difference Method," *Microwave Optical Tech. Letters*, vol.3, no. 5, pp. 150-154, May 1990.

[57] Lu, C. C., and W.C. Chew, "Fast algorithm for solving hybrid integral equations," *IEE Proceedings-H*, vol. 140, no. 6, pp. 455-460, December 1993.

[58] Lu, C. C., and W.C. Chew, "A Mutilevel Algorithm for Solving Boundary Integral Equation of Wave Scattering," *Microwave Opt. Technology Letter*, vol. 7, no. 10, pp. 466-470, July 1994.

[59] Mandelbrot, B. B., *The Fractal Geometry of Nature*, New York: W. H. Freeman & C., 1983.

[60] Maradudin, A. A., E. R. Mendez, and T. Michel, "Backscattering effects in the elastic scattering of p-polarization light from a large amplitude random grating," in *Scattering in Volumes and Surfaces*, M. Nieto-Vesperians and J. C. Dainty eds., Elsevier Science Publishers, North-Holland, 1990a.

[61] Maraudin, A., T. Michel, A. McGurn, and E. R. Mendez, "Enhanced Backscattering of Light form a Random Grating," *Annals Phys.*, vol. 203, no. 2, pp. 255-307, 1990b.

[62] Maystre, D., M. Saillard and J. Ingers, "Scattering by one- or two-dimensional randomly rough surfaces," *Waves in Random Media*, vol. 1, pp. 143-155, 1991.

[63] McGurn, A. R., and A. A. Maradudin, "Weak Transverse Localization of the Light Scattered Incoherently from a One-dimensional Random Metal Surfaces," *J. Optical Soc. Am. B*, vol. 10, no. 3, pp. 539-545, March 1993.

[64] Medgyesi, L. N., and J. M. Putnam, and M. B. Gedera, "Genralized method of moments for three-dimensional penetrable scatterers," *J. Optical Soc. Am. A*, vol.11, no. 4, pp. 1383-1398, April 1994.

[65] Michielssen, E. and A. Boag, "Multilevel Evaluation of Electromagnetic Fields for the Rapid Solution of Scattering Problems," *Microwave & Optical Tech. Letters*, vol. 7, no. 17, pp. 790-795, December 1994.

[66] Michielssen, E., A. Boag, and W. C. Chew, "Scattering from Elongated Objects: Direct Solution in O(N $\log^2$N) Operations," *IEE Proc.- Microwave Antennas Propagation*, vol. 143, no. 4, pp. 277-283, August 1996a.

[67] Michielssen, E. and W. C. Chew, "Fast Steepest Descent Path Algorithm for Analyzing Scattering from Two-dimensional Objects," *Radio Science*, vol. 31, no. 5, pp. 1215-1224, September-October 1996b.

[68] Mittra, R., *Computer Techniques for Electromagnetics*, New York: Pergamon, 1973.

[69] Mitzner, K. M., "An integral equation approach to scattering from a body of finite conductivity," *Radio Science*, vol. 2, pp. 1459-1470, 1967.

[70] Mo, T., T. J. Schmugge, and J. R. Wang, "Calculations of the Microwave Brightness Temperature of Rough Soil Surfaces: Bare Field," *IEEE Trans. Geosciences Remote Sensing*, vol. GE-25, no. 1, pp. 47-54, January 1987.

[71] Mori, A. and A. Freni, "A Modified BMIA/CAG Method for Fast Evaluation of the Electromagnetic Scattering by Rough Terrain," *Microwave Optical Tech. Letters*, vol. 20, no. 4, pp. 280-282, February 1999.

[72] Nieto-Vesperinas, M. and J. M. Soto-Crespo, "Monte-Carlo simulations for scattering of electromagnetic waves from perfectly conducting random rough surfaces," *Optics Letters*, vol. 12, pp. 979-981, 1987.

[73] Ogilvy, J. A., *Theory of Wave Scattering from Random Rough Surfaces*, Adam Hilger, Bristol, 1991.

[74] Pak, K., L. Tsang, C. H. Chan, and J. Johnson, "Backscattering Enhancement of Vector Electromagnetic Waves from Two-dimensional Perfectly Conducting Random Rough Surfaces Based on Monte Carlo Simulations," *J. Opt. Soc. Am. A*, vol. 12, no. 11, pp. 2491-2499, 1995.

[75] Pak, K., *Studies of Large-Scale Random Rough Surface Scattering Problems Based on Monte Carlo Simulations with the Efficient Computational integral Equation Methods*, Ph.D. Dissertation, University of Washington, 1996.

[76] Pak, K., L. Tsang, and J. Johnson, "Numerical Simulations and Backscattering Enhancement of Electromagnetic Waves from Two-dimensional Dielectric Random Rough Surfaces with the Sparse Matrix Canonical Grid Method," *J. Opt. Soc. Am. A*, vol. 14, no. 7, pp. 1515-1528, July 1997.

[77] Rao, S. M., D. R. Wilton, and A. W. Glisson, "Electromagnetic Scattering by the Surfaces of Arbitrary Shape," *IEEE Trans. Antennas Propagation*, vol. 30, no. 5, pp. 402-418, May 1982.

[78] Rino, C., T. Crystal, A. Koide, H. Ngo, and H. Guthart, "Numerical simulations of backscatterer from linear and nonlinear ocean surface realization," *Radio Science*, vol. 26, pp. 51-72, 1992.

[79] Rino, C. L., and H. D. Ngo, "Application of beam simulation to scattering at low grazing angles. 2. Oceanlike surfaces," *Radio Science*, vol. 29, no. 6, pp. 1381-1391, November 1994.

[80] Rino, C. L., and H. D. Ngo, "Numerical Simulation of Low-Grazing Angle Ocean Microwave Backscatter and Its Relation to Sea Spikes," *IEEE Trans. Antennas Propagation*, vol. 46, no. 1, pp. 133-141, January 1998.

[81] Rodriguez, E., Y. Kim, and S. L. Durden, "A Numerical Assessment of Rough Surface Scattering Theories: Horizontal Polarization," *Radio Science*, vol. 27, no. 4, pp. 497-513, July-August 1992.

[82] Rokhlin, V., "Rapid Solution of Integral Equations of Classic Potential Theory," *J. Computational Phys.*, vol. 60, pp. 187-207, 1983.

[83] Rokhlin, V., "Rapid Solution of Integral Equations of Scattering Theory in Two Dimensions," *J. Computational Phys.*, vol. 86, pp. 414-439, 1990.

[84] Sarabandi, K. and T. Chiu, "Electromagnetic Scattering from Slightly Rough Surfaces with Inhomogeneous Dielectric Profiles," *IEEE Tans. Antennas Propagation*, vol. 45, no. 9, pp. 1419-1430, September 1997.

[85] Schmugge, T. J., T. Wilheit, W. Webster, Jr., and P. Gloersen, "Remote sensing of soil moisture with microwave radiometers, II," *NASA TND-8321*, Goddard Space Flight Center, Greenbelt, MD, 1976.

[86] Schmugge, T., P. E. O'Neil, and J. R. Wang, "Passive Microwave Soil Moisture Research," *IEEE Trans. Geoscience Remote Sensing*, vol. GE-24, no. 1, pp. 12-22, January 1986.

[87] Song, J. M., and W.C. Chew, "Multilevel Fast-Multipole Algorithm for Solving Combined Field Integral Equations of Electromagnetic Scattering," *Microwave Opt. Technology Letters*, vol. 10, no. 1, pp. 14-19, September 1995.

[88] Thomas, B. A., "Approximate Boundary Conditions," *IEEE Tans. Antennas Propagation*, vol. 29, no. 5, pp. 826-829, September 1981.

[89] Thorsos, E. I., "The validity of the Kirchhoff approximation for rough surface scattering using a Gaussian roughness spectrum," *J. Acoustical Soc. Am.*, vol. 83, no. 1, pp. 78-92, January 1988.

[90] Thorsos, E. I., and D. R. Jackson, "The validity of the perturbation approximation for rough surface scattering using a Gaussian roughness spectrum," *J. Acoustical Soc. Am.*, vol. 86, no. 1, pp. 261-272, January 1989.

[91] Thorsos, E. I., and D. R. Jackson, "Studies of Scattering Theory Using Numerical Methods," *Waves in Random Media*, vol. 3, pp. 165-190, 1991.

[92] Toporkov, J. V., R. T. Marchand, and G. S, Brown, "On the Discretization of the Integral Equation Describing Scattering by Rough Conducting Surfaces," *IEEE Trans. Antennas Propagation*, vol. 46, no. 1, pp. 150-162, January 1998.

[93] Tran, P., V. Celli, and A. A. Maradudin, "Electromagnetic Scattering from a Two-dimensional, Randomly Rough, Perfectly Conducting Surface: Iterative Methods," *J. Optical Soc. Am. A*, vol.11, no. 5, pp. 1686-1689, May 1994a.

[94] Tran, P. and A. A. Maradudin, "The Scattering of Electromagnetic Waves from a Randomly Rough 2D Metallic Surface," *Optics Communications*, vol. 101, pp. 269-273, August 1994b.

[95] Tran, P. and J. M. Elson, "Banded Method of Ordered Multiple Interaction for the Scattering of Electromagnetic Waves from a Rough Surface," *J. Optical Soc. Am. A*, vol. 15, no. 6, pp. 1643-1643, June 1998.

[96] Tsang L., E. Njoku, and J. A. Kong, "Microwave Thermal Emission from a Stratified Medium with Nonuniform Temperature Distribution," *J. Applied Phys.*, vol. 46, no. 12, pp. 5127-5133, December 1975.

[97] Tsang, L. and R. W. Newton, "Microwave Emissions from Soils with Rough surfaces," *J. Geophysical Res.*, vol. 87, no. 11, pp. 9017-9024, October 1982.

[98] Tsang, L., J. A. Kong, and R. T. Shin, *Theory of Microwave Remote Sensing*, New York: Wiley-Interscience, 1985.

[99] Tsang, L., "Polarimetric Passive Microwave Remote Sensing of Random Discrete Scatterers and Rough Surfaces," *J. Electromagnetic Waves & Applications*, vol. 5, no. 1, pp. 41-57, 1991.

[100] Tsang, L., C. H. Chan and H. Sangani, "A banded matrix iterative approach to Monte Carlo simulations of scattering of waves by large-scale random rough surface problems: TM case," *Electronic Letters*, vol. 29, no. 2, pp. 166-167, January 1993a.

[101] Tsang, L., C. H. Chan and H. Sangani, "Application of a Banded Matrix Iterative Approach to Monte Carlo Simulations of Scattering of Waves by a Random Rough Surface: TM Case," *Microwave Optical Tech. Letters*, vol. 6, no. 2, pp. 148-151, February 1993b.

[102] Tsang, L., C. H. Chan, and K. S. Pak, " The Monte Carlo Simulations of A Two-dimensional Random Rough Surface Using the Novel Sparse-Matrix Flat-Surface Iterative Approach," *Electronic Letters*, vol. 29, no. 13, pp. 1153-1154, 1993c.

[103] Tsang, L., C. H. Chan, H. Sangani, A. Ishimaru, and P. Phu, "A banded matrix iterative approach to Monte-Carlo simulations of large-scale random rough surface scattering: TE case," *Journal of Electromagnetic Waves and Applications*, vol. 7, no. 9, pp. 1185-1200, 1993d.

[104] Tsang, L., C. H. Chan, K. Pak, and H. Sangani, "A BMIA/FFT algorithm for the Monte Carlo simulations of large scale random rough surface scattering: Application to grazing incidence," *Proceedings of the IEEE Antennas Propagation Soc. Int. Symp.*, pp. 2028-2031, 1994a.

[105] Tsang, L., C. H. Chan, and K. Pak, "Backscattering enhancement of a two-dimensional random rough surface (three-dimensional scattering) based on Monte Carlo simulations," *Journal of Optical Society of America, A*, vol. 11, no. 2., pp. 711-715, February 1994b.

[106] Tsang, L., C. H. Chan, K. Pak, H. sangani, A. Ishimaru, and P. Phu, "Monte Carlo Simulation of Large-scale Composite Random Rough Surface Scattering Based on

the Banded Matrix Iterative Approach," *Journal of Optical Society of America*, vol. 11, no. 2., pp. 691-696, February 1994c.

[107] Tsang, L., C. H. Chan, K. Pak and H. Sangani, "Monte Carlo simulations of large-scale problems of random rough surface scattering and applications to grazing incidence with the BMIA/canonical grid method," *IEEE Trans. Antennas Propagation*, vol. 43, no. 8, pp. 851-859, August 1995.

[108] Tsang, L., and Q. Li, "Numerical solution of scattering of waves by lossy dielectric surfaces using a physics-based two-grid method," *Microwave Opt. Technology Letter*, vol. 16, no. 6, pp. 356-364, December 20, 1997.

[109] Ulaby, F. T., R. K. Moore, and A. K. Fung, *Microwave Remote Sensing: Active and Passive*, vol. 2, Norwood, Massachusetts: Artech House, 1982.

[110] Umashankar, K., A. Taflove, and S. M. Rao, "Electromagnetic Scattering by Arbitrary Shaped Three-dimensional Homogeneous Lossy Dielectric Objects," *IEEE Tans. Antennas Propagation*, vol. 34, no. 6, pp. 758-766, June 1986.

[111] Voronovich, A. G., *Wave scattering from rough surfaces*, Berlin: Springer-Verlag, 1994.

[112] Wagner, R. L. and W. C. Chew, "A Ray-Propagation Fast Multipole Algorithm," *Microwave & Optical Tech. Letters*, vol. 7, no. 10, pp. 435-438, July 1994.

[113] Wagner, R. L., J. S. Song, and W. C. Chew, "Monte Carlo Simulation of Electromagnetci Scattering from Two-dimensional Random Rough Surfaces," *IEEE Tans. Antennas Propagation*, vol. 45, no. 2, pp. 235-245, February 1997.

[114] Wang, D. S., "Limits and Validity of the Impedance Boundary Conditions on Penetrable Surfaces," *IEEE Tans. Antennas Propagation*, vol. 35, no. 4, pp. 453-457, April 1987.

[115] Wang, J. R., and T. J. Schmugge, "An Empirical Model for the Complex Dielectric Permittivity of Soils as a Function of Water Content," *IEEE Trans. Geosciences Remote Sensing*, vol. GE-18, no. 4, pp. 288-295, October 1980.

[116] Wang, J. R., P. E. O'Neill, T. J. Jackson, and E. T. Engman, "Multi-frequency Measurements of the Effects of Soil Moisture, Soil Texture and Surface

Roughness," *IEEE Trans. Geoscience Remote Sensing*, vol. GE-21, pp. 44-51, 1983.

[117] Wang, J. R., "Microwave Emission from Smooth Bare Fields and Soil Moisture Sampling Depth," *IEEE Trans. Geoscience Remote Sensing*, vol. GE-25, no. 5, pp. 616-622, September 1987a.

[118] Wang, J. R., E. T. Engman, T. Mo, T. J. Schmugge, and J. C. Shiue, "The Effects of Soil Moisture, Surface Roughness, and Vegetation on L-Band Emission and Backscatter," *IEEE Trans. Geoscience Remote Sensing*, vol. GE-25, no. 6, pp. 825-833, November 1987b.

[119] West, J. C. and J.M. Sturm, "On iterative approaches for electromagnetic rough-surface scattering problems," *IEEE Transactions on Antennas and Propagation*, Vol.47, no.8, pp. 1281-1288, August 1999.

[120] Winebrenner, D.P. and A. Ishimaru, "Application of the phase-perturbation technique to randomly rough surface," *Journal of Optical Society of America A*, vol. 2, pp.2285-2294, 1985a.

[121] Winebrenner, D.P. and A. Ishimaru, "Investigation of a surface field perturbation technique for scattering from rough surface," *Radio Science*, vol. 20, pp.161-170, 1985b.

[122] D. J. Wingham and R. H. Devayya, "A Note on the Use of the Neumann Expansion in Calculating the Scatter from Rough Surfaces," *IEEE Trans. Antennas Propagation*, vol. 40, no. 5, pp. 560-563, May 1992.

[123] Yueh, S. H., R. Kwok, F. K. Li, S.V. Nghiem, W. J. Wilson, and J. A. Kong, "Polarimetric Passive Remote Sensing of Ocean Wind Vector," *Radio Science*, pp. 799-814, 1994.

[124] Yueh, S. H., "Modeling of Wind Direction Signal in Polarimetric Sea Surface Brightness Temperatures," *IEEE Tans. Geoscience Remote Sensing*, vol. 35, no. 6, pp. 1400-1418, November 1997.

VITA

QIN LI

University of Washington

MARCH, 2000

Qin Li was born in People's Republic of China on November 7, 1963. He received his Bachelor of Science in Space Physics from Wuhan University in Wuhan, P. R. China, July 1985, and his Master of Science in Space Physics from the same University, in July 1988. He was with the Department of Space Physics of Wuhan University from 1988 to 1996. He received his Doctor of Philosophy degree in Electrical Engineering from the University of Washington in March 2000.

Publications

Journal Papers

1. Qin Li, L. Tsang, J. C. Shi, C. H. Chan, "Application of Physics-based Two-Grid Method and Sparse Matrix Canonical Grid Method for Numerical Simulations of Emissivities of Soils with Rough Surfaces", accepted by *IEEE Transactions on Geoscience and Remote Sensing*, January 2000.
2. Qin Li, Leung Tsang, Kyung Pak, and Chi Hou Chan, "Bistatic Scattering and Emissivities of Rough Surfaces with the Physics-Based Two-Grid Method in Conjunction with the Sparse Matrix Canonical Grid Method," to be appeared on *IEEE Transactions on Antennas and Propagation*, January 2000.

3. Q. Li, C. H. Chan, and L. Tsang, "Monte-Carlo Simulations of Wave Scattering from Lossy Dielectric Random Rough Surfaces Using the Physics-Based Two-Grid Method and the Canonical Grid Method," *IEEE Transaction on Antennas and Propagation,* Vol. 47, No. 4, pp. 752-763, April. 1999.
4. C. H. Chan, L. Tsang, and Q. Li, "Monte Carlo Simulations of Large-Scale One-Dimensional Random Rough Surface Scattering at Near-Grazing Incidence," *IEEE Transaction on Antennas and Propagation,* Vol. 46, No. 1, pp. 142-149, Jan., 1998.
5. L. Tsang and Q. Li, "Numerical solution of scattering of waves by lossy dielectric surfaces using a physics-based two-grid method," *Microwave and Optical Technology Letters,* Vol.16, No.6, pp. 356-64. 20 Dec. 1997.
6. Shu-Qing Li, Chi Hou Chan, Leung Tsang, and Qin Li, "Parallel Implementation of the Sparse-Matrix/Canonical Grid Method for the Analysis of Two-Dimensional Random Rough Surfaces (Three-Dimensional Scattering Problem) on a Beowulf System," submitted to *IEEE Transactions on Geoscience and Remote Sensing,* Aug. 1999.

Conference

1. Qin Li, Leung Tsang, Kyung Pak, and Chi Hou Chan, "Scattering of Electromagnetic Waves and Emissivities of Random Rough Dielectric Lossy Surfaces with the Physics-Based Two-Grid Method Combined with the Sparse-Matrix Canonical Grid Method," *Progress In Electromagnetics Research Symposium (PIERS)*, Taiwan, 1999.
2. Qin Li, Leung Tsang, Chi Hou Chan and Kyung Pak, "Emissivity of Random Dielectric Rough Surfaces: A Comparison Between the Second Order Small Perturbation Method and 3-dimensional Monte-Carlo Simulations," *National Radio Science Meeting,* Boulder, Colorado, 1999.
3. Qin Li, Leung Tsang, Guifu Zhang, and Chi Hou Chan, "Wave Scattering from a Lossy Dielectric Rough Surface Using a Physics-Based Two-grid Method Combined with the Banded-Matrix Iterative Approach/Canonical Grid Method

and Applications to Passive Remote Sensing," *International Geoscience and Remote Sensing Symposium (IGARSS)*, Seattle, Washington, 1998.

4. Qin Li, Leung Tsang, Guifu Zhang, and Chi Hou Chan, "Numerical Solutions of Wave Scattering from a Lossy Dielectric Random Rough Surface at Low Grazing Incidence Using a Physics-Based Two-grid Method Combined with the Banded-Matrix Iterative Approach/Canonical Grid Method," *IEEE AP-S International Symposium and USNC/URSI National Radio Science Meeting*, Atlanta, Georgia, 1998.
5. Kyung Pak, Leung Tsang, Chi Hou Chan, Joel Johnson and Qin Li, "Scattering of Electromagnetic Waves in Large-Scale Rough Surface Problems Based on the Sparse-Matrix Canonical-Grid Method," *Applied Computational Electromagnetics Society (ACES) Symposium*, Monterey, CA, 1997.
6. Qin Li, Leung Tsang, Kyung Pak, and Chi Hou Chan, "Monte-Carlo Simulations of Emissivities of Random Dielectric Rough Surfaces and Comparisons with the Small Perturbation Method," *International Geoscience and Remote Sensing Symposium (IGARSS)*, German, 1999.
7. S. Li, C. H. Chan, L. Tsang, and Q. Li, "Parallel Implementation of the Sparse Matrix Canonical Grid Method for Two-dimensional Lossy Dielectric Rough Surfaces (3D scattering problems) on a Beowulf System," *IEEE AP-S International Symposium and USNC/URSI National Radio Science Meeting*, Orlando, Florida, 1999.
8. Qin Li, Leung Tsang, and Jiancheng Shi, "Numerical Simulations of Emissivities of Two-dimensional Random Dielectric Lossy Rough Surfaces with Gaussian and Non-Gaussian Spectrums," submitted to *National Radio Science Meeting*, Boulder, Colorado, 2000.
9. Leung Tsang, Qin Li, and Chi Hou Chan, "Scattering of electromagnetic Waves by Random Rough Surfaces Based on Monte Carlo Simulations," submitted to the *Asia Pacific Rim Microwave* Conference, Singapore, 1999.

Other Publications:

Leung Tsang and Qin Li, *Microwave Remote Sensing Theory*, John Wiley.

Encyclopedia of Electrical and Electronics Engineering, May 1999.